

ANKARA YILDIRIM BEYAZIT UNIVERSITY

GRADUATE SCHOOL OF NATURAL AND APPLIED SCIENCES



**ENERGY AND EXERGY ANALYSIS AND PERFORMANCE
OPTIMIZATION OF A SOLAR POWER TOWER SYSTEM**

M.Sc. Thesis by

Gürcan TİRYAKİ

Department of Mechanical Engineering

June, 2017

ANKARA

**ENERGY AND EXERGY ANALYSIS AND
PERFORMANCE OPTIMIZATION OF A SOLAR
POWER TOWER SYSTEM**

A Thesis Submitted to

The Graduate School of Natural and Applied Sciences of

Ankara Yıldırım Beyazıt University

**In Partial Fulfillment of the Requirements for the Degree of Master of Science
in Mechanical Engineering, Department of Mechanical Engineering**

by

Gürcan TIRYAKI

June, 2017

ANKARA

M.Sc. THESIS EXAMINATION RESULT FORM

We have read the thesis entitled “**ENERGY AND EXERGY ANALYSIS AND PERFORMANCE OPTIMIZATION OF A SOLAR POWER TOWER SYSTEM**” completed by **GÜRCAN TİRYAKİ** under the supervision of **PROF. DR. ÜNAL ÇAMDALI** and we certify that in our opinion it is fully adequate, in scope and in quality, as a thesis for the degree of Master of Science.

Prof. Dr. Ünal ÇAMDALI

Supervisor

Prof. Dr. Ahmet DURMAYAZ

Jury Member

Assoc. Prof. Dr. Malik M. NAUMAN

Jury Member

Prof. Dr. Fatih V. ÇELEBİ

Director

Graduate School of Natural and Applied Sciences

ETHICAL DECLARATION

I hereby declare that, in this thesis which has been prepared in accordance with the Thesis Writing Manual of Graduate School of Natural and Applied Sciences,

- All data, information and documents are obtained in the framework of academic and ethical rules,
- All information, documents and assessments are presented in accordance with scientific ethics and morals,
- All the materials that have been utilized are fully cited and referenced,
- No change has been made of the utilized materials,
- All the works presented are original,

and in any contrary case of above statements, I accept to renounce all my legal rights.

ACKNOWLEDGMENTS

Firstly, I would like to express my sincere gratitude to my supervisor, Prof. Dr. Ünal ÇAMDALI for his tremendous support and motivation during my study. His immense knowledge and precious recommendations constituted the milestones of this study. His guidance assisted me all the time of my research, and it was an incredible experience for me as I have gained lots of knowledge on CSP power plants.

I would like to thank Prof. Dr. Ahmet DURMAYAZ for his understanding and endless support. He always motivated me during my hard times and his advice helped me a lot to overcome many of my problems.

I also would like to thank Assoc. Prof. Dr. Malik Muhammed NAUMAN for his valuable contributions and constructive criticisms during my thesis defense examination.

I also would like to thank all of my friends and colleagues for their continuous support and motivation all days, during my hard times.

Finally, I must express my profound appreciations to my family especially my brother Gürkan TİRYAKİ for providing me emotional support, loving care and continuous encouragement throughout my years of study and through the period of this thesis. This accomplishment would not have been possible without them. Thank You.

2017, 13 June

Gürcan TİRYAKİ

ENERGY AND EXERGY ANALYSIS AND PERFORMANCE OPTIMIZATION OF A SOLAR POWER TOWER SYSTEM

ABSTRACT

Renewable energy is collected from resources which are naturally replenished and almost infinite in terms of human timescale. There are many forms of renewable energy which mostly depends on sunlight for producing heat and electricity. One of the methods to produce heat and electricity from solar energy is solar tower power plants. A solar tower power plant converts sunlight first to heat, then mechanical and ultimately electrical energy. The technology utilizes hundreds even thousands of sun-tracking mirrors which are called heliostats. They focus sunlight to a receiver which is usually constructed at the top of a tower. A heat transfer fluid that is the molten salt, is heated in the receiver. Then it is used to transfer its heat to the working fluid in the steam generator in order to generate steam. Finally, the steam is used in a conventional Rankine cycle to produce electricity.

In this study, a base solar power tower system with a cavity receiver with molten salt is analyzed according to *First and Second Laws of Thermodynamics* by using parameters which are taken from the literature. Then, the effects of direct normal irradiation, heliostat field area, the emissivity of the receiver, the reflectivity of the receiver, receiver tube diameter, view factor and concentration ratio on the energy and exergy efficiencies of the system, receiver surface temperature and receiver total heat loss are investigated.

Furthermore, a performance optimization of the system is carried out by modeling a *Carnot-like heat engine* of the system. For this purpose, the necessary equations are obtained by means of MATHEMATICA program. Then, these equations are solved by codes written in MATLAB program. Finally, the optimum parameters depending on max power and max power density generated by the system are obtained.

Keywords: Solar energy, concentrated solar systems, solar power tower systems, first law analysis, second law analysis, performance optimization.

BİR GÜNEŞ KULESİ SİSTEMİNİN ENERJİ VE EKSERJİ ANALİZİ VE PERFORMANS OPTİMİZASYONU

ÖZ

Yenilenebilir enerji doğal olarak yenilenen ve insan ömrü açısından neredeyse sonsuz gibi gözüken kaynaklardan elde edilir. Elektrik ve ısı enerjisi üretilen yenilenebilir enerjilerin çoğu güneş enerjisine bağlıdır. Güneş enerjisinden ısı enerjisi ve elektrik üretiminin yollarından biri de güneş enerjisi kulesi santralleridir. Güneş enerjisi kulesi santralleri, güneş ışığını önce ısıya daha sonrasında mekanik enerjiye ve son olarak da elektrik enerjisine çevirir. Söz konusu teknoloji heliostat denen güneşi takip eden yüzlerce hatta binlerce aynayı kullanmaktadır. Bu aynalar güneş ışığını genellikle bir kulenin tepesinde bulunan alıcıya yönlendirir. Alıcının içinde bulunan eriyik tuz almış olduğu ısıyı çalışma akışkanına aktararak buhar üretimini sağlar. Buhar ise Rankine çevriminde kullanılarak elektrik üretir.

Bu çalışmada taşıyıcı akışkan olarak eriyik tuz kullanan çukur alıcılı bir güneş kulesi sisteminin literatürden alınan parametreleri kullanılarak enerji ve ekserji analizi yapılmıştır. Daha sonra sistemin heliostat alanı, alıcının yayma katsayısı, alıcının yansıtma katsayısı, alıcı boru çapı, görüş faktörü ve konsantrasyon faktörünün değişiminin enerji ve ekserji verimi, alıcının yüzey sıcaklığı ve alıcının toplam ısı kaybı üzerindeki etkileri incelenmiştir.

Bu çalışmada ayrıca sistemin performans optimizasyonu da sistemin *Carnot benzeri bir makinasının* modellenmesi ile gerçekleştirilmiştir. Analiz için gerekli olan denklemler MATHEMATICA programı yardımı ile elde edilmiş ve elde edilen denklemler de MATLAB programında yazılan bir program yardımıyla çözülmüştür. Çözüm sonucunda sistemin ürettiği maksimum güç ve maksimum güç yoğunluğuna dayalı olarak optimum parametreler elde edilmiştir.

Anahtar Kelimeler: Güneş enerjisi, yoğunlaştırılmış termal güneş enerjisi santralleri, güneş enerji kule sistemleri, birinci yasa analizi, ikinci yasa analizi, performans optimizasyonu.

CONTENTS

M.Sc. THESIS EXAMINATION RESULT FORM	ii
ETHICAL DECLARATION	iii
ACKNOWLEDGMENTS	iv
ABSTRACT	v
ÖZ	vi
NOMENCLATURE	ix
LIST OF TABLES	xii
LIST OF FIGURES	xiii
CHAPTER 1 - INTRODUCTION	1
1.1 World's State of Energy	2
1.2 Solar Energy	3
1.2.1 Solar Thermal Power Systems (STPS)	3
1.2.2 Solar Power Tower Systems (SPTS)	4
1.3 Aim of the Study	7
1.4 Review of Related Works	8
CHAPTER 2 - ENERGY AND EXERGY ANALYSIS OF AN SPTS	14
2.1 Heliostat Field	15
2.2 Receiver	17
2.2.1 Energy and Exergy Balance of a Receiver	18
2.2.2 Convective Heat Loss of a Receiver	19
2.2.3 Emissive Heat Loss of a Receiver	19
2.2.4 Reflective Heat Loss of a Receiver	20
2.2.5 Conductive Heat Loss of a Receiver	20
2.3 Steam Generator	21
2.4 Conventional Power Cycle	22
CHAPTER 3 - ENERGY AND EXERGY ANALYSIS RESULTS	24
3.1 Effects of Direct Normal Irradiation (DNI)	27
3.2 Effects of the Heliostat Field Area	31
3.3 Effects of the Emissivity and Reflectivity	34
3.4 Effects of the Tube Diameter	39
3.5 Effects of the View Factor	43

3.6 Effects of the Concentration Ratio	50
CHAPTER 4 - OPTIMUM PERFORMANCE ANALYSIS OF AN SPTS WITH FINITE-RATE HEAT TRANSFER	54
CHAPTER 5 - OPTIMUM PERFORMANCE ANALYSIS RESULTS.....	63
CHAPTER 6 - DISCUSSION AND CONCLUSION.....	75
REFERENCES.....	80
APPENDICES	85
Appendix A – $\partial \bar{W} / \partial x = 0$ Performance Optimization Derivation by <i>MATHEMATICA</i>	86
Appendix B – $\partial \bar{W}_d / \partial x = 0$ Performance Optimization Derivation by <i>MATHEMATICA</i>	92
Appendix C – The Performance Optimization Codes Written in <i>MATLAB</i>	98
CURRICULUM VITAE	101

NOMENCLATURE

Roman Letter Symbols

A	Area, m^2
C	Concentration ratio
c_p	Specific heat, J/kgK
d	Diameter, m
ex	Exergy, J/kg
$\dot{E}x$	Exergy, W
F_r	View factor
h	Heat transfer coefficient, W/m^2K ; Enthalpy, J/kg
i	Irreversibility, W
k	Thermal conductivity $W/m \cdot K$
L	Thickness, m
$LMTD$	Logarithmic mean temperature difference
\dot{m}	Mass flow rate, kg/s
P	Pressure, Pa
\dot{Q}	Heat transfer, W
\bar{Q}	Non-dimensional heat transfer
q''^*	Direct normal irradiation, W/m^2
R	Ideal gas constant, kJ/kgK
\dot{S}_{gen}	Entropy generation rate, J/K
s	Entropy, J/kgK
T	Temperature, K
V	Volume, m^3
\dot{W}	Power, W
\bar{W}	Non-dimensional Work
\dot{W}_d	Power density, W
\bar{W}_d	Non-dimensional power density
x	$T_W/T_{H,i}$
y	$T_{H,o}/T_{H,i}$

Greek Letter Symbols

β	Allocation parameter
Δ	Difference
ε	Emissivity
η	Thermal efficiency
λ_{tube}	Thermal conductivity of the tube, $W/m \cdot K$
ρ	Receiver Surface Reflectivity; Density, kg/m^3
σ	Stefan-Boltzmann constant, $5,67 \times 10^{-8} W/m^2 K^4$
τ	T_L/T_{Hi}

Superscripts

*	Related to solar rays
---	-----------------------

Subscripts

0	Environment; Reference
2,3	State points of the power cycle
<i>a, b</i>	State points of the molten salt cycle
<i>abs</i>	Absorbed
<i>air</i>	Air
<i>ape</i>	Aperture
<i>avg</i>	Average
<i>c</i>	Convective
<i>c – c</i>	Convection to convection
<i>CNCA</i>	Chambadal-Novikov-Curzon-Ahlnorn
<i>cond</i>	Conductive
<i>conv</i>	Convective
<i>em</i>	Emissive
<i>ex</i>	Exit
<i>fc</i>	Forced convection
<i>H</i>	High temperature reservoir
<i>h</i>	Heliostat field
<i>I</i>	Related to energy
<i>i</i>	In
<i>II</i>	Related to exergy

<i>in</i>	Inlet
<i>insu</i>	Insulation
<i>L</i>	Low temperature reservoir
<i>loss</i>	Loss
<i>max</i>	Maximum
<i>min</i>	Minimum
<i>ms</i>	Molten salt
<i>nc</i>	Natural convection
<i>net</i>	Net
<i>o</i>	Out
<i>overall</i>	Overall system
<i>p</i>	Pump
<i>para</i>	Parasitic
<i>pc</i>	Power cycle
<i>r</i>	Radiative
<i>r – c</i>	Radiation to convection
<i>rec</i>	Receiver
<i>ref</i>	Reflective
<i>st</i>	Steam
<i>sur</i>	Surface
<i>t</i>	Turbine
<i>totloss</i>	Total loss
<i>W</i>	Warm
<i>w</i>	Receiver wall surface

Acronyms

CNCA	Chambadal-Novikov-Curzon-Ahlborn
CSP	Concentrated solar power
LFR	Linear fresnel reflectors
mp	Maximum power
mpd	Maximum power density
PTCS	Parabolic through collector system
SPTS	Solar power tower system
STPS	Solar thermal power system

LIST OF TABLES

Table 3.1 Base solar power tower system parameters.....	24
Table 3.2 Energy analysis results of the solar power tower system.....	25
Table 3.3 Exergy analysis results of the solar power tower system.....	26



LIST OF FIGURES

Figure 1.1 The schematics of energy conversion with the solar thermal power system	4
Figure 1.2 A solar power tower system	5
Figure 1.3 Basic schematic of solar power tower systems.....	5
Figure 1.4 Configurations of the heliostat field a) edge configuration (north) b) circular configuration	6
Figure 2.1 Schematic diagram of an SPTS using molten salt	14
Figure 2.2 Schematic diagram of a heliostat field.....	16
Figure 2.3 Schematic diagram of a typical cavity receiver	17
Figure 2.4 Schematic diagram of a steam generator	21
Figure 2.5 Schematic diagram of a simple Rankine cycle	22
Figure 3.1 Percentage loss of the energy and exergy of the each subsystem.....	27
Figure 3.2 Effects of the DNI on the energy and exergy efficiencies of the receiver	28
Figure 3.3 Effects of the DNI on the energy and exergy efficiencies of the overall system.....	28
Figure 3.4 Effects of the DNI on the receiver surface temperature	29
Figure 3.5 Effects of the DNI on the total heat loss of the receiver	30
Figure 3.6 Effects of the DNI on the receiver's convection, conduction, reflection and emission heat losses.....	30
Figure 3.7 Effects of the DNI on the electric production of the system	31
Figure 3.8 Effects of the heliostat field area on the energy and exergy efficiencies of receiver.....	32
Figure 3.9 Effects of the heliostat field area on the energy and exergy efficiencies of the overall system.....	32
Figure 3.10 Effects of the heliostat field area on the receiver surface temperature ..	33
Figure 3.11 Effects of the heliostat field area on the receiver total heat loss.....	33
Figure 3.12 Effects of the heliostat field area on the receiver's convection, conduction, reflection and emission heat losses	34
Figure 3.13 Effects of the emissivity on the receiver energy and exergy efficiencies	35
Figure 3.14 Effects of the reflectivity on the receiver energy and exergy efficiencies	35
Figure 3.15 Effects of the emissivity on the overall system energy and exergy efficiencies	36

Figure 3.16 Effects of the reflectivity on the overall system energy and exergy efficiencies	36
Figure 3.17 Effects of the emissivity on the receiver total heat loss.....	37
Figure 3.18 Effects of the reflectivity on the receiver total heat loss	37
Figure 3.19 Effects of emissivity on the receiver’s convection, conduction, reflection and emission heat losses.....	38
Figure 3.20 Effects of the reflectivity on the receiver’s convection, conduction, reflection and emission heat losses	39
Figure 3.21 Effects of the tube diameter on the energy and exergy efficiencies of receiver.....	40
Figure 3.22 Effects of the tube diameter on the energy and exergy overall system efficiencies	40
Figure 3.23 Effects of the tube diameter on the receiver surface temperature.....	41
Figure 3.24 Effects of the tube diameter on the receiver total heat loss	41
Figure 3.25 Effects of the tube diameter on the receiver’s convection, conduction, reflection and emission heat losses	42
Figure 3.26 Effects of the tube diameter on the concentration ratio of the system...	43
Figure 3.27 Effects of the view factor on the energy efficiencies of the receiver for the cases of aperture area dependence and receiver surface area dependence.....	44
Figure 3.28 Effects of the view factor on the energy efficiencies of the overall system for the cases of aperture area dependence and receiver surface area dependence.....	44
Figure 3.29 Effects of the view factor on the exergy efficiencies of the receiver for the cases of aperture area dependence and receiver surface area dependence.....	45
Figure 3.30 Effects of the view factor on the exergy efficiencies of the overall system for the cases of aperture area dependence and receiver surface area dependence.....	45
Figure 3.31 Effects of the view factor on the receiver surface temperature	46
Figure 3.32 Effects of the view factor on the receiver total heat loss for the cases of aperture area dependence and receiver surface area dependence	46
Figure 3.33 Effects of the view factor on the receiver conduction, convection, emission and reflection heat losses related to aperture area	47
Figure 3.34 Effects of the view factor on the receiver conduction, convection, emission and reflection heat losses related to receiver surface area	48
Figure 3.35 Percentages different type of heat losses for the cases of aperture area dependence.....	49
Figure 3.36 Percentages of different type of heat losses for the cases of receiver surface area dependence.....	49

Figure 3.37 Effects of the concentration ratio on the receiver energy and exergy efficiencies	50
Figure 3.38 Effects of the concentration ratio on the overall energy and exergy efficiencies	51
Figure 3.39 Effects of the concentration ratio of the receiver surface temperature ..	52
Figure 3.40 Effects of the concentration ratio of the receiver total heat loss.....	52
Figure 3.41 Effects of the concentration ratio of the receiver conduction, convection, emission and reflection heat losses	53
Figure 4.1 Simplified schematic diagram of an SPTS	54
Figure 4.2 T-s diagram of a simple ideal Rankine cycle.....	54
Figure 4.3 Carnot-like heat engine model.....	56
Figure 5.1 Change of x with respect to β_{c-c} for different τ and y values when $\beta_{r-c} = 0.1$	65
Figure 5.2 Change of x with respect to β_{r-c} for different τ and y values when $\beta_{c-c} = 0.1$	67
Figure 5.3 Change of η with respect to β_{c-c} for different τ and y values when $\beta_{r-c} = 0.1$	70
Figure 5.4 Change of η with respect to β_{r-c} for different τ and y values when $\beta_{c-c} = 0.1$	72
Figure 5.5 Variation of η with respect to β_{r-c} and β_{c-c} with different τ and y values at mp condition	73
Figure 5.6 Variation of η with respect to β_{r-c} and β_{c-c} with different τ and y values at mpd condition.....	74
Figure 5.7 Effect of τ on the efficiencies at $y = 0.9$ and different cases of $\beta_{r-c} = 0.1$ and $\beta_{c-c} = 0.1$ values	74

CHAPTER 1

INTRODUCTION

Mankind's need for energy is increasing with the technology improving with increasing rates in the last decades. Today, the energy we use is mostly produced from fossil fuels such as coal, petrol, natural gas etc. However, because of fossil fuels have finite energy resources which are facing with a depletion in the coming decades, and due to the rapid increase of energy consumption, mankind's need for more abundant and constant energy sources have become more important with each passing days. As a result, renewable energy sources are becoming more popular topics for governments, scientists, academicians and common people around the world.

There could be found plenty of different definition for the renewable energy but the most commonly it can be defined as energy that is produced using resources, which are naturally replenished and almost infinitely in terms of human timescale.

There are many forms of renewable energy sources such as solar energy, biogas, wind, waves, tides and geothermal heat. Most of these energy sources are directly or indirectly related to the sunlight. For example, while the amount of the wind and hydroelectric power potential are the indirect results of sunlight, solar energy is the direct conversion of sunlight using photovoltaic panels or collectors as an instrument for the process.

In this chapter, firstly a brief information of world's state of energy production and consumption is introduced. Then, solar energy and its applications especially solar thermal power systems are described. Last, the aim of this study and related works in the literature are reviewed.

1.1 World's State of Energy

Energy demand was supplied mostly by man, animal power and burning of primitive resources like wood before industrialization. Technological advances and the discovery of rich coal resources started the industrial revolution. Using coal as a fuel improved transportation sector. Steam engines, and mechanized production; all became the part of the daily life at that time. In time, with the discovery of oil finding new oil reservoirs became important and oil dependency increased with time as the technology advanced. More recently, economic growth has been dependent on natural gas. Today, these sources are mostly used to generate electricity. Electricity is the most important form of energy because of its wide variety of use and ease of distribution. Electricity demand is growing worldwide with time due to the increase in consumer electronics, industrial activities and the access to consumers in the world [1,2].

Due to the increase of the energy demand, major fossil fuel companies have been trying to find new resources of fossil fuels around the world. According to these companies, there are still new resources of oil, or new sources to be discovered yet. More accepted assumption about the oil availability of the world is that there is enough oil for 30 years for the present demand. Also, latest data for the global gas reserves show that there is roughly 50% more gas than oil, which is 60 years of present demand. Because of the gas is less explored than oil, there is a possibility to find more resources of gas. Since coal reserves are assessed to be many times more than those of oil and gas, they are expected to end after hundreds of years [1,2].

For the case of the nuclear energy, fuels used to produce electrical energy by using nuclear fission are also limited. In addition, there are political dangers due to the production of nuclear weapons by using the byproducts of the process [1,2].

In recent decades, because of the depletion of fossil fuels and the concerns about nuclear fuels, scientists, entrepreneurs and major companies start to show attention to the renewable energies. Even though there are varieties of different renewable energies, solar energy is probably the dominant energy source in this field.

1.2 Solar Energy

The sun releases energy continuously as solar radiation, supporting life on earth and driving the earth's climate and weather. The sun has a surface temperature of about 5500 K and generates its thermal energy by the nuclear fusion reaction. For the surface of the Earth, sunlight is the main source of thermal energy, which can be harnessed by natural synthetic processes [3].

Solar energy can be used in several different ways to provide people with a readily available power source. Early uses of solar energy were the utilization for common tasks such as drying clothes, curing meat and heating water. In the last decades, solar energy has been used in residential and commercial settings to power for heating and cooling systems such as furnaces, air conditioners, ventilations, HVAC and water heaters [4].

One of the methods of harnessing the solar energy to produce electricity is the use of photovoltaics fuel cells, which is a process of using solar cells to convert the solar radiation directly to electricity. Another method is solar thermal power systems (STPS) which convert the solar radiation to thermal energy before using conventional thermodynamic cycles to produce electricity.

1.2.1 Solar Thermal Power Systems (STPS)

Solar thermal power systems (concentrating solar power systems) can be defined as the systems that convert the solar radiation energy to thermal energy in order to produce electricity by using thermodynamic cycles [3,5].

Unlike the photovoltaic systems, solar thermal power systems have no complicated silicon manufacturing processes. The cost of thermal power systems is relatively lower than that of photovoltaics due to the comparably lower technology needed. However, unlike photovoltaic systems, concentrating power systems are applicable only for large-scale systems [3]. The schematics of energy conversion with the solar thermal power systems can be seen in Figure 1.1.

Some STPSs also have the thermal energy storage systems in order to be independent of temporary decrease of solar radiation by clouds, or nighttime. Due to the use of conventional thermodynamic cycles to produce electricity, these systems can easily work as a hybrid system with a fossil or biomass energy sources thus allows all time heat and electricity production. [3,5,6].

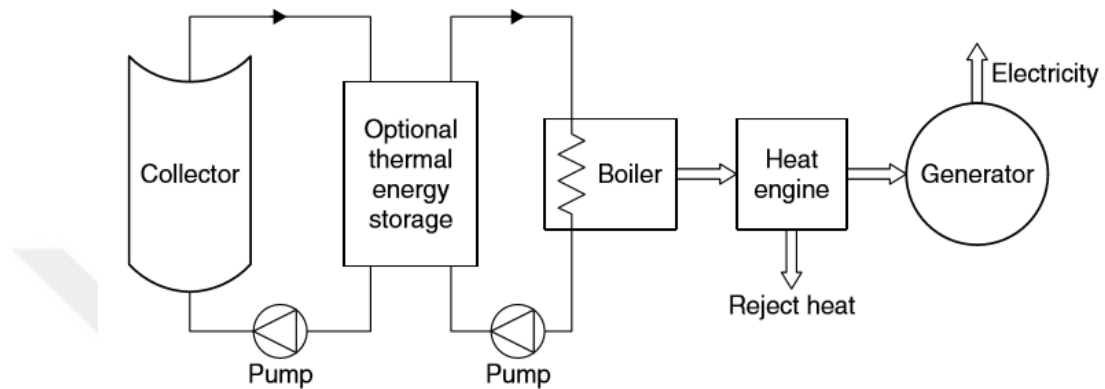


Figure 1.1 The schematics of energy conversion with the solar thermal power system [3]

There are six different main systems for solar thermal power systems under two main categories [3]. These are,

- *Low-temperature systems*
 - Solar ponds
 - Solar updraft tower
- *High-temperature systems*
 - Dish systems
 - Parabolic trough collector systems (PTCS)
 - Linear Fresnel reflectors (LFR)
 - Solar power tower systems (SPTS)

1.2.2 Solar Power Tower Systems (SPTS)

Solar power tower systems as seen in Figure 1.2 are developed in order to get over the limitations of size and power which other systems suffer. These systems contain five main components which are heliostat field, receiver, thermal storage, steam

generator and conventional power cycle. A schematic of solar power tower systems can be seen in Figure 1.3.

These systems contain mirrors, which are called heliostats. Heliostats are operated with two-axis tracking systems. They follow the sun and reflect the solar radiation to the top of the tower which is known as a receiver. An ideal position for each of these mirrors is calculated by a computer program to ensure the most efficient focus on the receiver [5,6].



Figure 1.2 A solar power tower system [7]

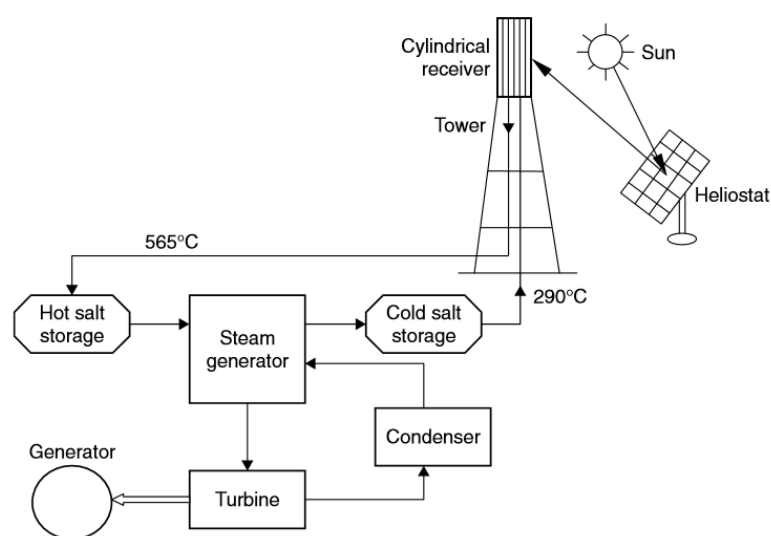


Figure 1.3 Basic schematic of solar power tower systems [3]

The configuration of the heliostats and the tower height are optimized to make the mirrors visible by the receiver depending on the latitude where the system is constructed. In latitudes greater than 35, the tower is constructed at the edge of the field of heliostats. On the other hand, in latitudes lower than 35, it is placed at a central position as seen in Figure 1.4. The type of the receiver should also be adapted to the heliostats field related to the configuration of the heliostats. While external receivers are used by the systems that have a central configuration, cavity receivers are used that have a lateral configuration [5,6,8].

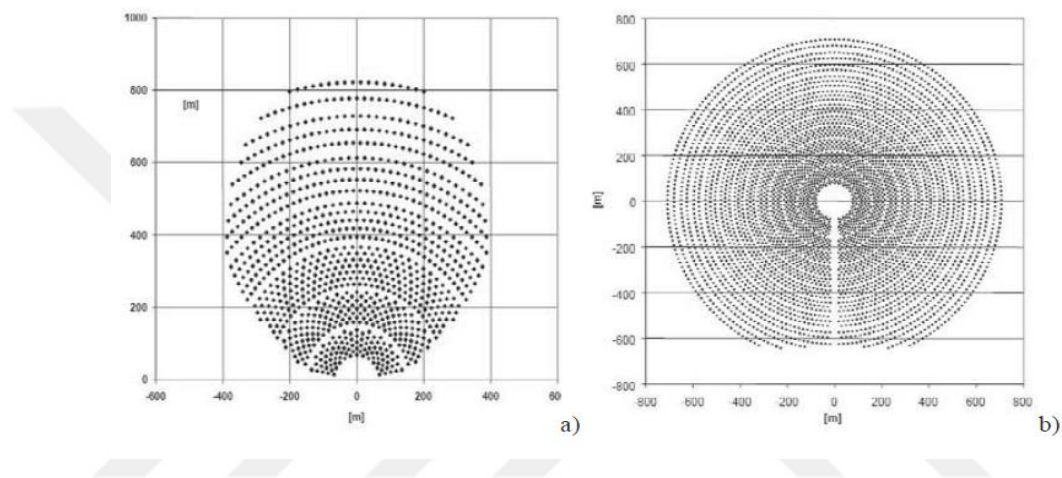


Figure 1.4 Configurations of the heliostat field a) edge configuration (north) b) circular configuration [5]

The heliostat effectiveness in concentrating solar radiation depends on the sun's location. Concentration factor of tower systems are usually greater than 500 and reaches high temperatures making them a perfect candidate as a heat source of the thermodynamic cycles. As the transfer fluid, hot air or molten salt are used to transfer heat from the receiver to a steam generator. The steam produced by the steam generator drives a turbine to produce electricity [5,6,9].

To keep the power plant operational for a certain time at constant power, usually, a thermal storage unit is integrated into the system. It is used to store energy in times of high irradiation, so the system can continue to work at cloudy weather and night [4].

In these systems, Rankine or Brayton cycles can be used for power generation. However, using Rankine cycle allows the use of smaller receivers and high energy densities due to the high heat transfer coefficient [3].

In solar power tower systems, the collectors represent the largest cost in the systems. Therefore, to obtain the maximum conversion of the solar energy, an efficient engine is required. So, the solar tower power plants can be established as quite large systems with the optimum size of 50–400 MW in order to minimize cost [3,9]. Taggart declared that solar power tower systems could generate electricity at 0.04 US\$/kWh by 2020 [10].

1.3 Aim of the Study

In the last decades, renewable energy became more popular due to the limited resources of common fuels and the environmental problems caused by them. Among the many different renewable energy sources, solar energy is probably taking the most of the credits.

One of the methods of harnessing the sun's energy to produce electricity is using solar thermal power systems (STPS). These systems convert the solar radiation energy to heat to produce electricity by using conventional thermodynamic cycles such as *Rankine cycle*. Solar power tower systems (SPTS) are the more popular ones due to their greater capacity to produce electricity and working at night.

In this study, the main purpose is to theoretically examine the SPTSs thermodynamically using the first and second laws of thermodynamics. SPTSs can be divided into five main components which are the heliostat field, receiver, heat storage, steam generator and power cycle. Each component of the system has its own challenges and characteristics depending on the types used in the system.

The initial parameters of SPTS are taken from the various studies in the literature. So, there is a possibility of comparison between the literature and this study. After obtaining results matching with the literature satisfactorily, various parameters are changed in reasonable ranges to analyze the system.

Another purpose of this study is to achieve a performance optimization of the SPTS. To achieve this goal a *Carnot-like heat engine* of SPTS is modeled and the necessary mathematical formulas are derived. Then, in order to remove dimensions of the system, non-dimensional parameters of the system are defined. Finally, a program in MATLAB is written to achieve the optimization of the SPTS.

1.4 Review of Related Works

In the literature, many different studies were found for solar systems carried out by different researchers around the world. In this section, summaries about some of these studies are presented to the readers to better understand the solar concentrating systems

Xu et al. [9] presented a model for the SPTS with molten salt by considering the first and second laws analysis. In this study, several different power cycles are designed and analyzed. As a result of this study, It is found that even though the maximum energy loss occurs in the power cycle system, the maximum exergy loss occurs in the receiver system and the heliostat field system, respectively.

Fernandez and Miller [11] performed a design optimization for a 5 MW_{th}, *small particle heat exchange receiver*, which is a high-temperature central receiver designed to drive a Bryton cycle or combined-cycle for the concentrated solar power plant. In this study, optimization for the various parts of the receiver, which consists of wall properties, window geometry and receiver geometry, is carried out. As a result of this optimization, it is declared that the receiver efficiency is increased by 6% for the proposed system.

Atace and Ameri [12] modeled all-glass evacuated solar collector tubes with the coaxial fluid conduit. In this study, the effect of changing various parameters of working fluid and the properties of the delivery tube and absorber tube is investigated. As a result of this study, when working fluid is carbon dioxide or air, the H-type model is superior to the T-type model in terms of the outlet flow temperature and exergy efficiency, is emphasized.

McGovern and Smith [13] investigated the effects of the receiver temperature and Rankine-cycle efficiency with a change of various parameters for solar through (parabolic trough collector systems) and solar-tower with direct-steam and molten salts. As a result of this study, it is suggested to use *sub-critical Rankine cycles* for solar through plants and *supercritical Rankine cycles* for solar tower power plants, with molten salts as a transfer fluid.

Ranjan and Kaushik [14] investigated academic literature about the energy, exergy and thermo-economic analysis for solar distillation systems. The investigation touched upon the significance of the many key points for the systems. As a result, it is concluded that energy and exergy efficiencies of the systems have increased reasonably by the use of integrated solar stills with better efficiencies.

Arora et al. [15] studied the thermo-economic optimization of solar parabolic dish driven *Stirling heat engine*. This study is analyzed the optimal values of different decision variables of the system using MATLAB-Simulink. At the end of the study, it is suggested that the proposed algorithm could be used while designing a real *Stirling heat engine*.

Zhao et al. [16] studied the optimization of the solar multiple for the solar-coal hybrid system. In this study, three different power plants with different parameters are considered. As a result of this study, the levelized cost of energy is found for certain solar multiple values within the considered range.

Calise et al. [17] studied the optimal thermoeconomical configuration of solar heating and cooling systems (SHC). In the study, analysis for three different SHC configurations of a building is made by developing a zero-dimensional transient simulation model in TRNSYS. Also, a cost model for each plant layout is developed. As a result, it is found the best SCH system can be achieved by selecting the suitable solar collector area and the volume of the storage tank in terms of economic profitability.

Silva et al. [18] studied the thermo-economic design optimization of a PTCS for industrial processes with memetic algorithms. In the study, the influence on optimal

design point location by comparing life cycle savings, levelized cost of energy, and payback time functions is studied. As a result of this study, it is found that while the short-term payback time criteria show the small plants with high solar field efficiency and small solar fractions are more favorable. However, in the case of the long-term criteria, the reverse conclusions are more favorable.

Zhu et al. [19] studied the heat transfer characteristics of a coil type solar dish receiver. This study is made under actual concentrate solar radiation conditions experimentally. The data, which are taken from the structure, are analyzed using the first and second laws of thermodynamics methods. As a result, the data of solar radiation, the efficiency of the solar receiver, heat loss, the impact of the exergy factor, energy and exergy efficiencies are evaluated.

Gholampour and Ameri [20] fabricated and tested a prototype PV/thermal flat transpired collector. A mathematical model by using correlations for Nusselt numbers, PV panel and transpired plate which were obtained by using CFD technique is developed. As a result, optimum values for suction velocity and PV coverage percent under different conditions are found.

Spelling et al. [21] developed a dynamic model of a pure-solar combined-cycle power plant in order to determine the thermodynamic and economic performance of the plant for different superstructure layouts and operating conditions. As a result, It is declared that the proposed system can compete with current solar thermal technology when the initial investment is big enough.

Tempesti and Fiaschi [22] analyzed a micro-combined heat power plant operating through an Organic Rankine Cycle (ORC) using geothermal and solar energy. In the analysis, different working fluids (e.g. R134a, R236fa, R245fa) are considered and the system is sized by considering the weather data from the center of Italy for different months. As a result of this analyze, it is shown that R245fa allows the lowest cost of electricity production and the lowest overall cost of the CHP plant.

Petela [23] studied the exergy of thermal radiation. In this study, formulas for the computation of exergy of thermal radiation are derived. Furthermore, some numerical examples by using the derived formulas are given.

Al-Sulaiman and Atif [24] compared five types Brayton cycles which operate by using supercritical carbon dioxide for a solar power tower system. At the end of the study, it is found that recompression Brayton cycle has the highest thermal efficiency and the highest net power output.

Carrizosa et al. [25] studied the optimization of a solar power tower system that has multiple receivers. In this study, the receiver and the heliostat field layout are optimized in order to minimize the levelized cost of thermal energy. As a result of this study, the number of heliostats and their locations of the aiming regions could be obtained with the proposed procedure.

Sogut and Durmayaz [26] performed an optimum performance analysis of a solar driven heat engine of a PTCS with direct-steam-generation (DSG) system for the maximum power (mp) and the maximum power density (mpd) conditions. As a result of this study, a discussion on the effect of heat transfer mechanisms is presented.

Li et al. [27] developed a design of a thermal model of a cavity receiver with a molten salt for steady-state conditions. As a result of this study, necessary parameters are found which satisfy the requirements defined by the authors.

Kalogirou et al. [28] presented a review of exergy analysis for solar thermal systems. In the review the analysis of different solar collectors, solar thermal system applications and processes are investigated.

Wang et al. [29] proposed an integrated simulation approach to simulate solar radiation transfer for a solar power tower system with a cavity receiver. As a result, it is found that reflection loss and homogenization of energy distribution on internal surfaces can be greatly reduced by the cavity effect.

N'Tsoukpoe et al. [30] designed a micro-central tower power plant of 10 kWe for Sahelian countries. The system is designed to make locally possible the

manufacturing of most of the components. In this study, the challenges faced during the design process is also reported. Finally, it is proposed that CSP technology could be offered as a potential of power generation in rural areas in Africa where the electrification rate remains very low.

Zheng et al. [31] presented an ideal model of the SPTS. This study investigated the effects of different parameters on the thermal and exergy conversion efficiencies. As a result, it is found that raising the receiver working temperature, increased the thermal and exergy conversion efficiencies until an optimum temperature value.

Luo et al. [32] proposed a novel dual-receiver with a heliostat field in order to increase the efficiency of a solar power tower system. As a result, it is found that the proposed design could improve the thermal efficiency dramatically.

Desai and Bandyopadhyay [33] studied the thermo-economic comparisons of organic/steam Rankine cycles using parabolic through collectors and linear *Fresnel* reflector. This study presented a selection methodology which is based on thermo-economic analysis and a comparison diagram for working fluids. According to the authors by using the selection methodology, any collector technology and any power generating need can be compared. As a result of this study, simulation results show that R-113 was achieved the lowest levelized cost of energy (0.344 \$/kWh) and toluene based organic Rankine cycle was achieved the highest cycle efficiency (31.2%).

Okoroigwe and Madhlopa [34] investigated progress in the development of *a solar tower-integrated solar combined cycle systems*. In this study, the thermodynamic and economic performances of *the solar tower integrated solar combined cycle systems* also reviewed. As a result of this study, it is found that solar tower technology has great potential for integration with *the integrated solar combined cycle system* from the view point of thermodynamic and economic perspectives.

Faille et al. [35] studied the development of a control model design for a 1 MW solar tower system with a thermal storage. The designed model successfully validated by closed loop simulations in Matlab/Simulink.

Desai et al. [36] proposed a methodology to thermodynamically determine the cost optimum design radiation for CSP plants without hybridization and storage. In this study, the usability of this methodology is demonstrated by using the case studies incorporating PTCS as well as LFR. As a result of this study, it is declared that design radiation obtained through proposed methodology is very close to that obtained with detailed multiple simulations.

Han et al. [37] studied the performance enhancement of a solar trough power plant by integrating tower collectors. As a result of this study, simulation results are showed the thermal efficiency of the integrating system can reach higher percentage points compared with that of the individual trough power plants. It is suggested the study could provide a new approach for utilizing solar energy more efficiently and more economically.

Kalogirou [38] studied the solar thermal collectors and its applications showing the various types of solar thermal collectors and applications. It is also presented typical applications of the various types of collectors such as solar water heating, space heating and cooling, refrigeration, industrial process heat and thermal power systems.

Yao et al. [39] achieved the modeling and simulation of 1 MW solar thermal central receiver system under construction nearby Beijing in China. In this study, a software tool called HFLD is developed in order to carry out the heliostat field layout design and performance calculations.

Liu et al. [40] proposed a novel parabolic trough solar power system with a dual-solar field with oil and molten salt. In this study, energy and exergy analysis is implemented in order to evaluate the feasibility of the proposed system.

Behar et al. [41] reviewed some studies achieved for the major components of SPTS such as the heliostat field, the solar receiver, and the power conversion system.

Bejan et al. [42] studied the second law analysis for solar collector systems. In this study, the optimum working conditions for maximum exergy delivery are derived by using sample examples.

CHAPTER 2

ENERGY AND EXERGY ANALYSIS OF AN SPTS

Energy and exergy analysis of STPS is performed at steady state conditions. Therefore, there is no need to consider the thermal storage of the system. Without the thermal storage, the whole system can be considered to have four main parts that are heliostat field, receiver, steam generator and the conventional power cycle. In this study, as a power cycle, the basic ideal Rankine cycle is used [9]. A schematic of an SPTS can be seen in Figure 2.1.

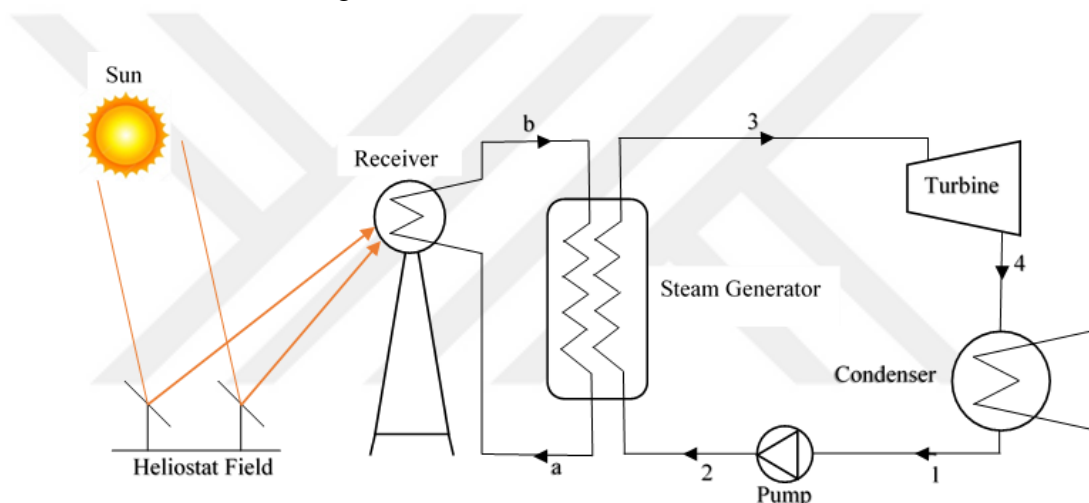


Figure 2.1 Schematic diagram of an SPTS using molten salt

When the sunlight falls on the heliostat field where hundreds even thousands of mirrors or reflective metal plates with double axis tracking equipment to track the sun for higher efficiency, it is reflected the to a receiver at the top of a tower to raise its temperature. Concentrated power of the heliostat field enables the receiver to reach the higher temperatures, thus keeping the molten salt in liquid state which is flowing inside the tubes that buried inside the receiver. The heat carried by the molten salt is transferred to the water at the steam generator to produce steam. Then, steam circulated in the Rankine cycle is used to produce first mechanical work and then electricity [9].

In this study, energy and exergy analysis of the system can be made for each part and then, by putting together the results of all of the parts. Since each part is considered separately, this analysis can be made by using energy and exergy balance for a selected control volume. For this analysis, some assumptions are made. These are;

1. The system is working at the steady-state conditions
2. The system has constant solar irradiation
3. Pressure drops in pipe installations are neglected
4. Heat loss in pipe installations are neglected
5. The changes in potential and kinetic energies are ignored through all the system
6. The changes in chemical exergies of the system's materials are neglected
7. Parasitic efficiency (η_{para}) of the system is 88% [9]
8. The thermal efficiency of the *Rankine cycle* is assumed to be independent of the power output of the turbine.

The rate of total energy and exergy balance for a control volume for the steady-state processes can be expressed as

$$\dot{W} = \sum_j \dot{Q}_j + \sum_{in} \dot{m}_{in} h_{in} - \sum_{out} \dot{m}_{out} h_{out} \quad (2.1)$$

$$\dot{W} = \sum_j \left(1 - \frac{T_0}{T_j}\right) \dot{Q}_j + \sum_{in} \dot{m}_{in} ex_{in} - \sum_{out} \dot{m}_{out} ex_{out} - T_0 \dot{S}_{gen} \quad (2.2)$$

where $T_0 \dot{S}_{gen}$ denotes the rate of exergy destruction because of the entropy generation which is equal to the rate of irreversibility $I\dot{R}$.

The rate of total exergy at each station can be expressed as

$$\dot{Ex} = \dot{m} ex = \dot{m}[(h - h_0) - T_0(s - s_0)] \quad (2.3)$$

2.1 Heliostat Field

Heliostat field has an aperture area of A_h , which concentrates the sun light to the cavity receiver by means of reflecting it and can be seen in Figure 2.2.

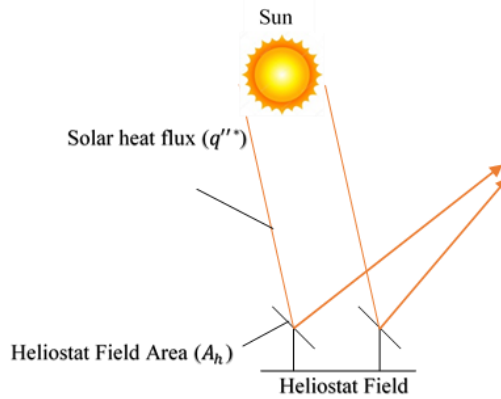


Figure 2.2 Schematic diagram of a heliostat field

The rate of total irradiation by the incident solar radiation can be given as

$$\dot{Q}^* = A_h q''^* \quad (2.4)$$

Where q''^* defined as the solar heat flux which is treated as the rate of direct normal irradiation (DNI) per unit area. Even though DNI changes depending on the geographical position on the earth, the meteorological conditions and the duration of a day, in this study, all of them are assumed to be constant.

A fraction of the \dot{Q}^* is transferred to the receiver as the rate of solar irradiation \dot{Q}_{rec}^* via heliostat field. The remaining of \dot{Q}^* which is called \dot{Q}_0^* is lost to the surroundings because of various parameters such as cosine efficiency, blocking, shading, reflectivity, tracking error, etc. [9].

The rate of total energy and exergy balance of the heliostat field can be expressed as

$$\dot{Q}^* = \dot{Q}_{rec}^* + \dot{Q}_0^* \quad (2.5)$$

$$\dot{E}x^* = \dot{E}x_{rec}^* + \dot{E}x_0^* \quad (2.6)$$

where $\dot{E}x_{rec}^*$ is the delivered exergy of the receiver and $\dot{E}x_0^*$ is the exergy loss due to heat loss.

$\dot{E}x^*$ can also be expressed as

$$\dot{E}x^* = \dot{Q}^* \left(1 - \frac{T_0}{T^*}\right) \quad (2.7)$$

T^* is the apparent temperature of the sun as an exergy source which is showed by Petela and calculated by Bejan as around 4500 K [23,42]

The exergy delivered to the receiver can be expressed as

$$\dot{E}x_{rec}^* = \dot{Q}_{rec}^* \left(1 - \frac{T_0}{T^*}\right) \quad (2.8)$$

It is assumed receiver subsystem receives 75 percentages of the total energy and exergies coming to the heliostat field.

2.2 Receiver

The receiver is an essential part of the solar power tower systems. It absorbs radiation energy and converts it into thermal energy by using molten salt (a mixture of wt% 60 NaNO_3 +wt%40 KNO_3) [27]. Receivers of the solar power tower systems have various shapes like cavity receiver or cylindrical receivers. In this study, calculations are made only for cavity receivers which are the most common ones. A cavity receiver's schematic diagram is shown in Figure 2.3.

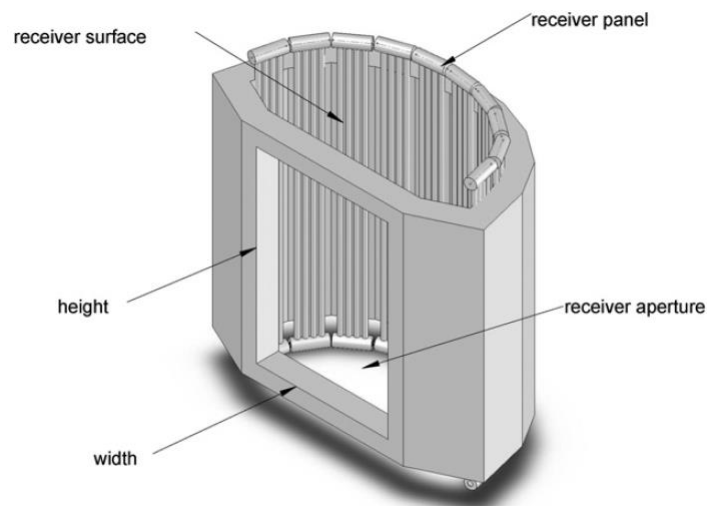


Figure 2.3 Schematic diagram of a typical cavity receiver [27]

2.2.1 Energy and Exergy Balance of a Receiver

The rate of energy and exergy balance for the receiver can be expressed as

$$\dot{Q}_{rec}^* = \dot{Q}_{rec,abs} + \dot{Q}_{rec,totloss} = \dot{m}_{ms}(h_{ms,b} - h_{ms,a}) + \dot{Q}_{rec,totloss} \quad (2.9)$$

$$\dot{E}x_{rec}^* = \dot{E}x_{rec,abs} + \dot{E}x_{rec,loss}^* + \dot{I}_{rec}^* \quad (2.10)$$

In the heat transfer process, some of the energy is lost to the surroundings due to convective, emissive, reflective and conductive heat losses [9,27]

$$\dot{Q}_{rec,totloss} = \dot{Q}_{rec,conv} + \dot{Q}_{rec,em} + \dot{Q}_{rec,ref} + \dot{Q}_{rec,cond} \quad (2.11)$$

$$\eta_{I,rec} = \frac{\dot{Q}_{rec,abs}}{\dot{Q}_{rec}^*} \quad (2.12)$$

$\dot{E}x_{rec,loss}^*$ can also be expressed as

$$\dot{E}x_{rec,loss}^* = \dot{Q}_{rec,totloss} \left(1 - \frac{T_0}{T_{rec,sur}} \right) \quad (2.13)$$

The rate of change of total stream exergy of the working fluid (molten salt) through the receiver can be shown as

$$\begin{aligned} \dot{E}x_{rec,abs} &= \dot{m}_{ms} [(h_{ms,b} - h_{ms,a}) - T_0 (s_{ms,b} - s_{ms,a})] \\ &= \dot{m}_{ms} C_{pms,avg} \left[T_{ms,b} - T_{ms,a} - T_0 \ln \left(\frac{T_{ms,b}}{T_{ms,a}} \right) \right] \end{aligned} \quad (2.14)$$

\dot{I}_{rec}^* can be expressed as

$$\dot{I}_{rec}^* = \dot{m}_{ms} T_0 (s_{ms,b} - s_{ms,a}) \quad (2.15)$$

When \dot{Q}_{rec}^* is known, the receiver surface temperature could be determined using an iteration method presented by [27].

Receiver's exergy efficiency can be expressed as

$$\eta_{II,rec} = \frac{\dot{E}x_{rec,abs}}{\dot{E}x_{rec}^*} \quad (2.16)$$

Receiver surface temperature can be defined as

$$\frac{\dot{Q}_{rec}^*}{\frac{A_h}{F_r C}} = \frac{T_{rec,sur} - T_{ms}}{\frac{d_o}{d_i h_{ms}} + \frac{d_o \ln\left(\frac{d_o}{d_i}\right)}{2\lambda_{tube}}} \quad (2.17)$$

where d_o and d_i are the outer and inner diameters of the tubes buried inside the receiver respectively, and λ_{tube} is the conductivity of the tubes.

2.2.2 Convective Heat Loss of a Receiver

Convective heat loss from the cavity receivers occurs as natural and forced convection at the same time due to its design. Due to the height of the tower, forced convection affects the receiver via wind force. Furthermore inside the receiver air almost has no movement thus creating an environment feasible for natural convection. The convective heat loss from the receiver can be found as

$$\dot{Q}_{rec,conv} = \left[h_{air,fc}(T_{rec,sur} - T_0) + \frac{h_{air,nc}(T_{rec,sur} - T_0)}{F_r} \right] \frac{A_h}{C} \quad (2.18)$$

F_r and C refers to view factor and concentration ratio, respectively and shown as

$$C = \frac{A_h}{A_{ape}} \quad (2.19)$$

$$F_r = \frac{A_{ape}}{A_{rec,sur}} \quad (2.20)$$

where A_{ape} is the aperture area of the receiver and $A_{rec,sur}$ is the area of the receiver surface. Therefore, convective heat loss from the receiver can also be written as

$$\dot{Q}_{rec,conv} = A_{ape} h_{air,fc}(T_{rec,sur} - T_0) + A_{rec,sur} h_{air,nc}(T_{rec,sur} - T_0) \quad (2.21)$$

2.2.3 Emissive Heat Loss of a Receiver

Emissive heat loss which occurs at the cavity receiver is affected by the change of the temperature of different parts of the receiver as well as the emissivity of their

surfaces. However, by calculating the average receiver surface temperature, the assumption having no heat transfer between different parts of the receiver can be made. Therefore, emissive heat loss can be defined as

$$\dot{Q}_{rec,em} = \varepsilon_{avg} \sigma (T_{rec,sur}^4 - T_0^4) \frac{A_h}{C} \quad (2.22)$$

Formula of ε_{avg} is taken from [27] and can be written as

$$\varepsilon_{avg} = \frac{\varepsilon_w}{\varepsilon_w + (1 - \varepsilon_w) F_r} \quad (2.23)$$

ε_{avg} and ε_w denote the average and surface emissivity of the receiver, respectively.

2.2.4 Reflective Heat Loss of a Receiver

For complex simulations of the receiver, Monte-Carlo ray tracing technique is used by considering emissive and reflective heat loss together [44]. In this study assumes that there is no change of reflectivity with the change of surface temperature is made. Therefore, reflective heat loss associated only with the surface reflectivity and the view factor and can be written as

$$\dot{Q}_{rec,ref} = \dot{Q}_{rec}^* F_r \rho \quad (2.24)$$

where ρ is the reflectivity of the receiver.

2.2.5 Conductive Heat Loss of a Receiver

In cavity receivers, conductive heat loss can be considered in three types which are insulation layer, support structure, and conduction of air between the insulation and receiver panel. However, conduction heat loss occurs from the receiver panel and air between the insulation and receiver panel are too small therefore can be neglected [27]. Conduction heat loss from the insulation is shown as

$$\dot{Q}_{rec,cond} = \frac{(T_{rec,sur} - T_0) A_h}{\left(\frac{L_{insu}}{k_{insu}} + \frac{1}{h_{air,nc} + h_{air,fc}} \right) F_r C} \quad (2.25)$$

where L_{insu} and k_{insu} are the thickness and the conduction coefficient of the insulation, respectively.

2.3 Steam Generator

The steam generator is a part where heat transfer fluid (molten salt) transfers its heat to the working fluid (water) through series of heat exchangers to produce steam for electricity generation and can be seen in Figure 2.4.

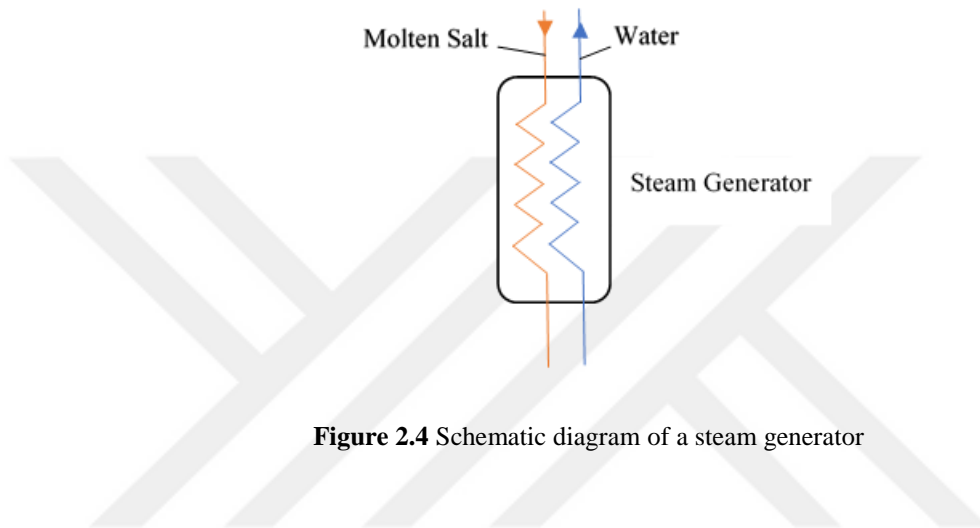


Figure 2.4 Schematic diagram of a steam generator

In this study, it is assumed that steam generator is well insulated and heat loss to the surrounding is negligible.

The thermophysical properties of the molten salt obtained by [9] can be determined as

$$\rho_{ms} = 2090 - 0.636T(^{\circ}\text{C}) \quad (2.26)$$

$$C_{p,ms} = 1443 + 0.172T(^{\circ}\text{C}) \quad (2.27)$$

$$k = 0.443 + 1.9 \times 10^{-4}T(^{\circ}\text{C}) \quad (2.28)$$

The rate of total energy and exergy balance for the steam generator can be expressed as

$$\dot{Q}_{rec,abs} = \dot{m}_{ms}(h_{ms,b} - h_{ms,a}) = \dot{Q}_{st,abs} = \dot{m}_{st}(h_{st,3} - h_{st,2}) \quad (2.29)$$

$$\dot{E}x_{rec,abs} = \dot{E}x_{st,abs} + \dot{I}_{sgs} \quad (2.30)$$

Exergy which is absorbed by the working fluid (water) can be expressed by using enthalpies and entropies of the working fluid as

$$\dot{E}x_{st,abs} = \dot{m}_{st}[(h_{st,3} - h_{st,2}) - T_0(s_{st,3} - s_{st,2})] \quad (2.31)$$

The energy and exergy efficiencies of the steam generator can be defined as

$$\eta_{I,sgs} = \frac{\dot{Q}_{st,abs}}{\dot{Q}_{rec,abs}} \quad (2.32)$$

$$\eta_{II,sgs} = \frac{\dot{E}x_{st,abs}}{\dot{E}x_{rec,abs}} \quad (2.33)$$

2.4 Conventional Power Cycle

The power cycles used in the SPTSs are usually Rankine cycles. These cycles use water as their working fluid and consist of a steam generator, turbine usually with high and low pressure stages, condensers, feed water heaters (open and closed) and pumps. In this study, only simple Rankine cycle which can be seen in Figure 2.5 is considered.

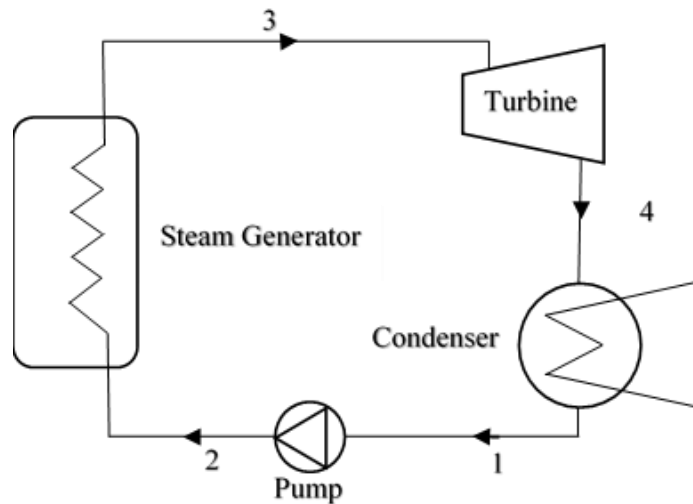


Figure 2.5 Schematic diagram of a simple Rankine cycle

Energy and exergy balance for the power cycle can be expressed as

$$\dot{Q}_{st,abs} = \dot{W}_{net} + \dot{Q}_{ps,totloss} \quad (2.34)$$

$$\dot{E}x_{st,abs} = \dot{W}_{net} + \dot{E}x_{ps,totloss} + \dot{I}_{pc} \quad (2.35)$$

The net power output of the power cycle can be expressed as

$$\dot{W}_{net} = \dot{W}_t - \dot{W}_p \quad (2.36)$$

and the energy and exergy efficiencies of the steam generator can be written as

$$\eta_{I,pc} = \dot{W}_{net} / \dot{Q}_{st,abs} \quad (2.37)$$

$$\eta_{II,pc} = \dot{W}_{net} / \dot{E}x_{st,abs} \quad (2.38)$$

As a result, the overall energy and exergy efficiencies can be defined as

$$\eta_{I,overall} = \frac{\dot{W}_{net} \eta_{para}}{\dot{Q}^*} \quad (2.39)$$

$$\eta_{II,overall} = \frac{\dot{W}_{net} \eta_{para}}{\dot{E}x^*} \quad (2.40)$$

where η_{para} , is defined as the parasitic efficiency of the system and taken 88% [9].

CHAPTER 3

ENERGY AND EXERGY ANALYSIS RESULTS

Base system parameters used in the analysis is taken from literature and can be seen in Table 3.1.

Table 3.1 Base solar power tower system parameters [9,24,45-48]

Subsystem	Properties	Value	Unit
Heliostat Field	Radiation (DNI) (<i>For Çubuk sub-province</i>)	375	W/m^2
	Overall Field Reflectivity	75	%
	Number of Heliostats	360	–
	Heliostat Height	9.75	m
	Heliostat Width	12.3	m
	Fraction of Mirror Area of Heliostat	0.9642	–
Receiver	Molten Salt's Inlet Temperature	290	$^{\circ}C$
	Molten Salt's Outlet Temperature	565	$^{\circ}C$
	View Factor	0.8	–
	Tube Diameter	0.019	m
	Tube Thickness	0.00165	m
	Passes	14	–
	Surface Emissivity	0.85	–
	Reflectivity	0.04	–
	Wind Velocity	5	m/s
	Stefan-Boltzmann Constant	5.67×10^{-8}	$m^2 K^4$

Table 3.1 (Continued) Base solar power tower system parameters [9,24,45-48]

Subsystem	Properties	Value	Unit
Receiver	Thickness of Insulation Layer	0.07	<i>m</i>
	Height of Receiver	6	<i>m</i>
	Area of Receiver	21.2	<i>m</i> ²
	Conductivity of the Tube	19.7	<i>W/m · K</i>
Steam Generator	Water's Inlet Temperature	46.3	°C
	Water's Outlet Temperature	552	°C
	Surrounding Temperature	25	°C
Power Generation Cycle	Pressure at the SGS	12600	<i>kPa</i>
	Pressure at the Condenser	10	<i>kPa</i>

The base system results of energy and exergy analysis can be seen in Table 3.2 and Table 3.3. According to the results obtained from the analysis, while energy efficiency of the overall system is found 24.69%, exergy efficiency of the overall system is found 26.44%.

Table 3.2 Energy analysis results of the solar power tower system

Subsystem	Energy Analysis			
	Received (kW)	Delivered (kW)	Loss (kW)	Efficiency (%)
Heliostat Field	15610.28	11707.71	3902.57	-
Receiver	11707.71	10487.04	1220.67	89.57
Steam Generator	10487.04	10487.04	0.00	100.00
Power Generation Cycle	10487.04	4379.42	6107.62	41.76
Overall System	15610.28	3853.89	11756.39	24.69

The energy efficiencies of the system are 75%, 89.57%, 100% and 41.76% for heliostat field subsystem, receiver subsystem, SGS subsystem and power generation subsystem, respectively. Biggest energy loss of the system is 6107.62 kW, which is occurred at the power generation subsystem. This is due to the use of basic Rankine cycle that, can be improved by the use of the reheat, open feedwater, closed feedwater processes or implementing supercritical Rankine cycle.

The exergy efficiencies of the system are 75%, 52.43%, 83.38% and 91.63% for heliostat field subsystem, receiver subsystem, SGS subsystem and power generation subsystem respectively. Even though the greatest energy loss occurs at the power generation subsystem, biggest exergy loss of the system can be seen at the receiver subsystem with a loss of 5200.17 kW.

Table 3.3 Exergy analysis results of the solar power tower system

Subsystem	Exergy Analysis			
	Received (kW)	Delivered (kW)	Loss+Destroyed (kW)	Efficiency (%)
Heliostat Field	14576.53	10932.40	3644.13	-
Receiver	10932.40	5732.23	5200.17	52.43
Steam Generator	5732.23	4779.63	952.60	83.38
Power Generation Cycle	4779.63	4379.42	400.21	91.63
Overall System	14576.53	3853.89	10722.64	26.44

Energy percentage losses and exergy percentage losses and destroyed, of the each subsystem can be seen in Figure 3.1. As seen even though the main energy loss occurred at the power generation subsystem, only the 3.73% of the exergy loss can be seen. Furthermore, while the receiver energy loss is as small as 10.38%, exergy loss at the receiver subsystem is 48.50% which is the highest among the subsystems. That distinct behavior is caused by the quality of the energy used in the subsystem. Since the solar irradiation has very high quality, which is converted to the thermal

energy, it contains lots of exergies. On the other hand, even though the power generation has the biggest energy loss due to the low quality energy, exergy loss is very little compared to the energy loss. Therefore even though receiver subsystem's energy loss is less compared to the power generation subsystem, exergy loss is much greater in receiver subsystem.

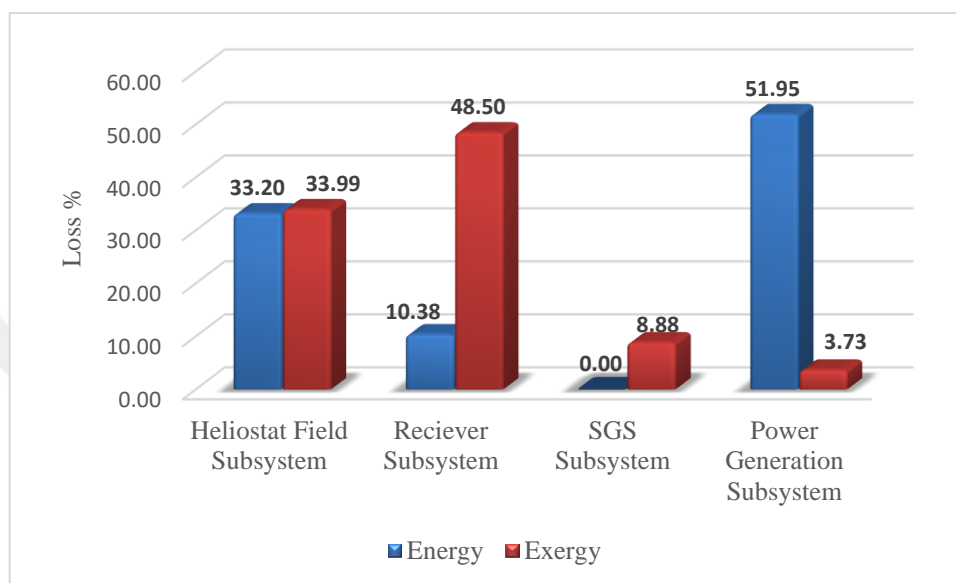


Figure 3.1 Percentage loss of the energy and exergy of the each subsystem

3.1 Effects of Direct Normal Irradiation (DNI)

Since the source of energy is the sun itself, the place where a solar tower power plant constructed is very important. In Figure 3.2, effects of the direct solar irradiation (DNI) on the energy and exergy efficiencies of the receiver can be seen. Also, effects of the DNI on the energy and exergy efficiencies of the overall system is shown in Figure 3.3. As seen from the figures, at the solar irradiation at 200 W/m^2 , energy efficiencies of the receiver and the system are 68.89% and 18.99%, respectively. When solar irradiation increased to 2000 W/m^2 , efficiencies are increased up to the 89.99% and 24.80%, respectively. Similarly, while the exergy efficiencies of the receiver and the overall system at the solar irradiation of 200 W/m^2 , are 40.32 % and 20.33%, respectively, at the solar irradiation of 2000 W/m^2 , efficiencies are increased up to 52.68% and 26.56%, respectively. Although the increase occurs at both energy

and exergy efficiencies as long as DNI increased, the rate of increase is diminished with the increase of DNI.

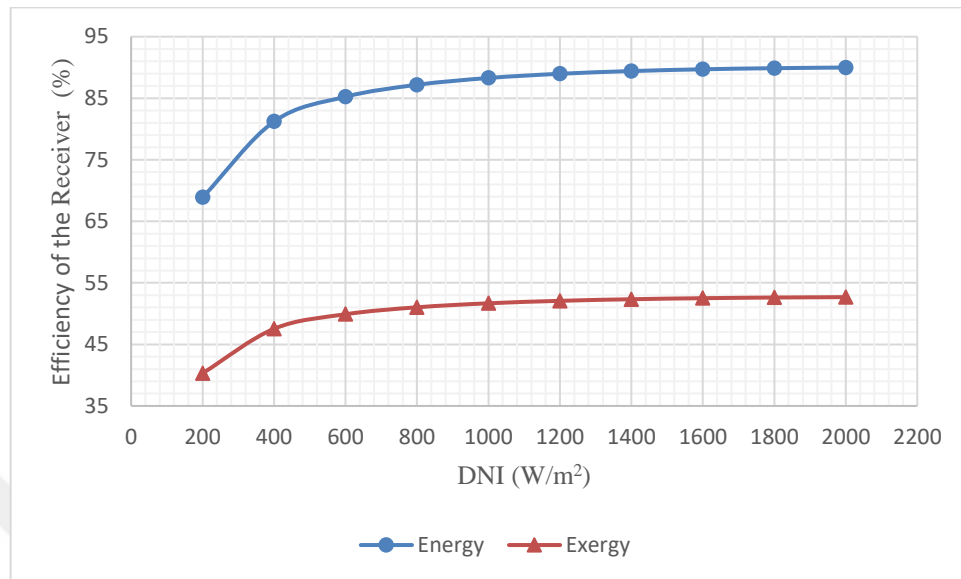


Figure 3.2 Effects of the DNI on the energy and exergy efficiencies of the receiver

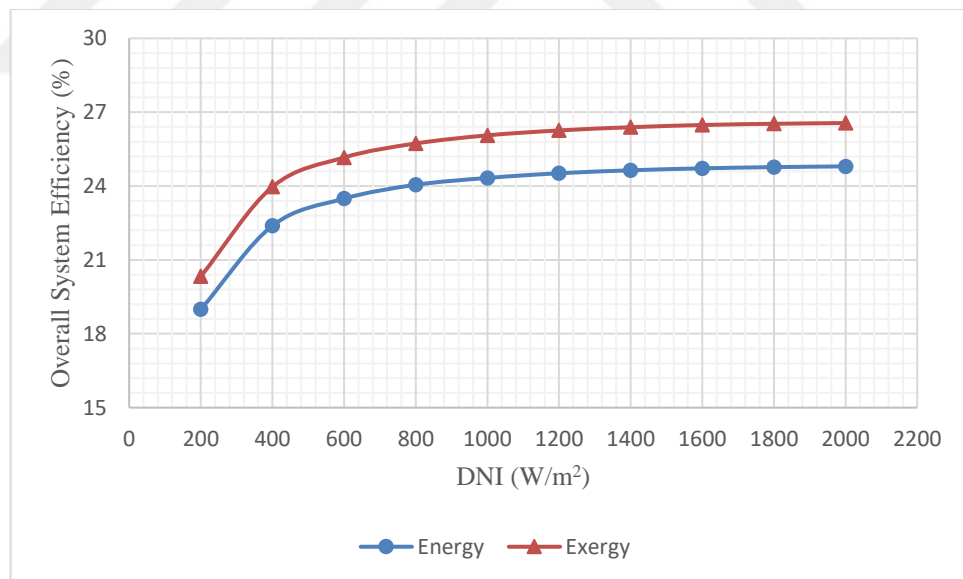


Figure 3.3 Effects of the DNI on the energy and exergy efficiencies of the overall system

In Figure 3.4, effects of the direct normal irradiation on the receiver surface temperature are seen. As expected, with the increase of DNI from 200 W/m² to 2000 W/m², receiver surface temperature is increased linearly from 726.45 K to 960.04 K.

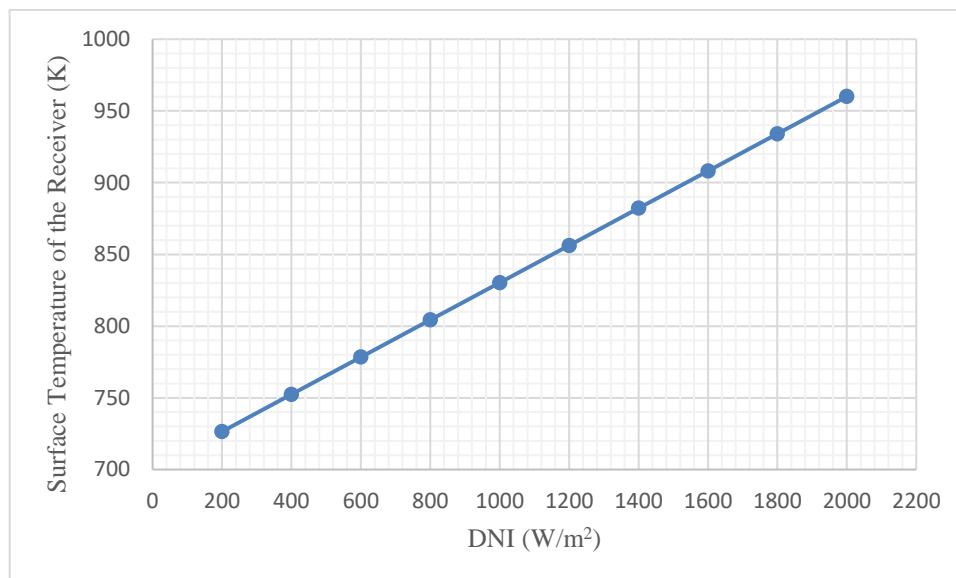


Figure 3.4 Effects of the DNI on the receiver surface temperature

Variation of the total heat loss of the receiver with respect to the increase of DNI is seen in Figure 3.5. As seen in the figure total heat loss increases with a slow increment rate. Total heat loss of the receiver is found 485.69 kW at DNI of 200 W/m². When DNI is increased to 2000 W/m², total heat loss becomes 1562.49 kW. In order to explain the increase of the total heat loss of the receiver in more detail, individual heat losses needed to be examined. The effects on the individual heat losses by convection, conduction, reflection, and emission with an increase of DNI is seen in Figure 3.6. In accordance with the figure, all of the individual heat losses are increased with an increase of DNI. At DNI of 200 W/m², convective, conductive, reflective and emissive heat losses are found 158.78 kW, 48.92 kW, 49.95 kW and 228.04 kW, respectively. When the DNI is increased to 2000 W/m², individual heat losses are found 275.95 kW, 77.82 kW, 499.53 kW and 709.19 kW, respectively. Therefore, it is understood that the increase of DNI effects reflective and emissive heat losses much greater than convective and conductive heat losses.

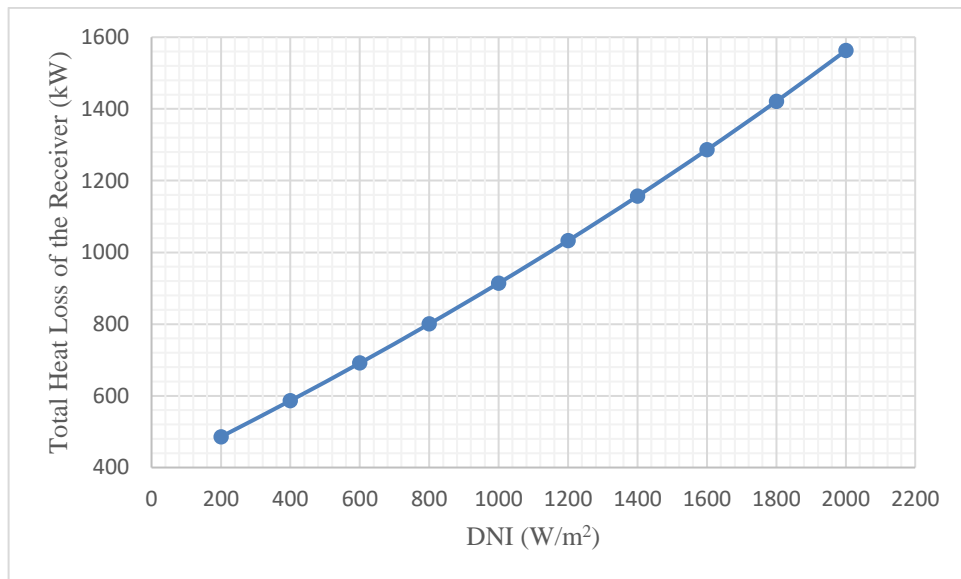


Figure 3.5 Effects of the DNI on the total heat loss of the receiver

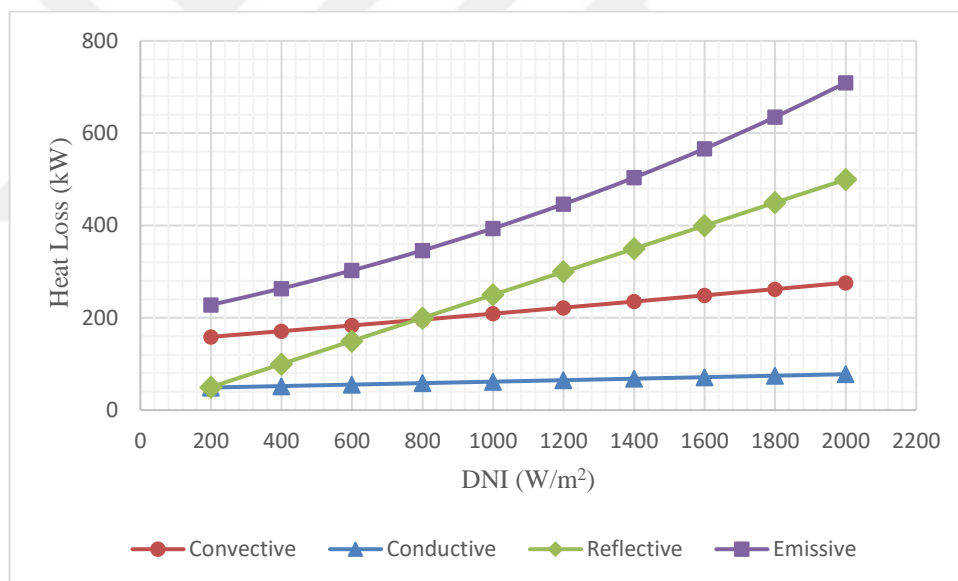


Figure 3.6 Effects of the DNI on the receiver's convection, conduction, reflection and emission heat losses

In Figure 3.7, effects of the DNI on the electricity generation of the system can be seen. As seen from the figure, with the increase of DNI from 200 W/m² to 2000 W/m², electricity generation is increased linearly from 449.06 kW to 5866.4 kW.

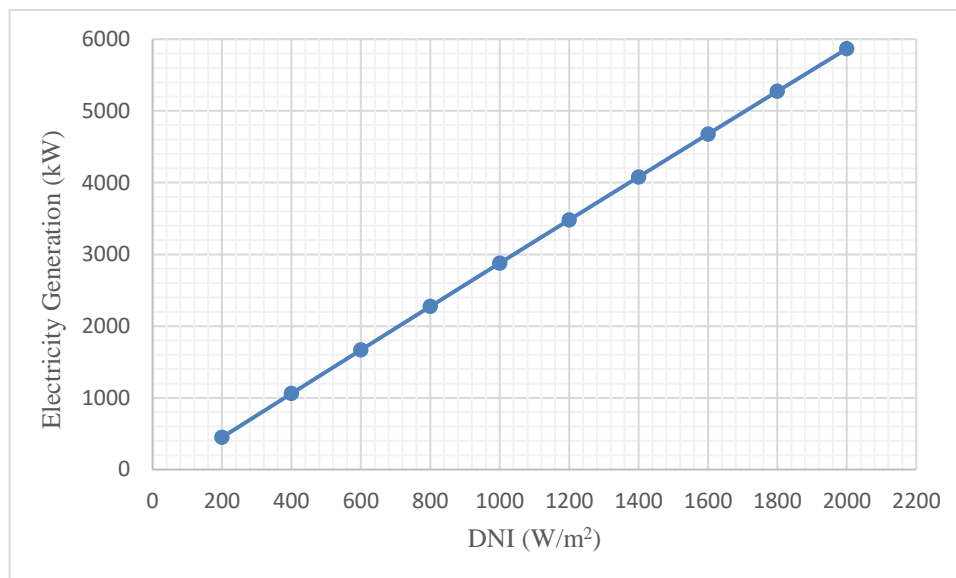


Figure 3.7 Effects of the DNI on the electric production of the system

3.2 Effects of the Heliostat Field Area

Heliostat field is basically the power source of the solar power tower systems, thus making it has a very important role for the system. Heliostat field area effect on the system is very straight forward.

Heliostat field area effect on the receiver energy and exergy efficiencies can be seen in Figure 3.8. Basically, with heliostat field area increase, efficiencies of the receiver increase with lower increase rate. While the heliostat field area is 3000 m², receiver energy and exergy efficiencies are found to be 82.13% and 48.08%, respectively, at 18000 m² efficiencies are increased to the 90.02% and 52.69%, respectively.

Similarly, heliostat field area effect on the energy and exergy efficiencies of the overall system can be seen in Figure 3.9. As can be deduced from the figure, at DNI of 3000 m², overall system energy and exergy efficiencies are found to be 22.64% and 24.24%, respectively. When heliostat field is increased to 18000 m², efficiencies are increased to the 24.81% and 26.57%, respectively.

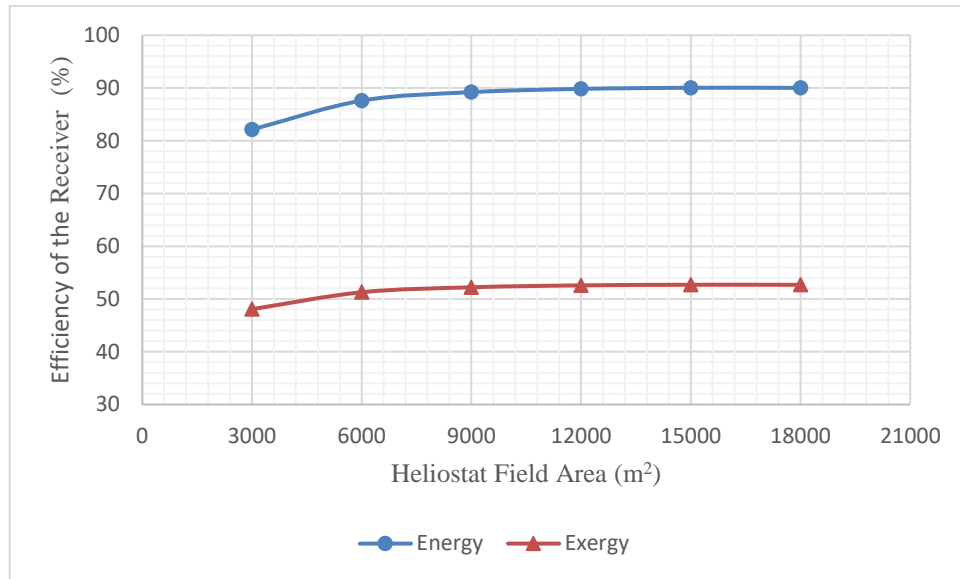


Figure 3.8 Effects of the heliostat field area on the energy and exergy efficiencies of receiver

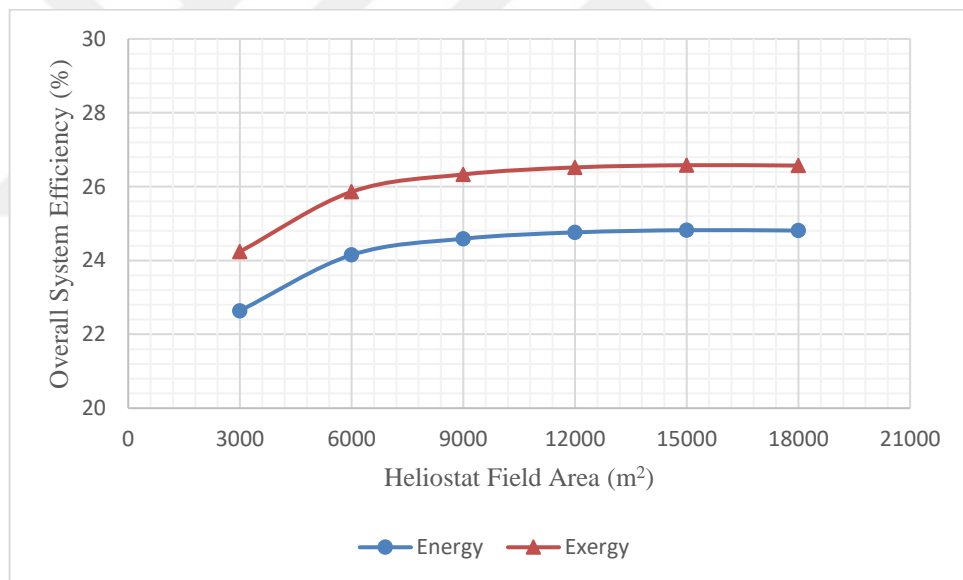


Figure 3.9 Effects of the heliostat field area on the energy and exergy efficiencies of the overall system

Increasing the heliostat field area increase the surface temperature and total heat loss of the receiver almost linearly, which can be seen in Figure 3.10 and Figure 3.11, respectively. When heliostat field area is 3000 m², the results of surface temperature and total heat loss of the receiver are 756.61 K and 603.13 kW, respectively. At

heliostat field area is increased to 18000 m², the results of surface temperature and total heat loss of the receiver are increased to 1037.18 K and 2021.85 kW, respectively.

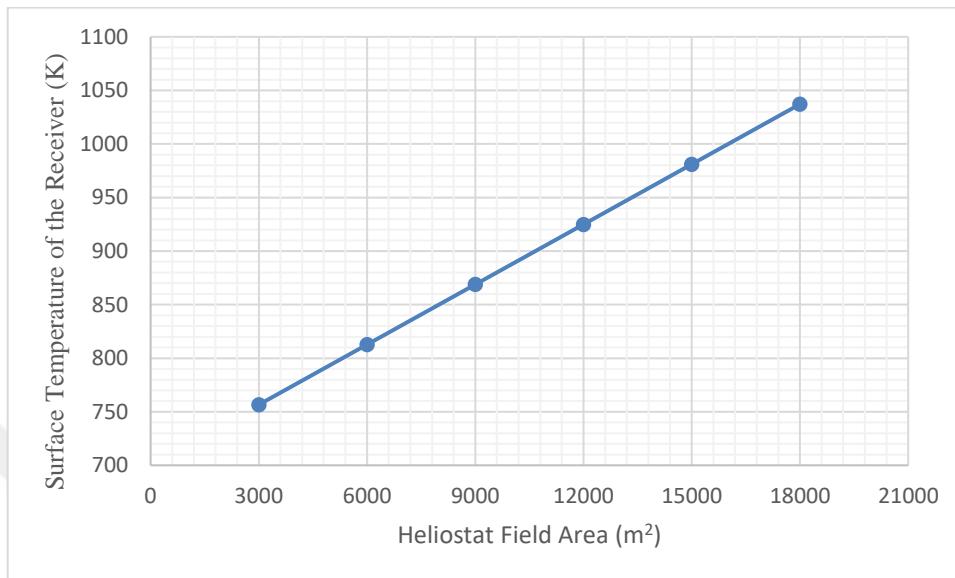


Figure 3.10 Effects of the heliostat field area on the receiver surface temperature

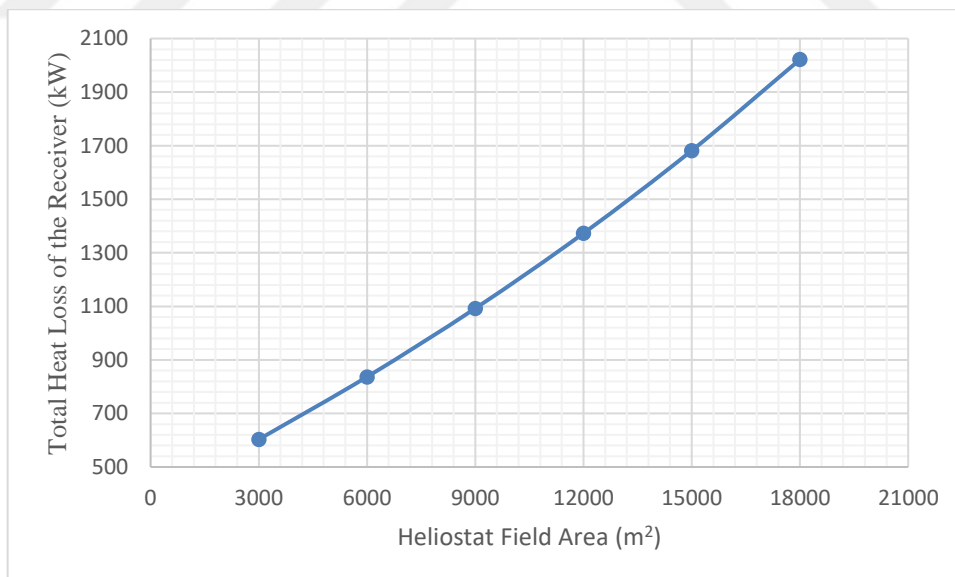


Figure 3.11 Effects of the heliostat field area on the receiver total heat loss

Effects on the individual heat losses with an increase of the heliostat field area behave similarly to the case of DNI and are seen in Figure 3.12. When heliostat field

area is 3000 m², convective, conductive, reflective and emissive heat losses are found 173.02 kW, 52.6 kW, 108 kW and 269.51 kW, respectively. When heliostat field area is increased to 18000 m², individual heat losses are increased to 317.81 kW, 87.53 kW, 648 kW and 968.51 kW, respectively.

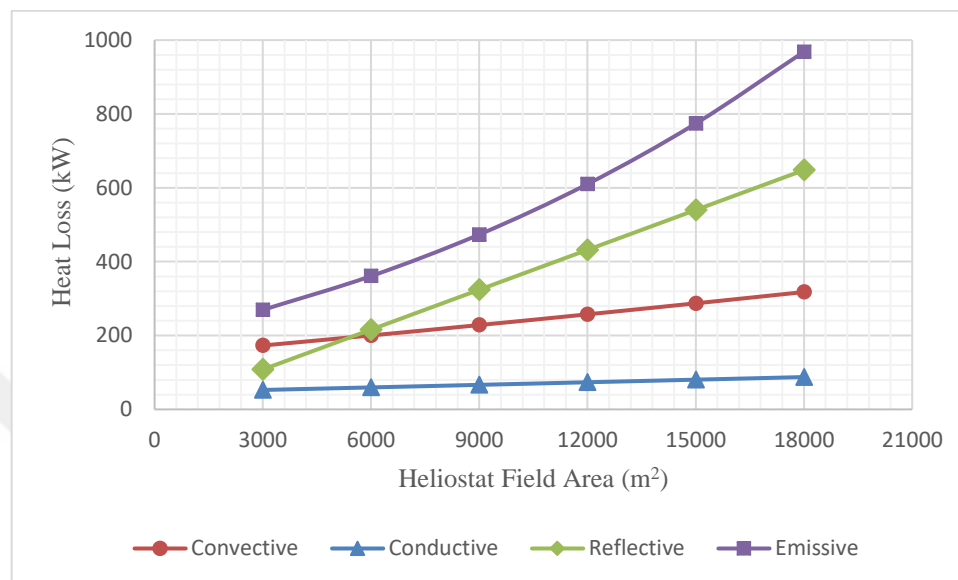


Figure 3.12 Effects of the heliostat field area on the receiver's convection, conduction, reflection and emission heat losses

3.3 Effects of the Emissivity and Reflectivity

Emissivity and reflectivity of the receiver are very important for the solar power tower systems due to the high energy quality. Therefore choosing the right material for the receiver has a great role for the efficiency of the system. Figure 3.13 and Figure 3.14 are showing the effects of the emissivity and reflectivity on the receiver energy and exergy efficiencies, respectively. The effect of the emissivity on the efficiencies of the receiver is relatively less than the reflectivity. While at the emissivity of 0.1, the energy and exergy efficiencies of the receiver are 93.50% and 54.73%, respectively, at the emissivity of 0.9, efficiencies are found to be 89.36% and 52.31%, respectively. On the other hand, while the receiver energy and exergy efficiencies at the reflectivity of 0.1, are 84.77% and 49.62%, respectively, with an

increase of reflectivity to 0.9, efficiencies are decreased to the 20.77% and 12.16%, respectively.

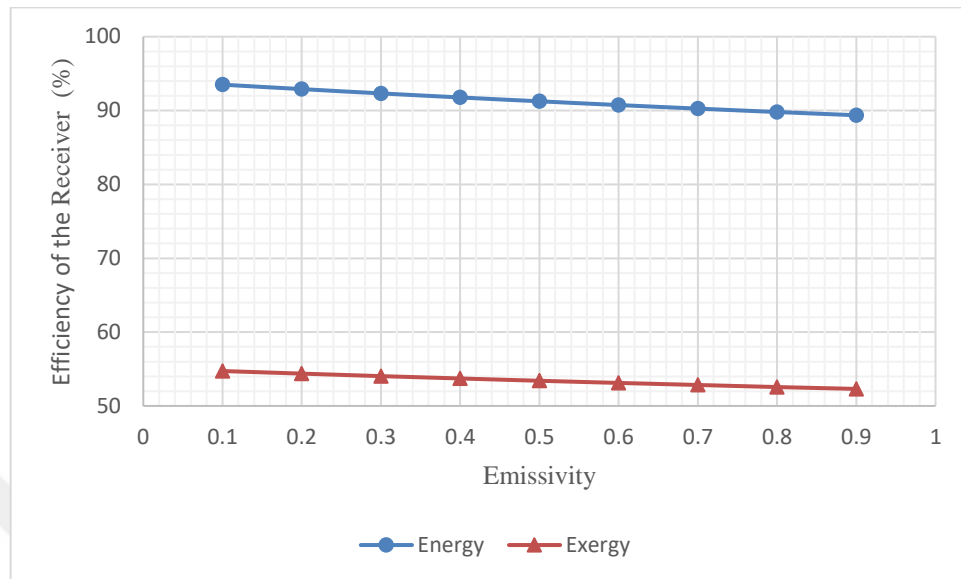


Figure 3.13 Effects of the emissivity on the receiver energy and exergy efficiencies

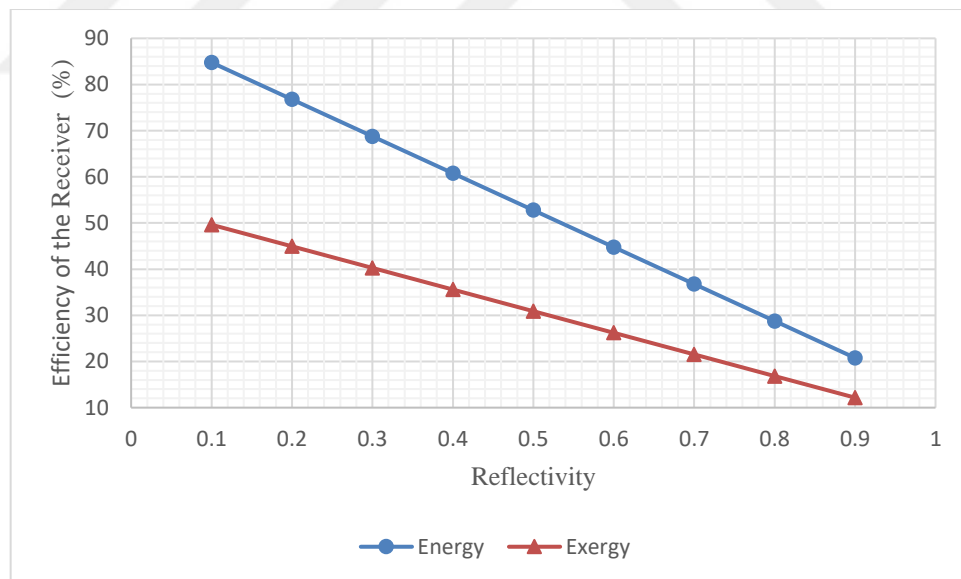


Figure 3.14 Effects of the reflectivity on the receiver energy and exergy efficiencies

Change of the emissivity and reflectivity effects, on the overall system energy and exergy efficiencies can be seen in Figure 3.15 and Figure 3.16, respectively. As seen from the figures reflectivity change affects the system greater than emissivity.

Furthermore, when reflectivity increases, energy and exergy efficiencies of the system approach to each other. When emissivity is increased from 0.1 to 0.9, overall energy and exergy efficiencies are decreased from 25.77% and 27.6% to 24.63% and 26.37%, respectively. Similarly, when the increase of reflectivity from 0.1 to 0.9, overall energy and exergy efficiencies are decreased from 25.57% and 27.38% to 3.52% and 3.77%, respectively.

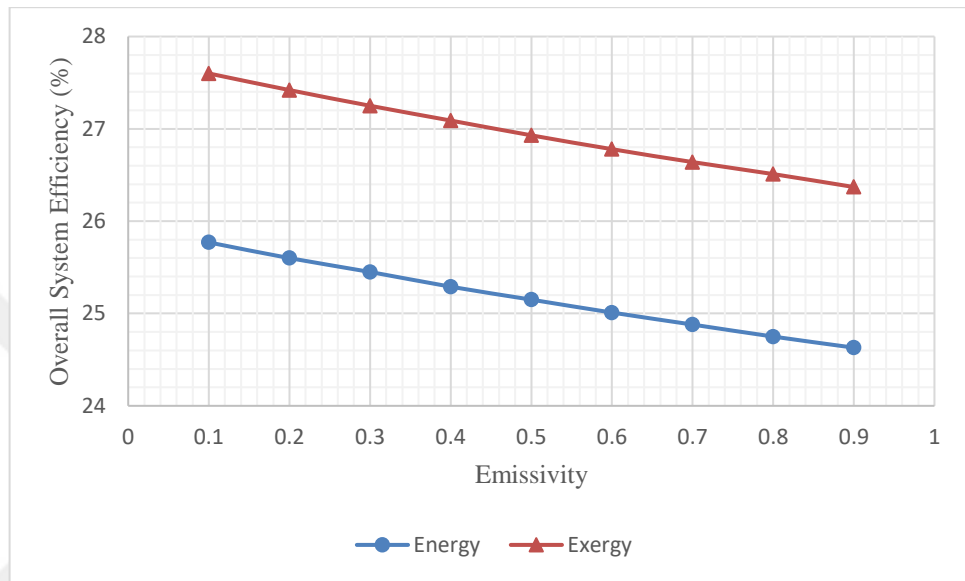


Figure 3.15 Effects of the emissivity on the overall system energy and exergy efficiencies

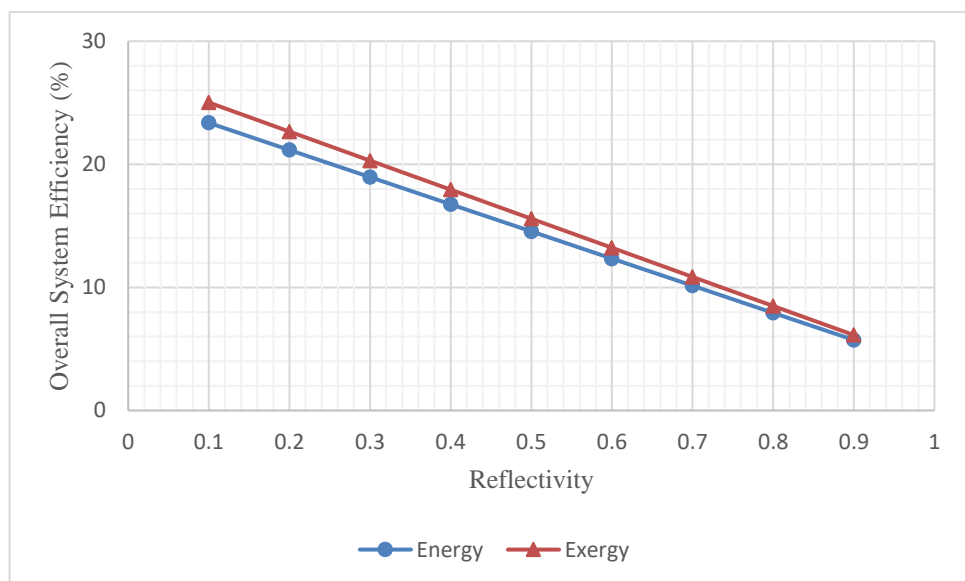


Figure 3.16 Effects of the reflectivity on the overall system energy and exergy efficiencies

There are no effects of the emissivity and reflectivity change on the surface temperature of the receiver because of both parameters are independent of it. However, both parameters effects on the total heat loss of the receiver can be seen in Figures 3.17 and Figure 3.18, respectively. As expectedly the increase of the receiver total heat loss for emissivity is lower than the reflectivity. While the heat loss of the receiver at the emissivity of 0.1, is 760.62 kW, at the reflectivity of 0.1, the heat loss of the receiver found to be 1782.64 kW. When emissivity is increased to 0.9, the heat loss of the receiver is increased to 1246.33 kW. In addition, at the reflectivity of 0.9, the heat loss of the receiver found to be 9275.57 kW.

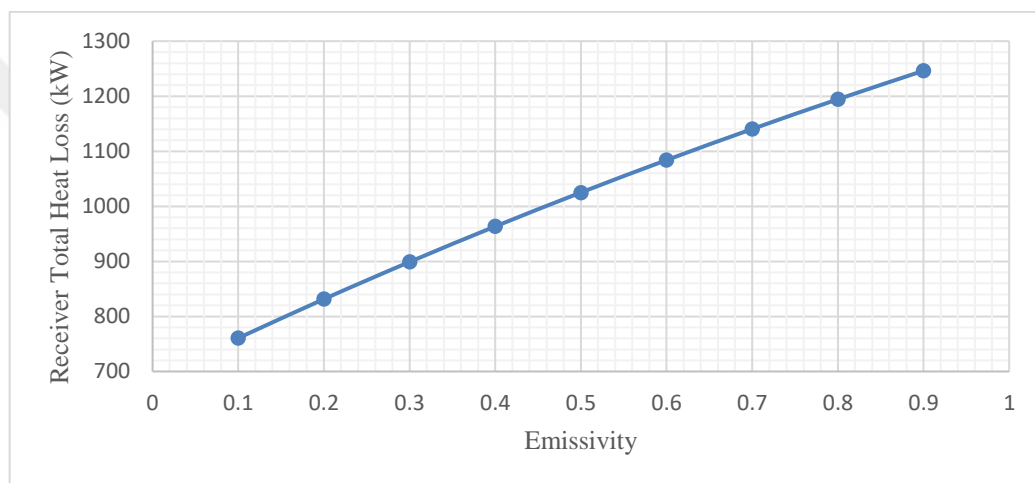


Figure 3.17 Effects of the emissivity on the receiver total heat loss

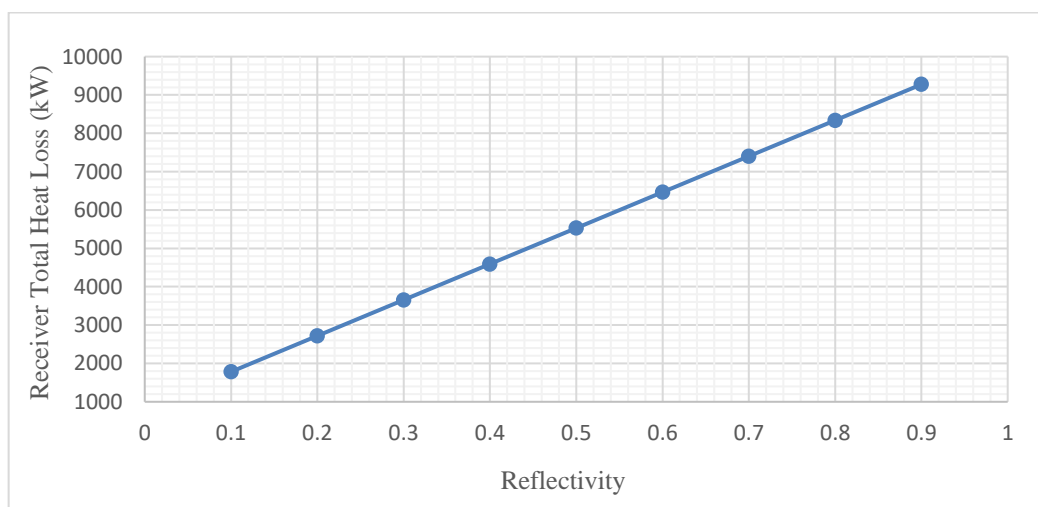


Figure 3.18 Effects of the reflectivity on the receiver total heat loss

Individual heat losses with an increase of emissivity can be seen in Figure 3.19. According to the figure increase of emissivity only affects the emissive heat loss as expected. When emissivity is increased from 0.1 to 0.9, emissive heat loss is increased from 74.37 kW to 560.08 kW.

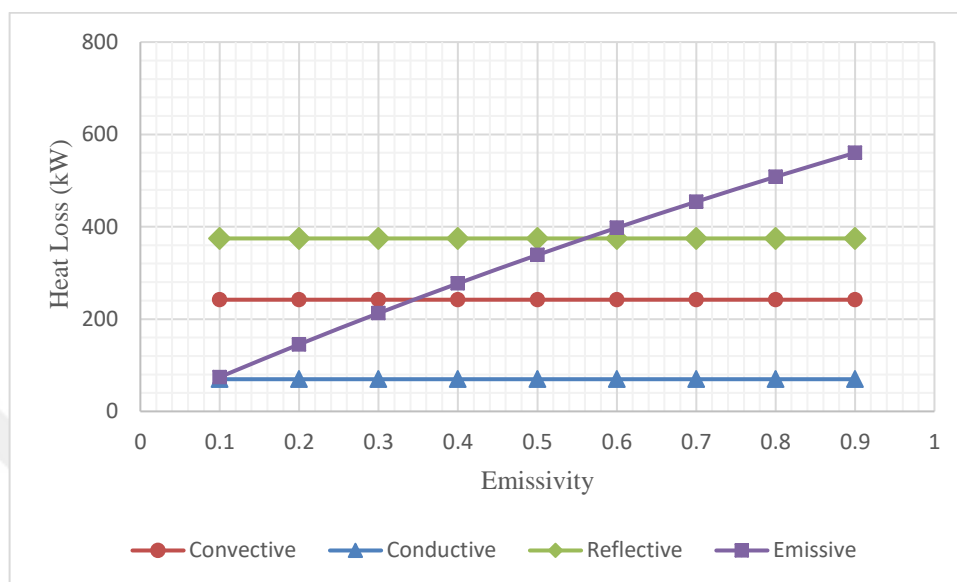


Figure 3.19 Effects of emissivity on the receiver's convection, conduction, reflection and emission heat losses

Individual heat losses with an increase of reflectivity can be seen in Figure 3.20. As seen from the figure increase of reflectivity only affects the reflective heat loss. When reflectivity is increased from 0.1 to 0.9, reflective heat loss is increased from 936.62 kW to 8429.55 kW. As seen from the figures, the change of emissive heat loss in emissivity change is in the order of hundreds, while the change in reflective heat loss in the change of reflectivity is measured in the order of thousands. Therefore, a conclusion of reflectivity is immensely more important parameter than the emissivity in terms of heat loss, can be made.

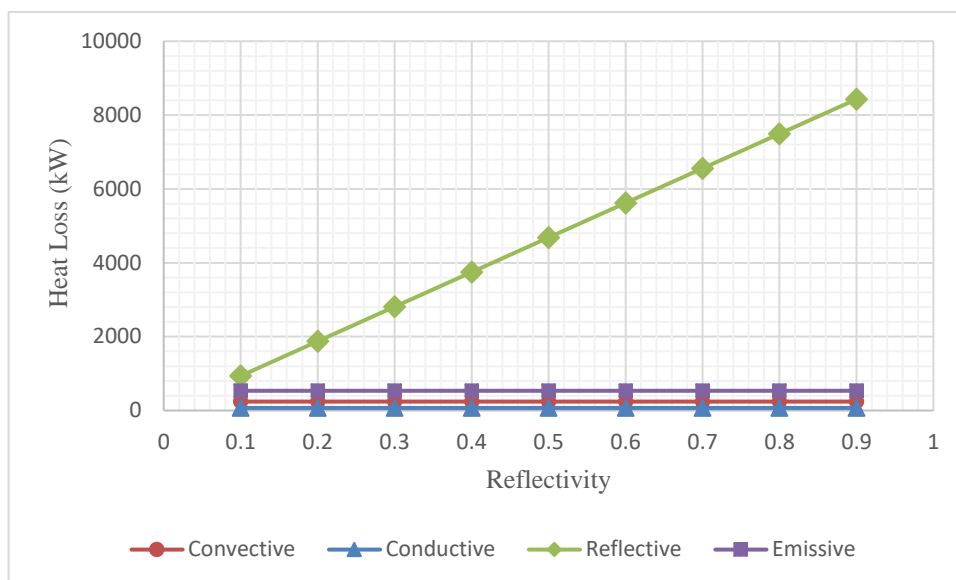


Figure 3.20 Effects of the reflectivity on the receiver's convection, conduction, reflection and emission heat losses

3.4 Effects of the Tube Diameter

Tube diameter in the receivers plays a grand role in the solar power tower systems. Receiver tubes are very delicate part of the system, due to the containing the thermal salt in them, to transfer heat to the power cycle subsystem.

Energy and exergy efficiencies of the receiver and the overall system with a change of tube diameter can be seen in Figure 3.21 and Figure 3.22 respectively. Analysis results showed that receiver efficiency is affected more than overall efficiency. At 8 mm tube diameter, energy efficiencies of the receiver and the whole system are found 85.36% and 23.53%, respectively. When the tube diameter increased to the 24 mm, energy efficiencies of the receiver and the whole system are increased with a decreasing increment, to 89.1% and 24.56%, respectively. In addition, at 8 mm tube diameter, exergy efficiencies of the receiver and the whole system are found 49.97% and 25.2%, respectively. When the tube diameter increased to the 24 mm, exergy efficiencies of the receiver and the whole system are increased with a decreasing rate to 52.16% and 26.3%, respectively.

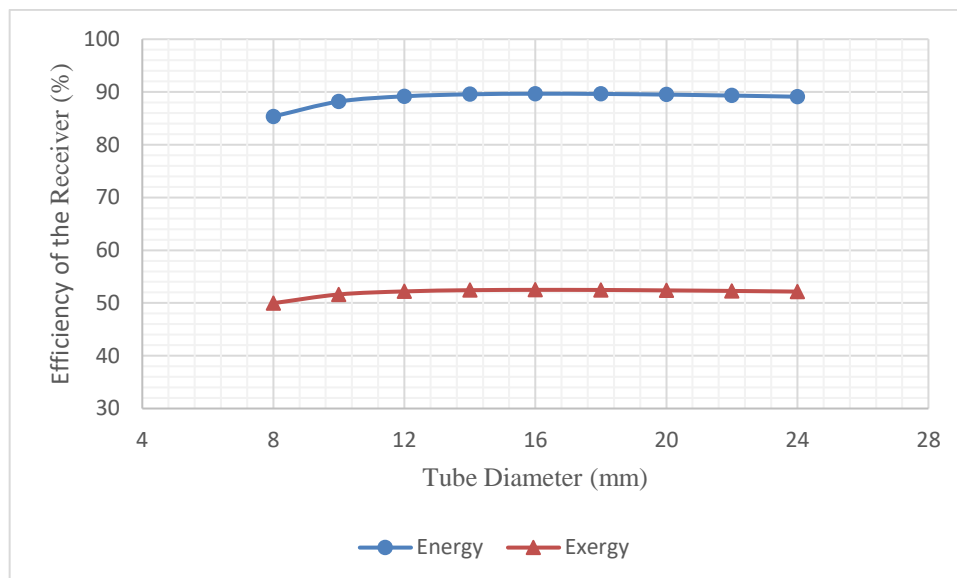


Figure 3.21 Effects of the tube diameter on the energy and exergy efficiencies of receiver

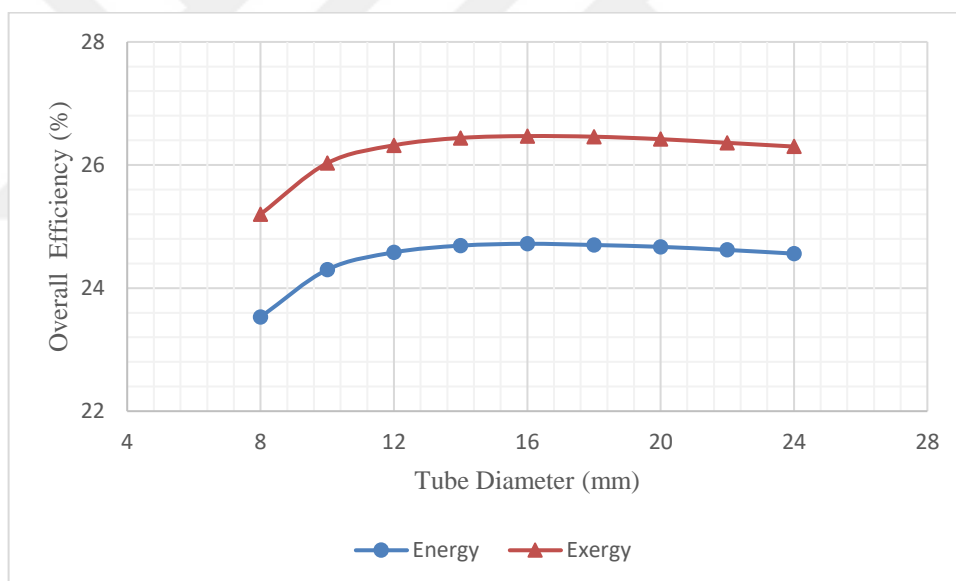


Figure 3.22 Effects of the tube diameter on the energy and exergy overall system efficiencies

Effect of the change in the tube diameter on the receiver surface temperature can be seen in Figure 3.23. While the tube diameter is 8 mm, receiver surface temperature is calculated as 1322,66 K. When tube diameter increased to the 24 mm, receiver surface temperature decrease with a parabolic behavior to the 849 K.

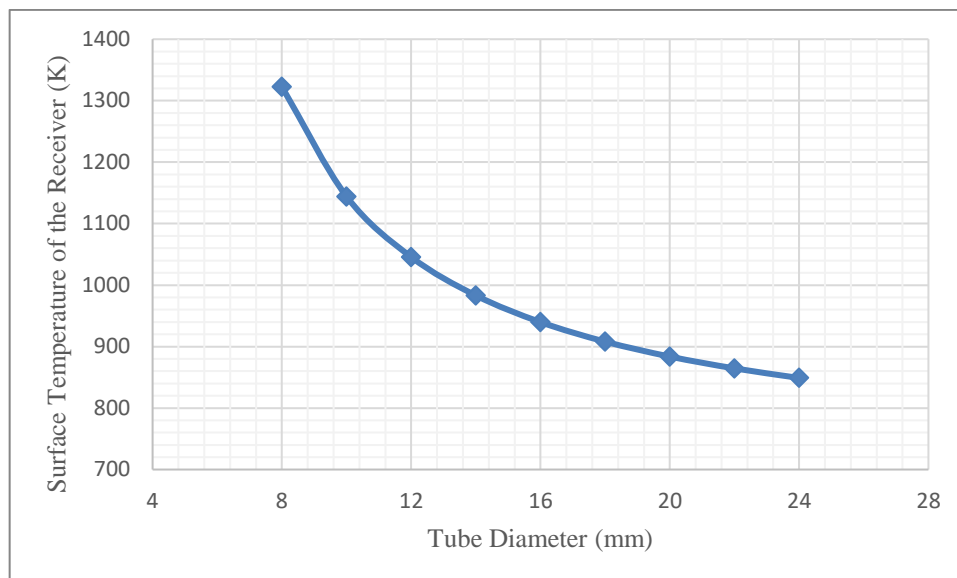


Figure 3.23 Effects of the tube diameter on the receiver surface temperature

Change in tube diameter relative to the receiver total heat loss shows interesting behavior, which can be seen in Figure 3.24. Analysis results show that between 8 mm and 16 mm tube diameters, receiver total heat loss decreases with values of 1713.88 kW and 1209.47 kW respectively. But between 16 mm and 24 mm tube diameters, receiver total heat loss starts to increase from 1209.47 kW to 1275.87 kW, respectively.

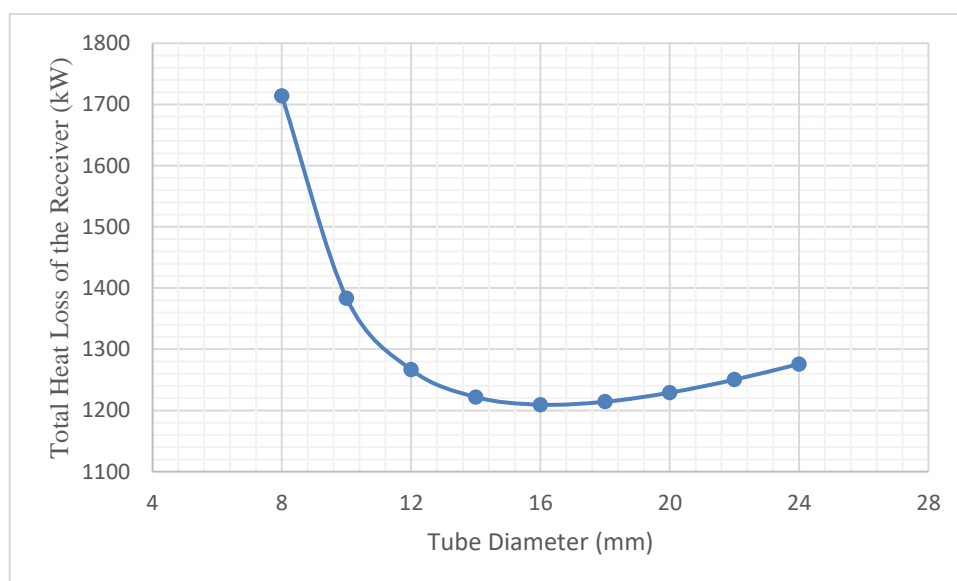


Figure 3.24 Effects of the tube diameter on the receiver total heat loss

In Figure 3.25, effects of individual heat losses by the increase of tube diameter are given. Emissive heat loss is showing an aggressive change with a downward trend until tube diameter of 20 mm, then slight increase until tube diameter of 24 mm. On the other hand, reflective heat loss has stayed constant throughout the analysis. Furthermore convective and conductive heat losses are showing slight increases with the increase of tube diameter. At tube diameter of 8 mm, convective, conductive, reflective and emissive heat losses are found 203.94 kW, 52.2 kW, 374.65 kW and 1083.1 kW, respectively. In addition at tube diameter of 24 mm, convective, conductive, reflective and emissive heat losses are found 275.79 kW, 80.81 kW, 374.65 kW and 544.62 kW, respectively.

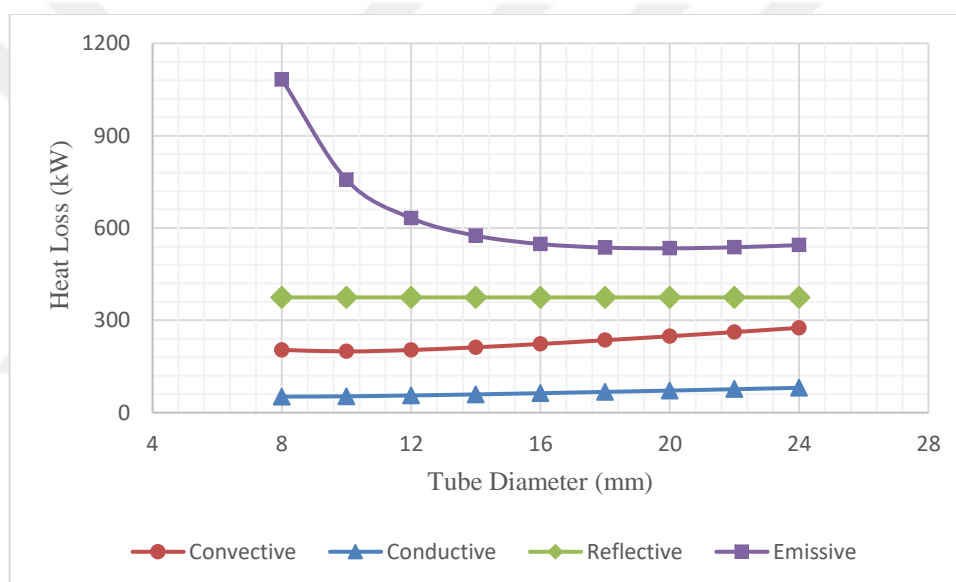


Figure 3.25 Effects of the tube diameter on the receiver's convection, conduction, reflection and emission heat losses

In Figure 3.26 effects of the concentration ratio relative to the tube diameter change, is given which has the similar behavior with receiver surface temperature change. According to the analysis when tube diameter changes 8 mm to 24 mm, concentration ratio decreased from 1457.33 to 485.78.

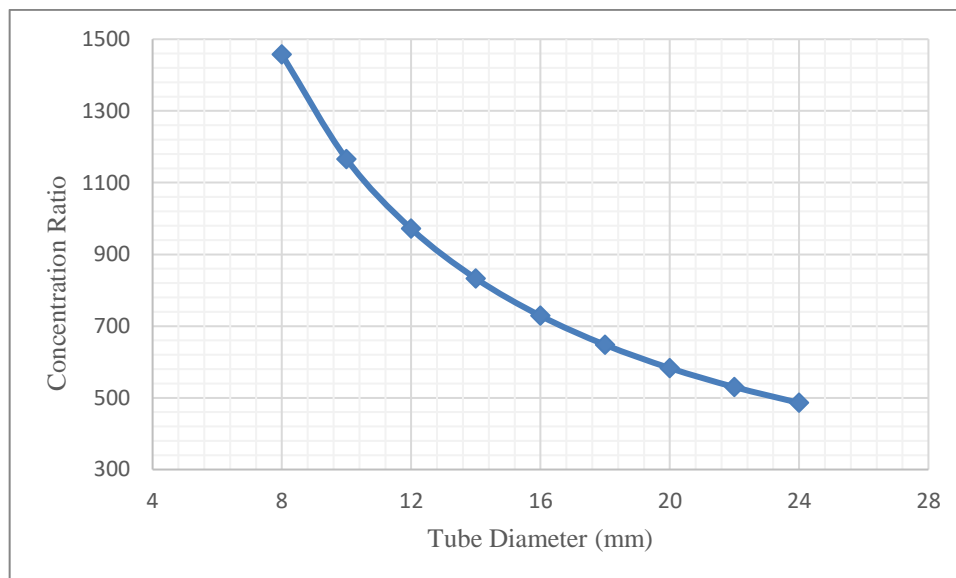


Figure 3.26 Effects of the tube diameter on the concentration ratio of the system

3.5 Effects of the View Factor

View factor is defined as the ratio of the aperture area of the receiver to the surface area of the receiver. Because of that, we can inspect the effect of the view factor two different way. These are the case of aperture area dependent and the case of receiver surface area dependent. Energy efficiencies of the receiver and the system for the both cases can be seen in Figure 3.27 and Figure 3.28, respectively. When view factor dependent to the aperture area, efficiencies are decreased almost linearly. While the case of aperture area dependent, at view factor of 0.1, efficiencies of the receiver and the system is 96.94% and 26.72%, respectively, at the view factor of 1.0, efficiencies decreased to the 87.62% and 24.15%, respectively.

For the case of the receiver surface dependent, the efficiencies first increased up to view factor of 0.4, then started to fall. While at view factor of 0.1, efficiencies of the receiver and the system are 86.97% and 23.97%, respectively, at the view factor of 0.4, efficiencies made its peak with 91.69% and 25.27%, respectively. Furthermore, at the view factor of 1.0, efficiencies are found to be 88.01% and 24.26%, respectively.

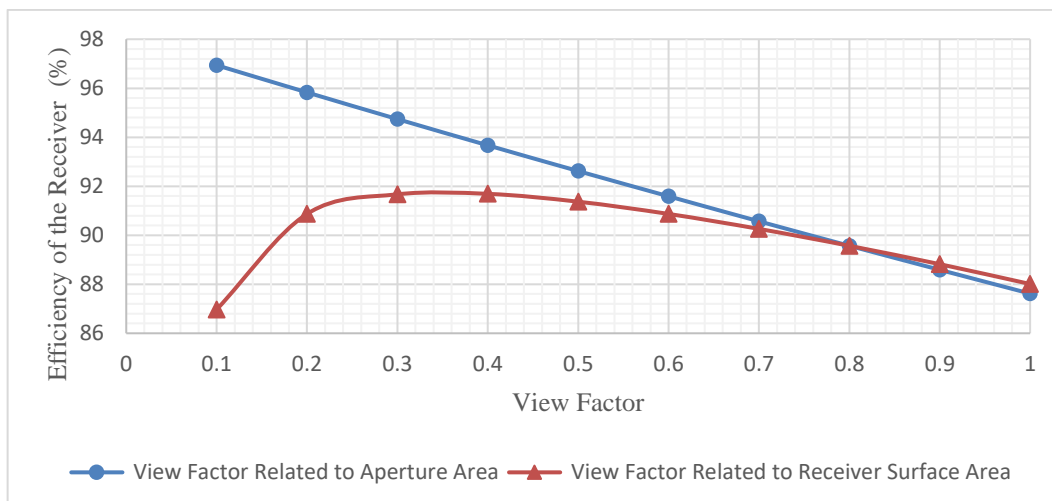


Figure 3.27 Effects of the view factor on the energy efficiencies of the receiver for the cases of aperture area dependence and receiver surface area dependence

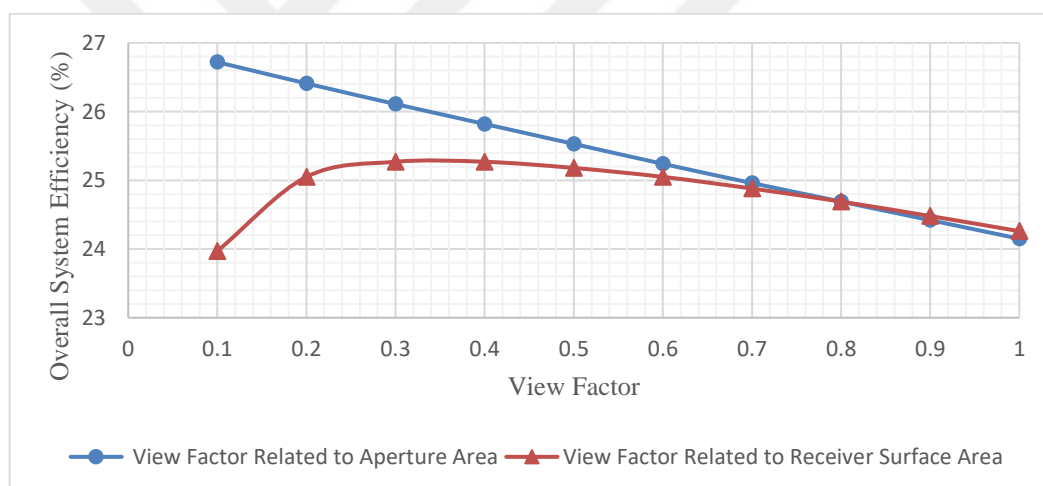


Figure 3.28 Effects of the view factor on the energy efficiencies of the overall system for the cases of aperture area dependence and receiver surface area dependence

Exergy efficiencies of the receiver and the system for the both cases can be seen in Figure 3.29 and Figure 3.30, respectively. When view factor depending on the aperture area exergy efficiencies behaves similarly to the energy efficiencies. While view factor is 0.1, in the case of aperture area dependent, efficiencies of the receiver and the system are 56.75% and 28.61%, respectively, at the view factor of 1.0 efficiencies decreased to the 51.29% and 25.86%, respectively.

For the view factors depending on receiver surface area just like the energy efficiencies the exergy efficiencies first increased up to view factor of 0.4, then started to fall. While view factor of 0.1, exergy efficiencies of the receiver and the system are 50.91% and 25.67%, respectively, at the view factor of 0.4, efficiencies made its peak with 53.67% and 27.06%, respectively. Furthermore, at the view factor of 1.0, efficiencies are found to be 51.52% and 25.98%, respectively.

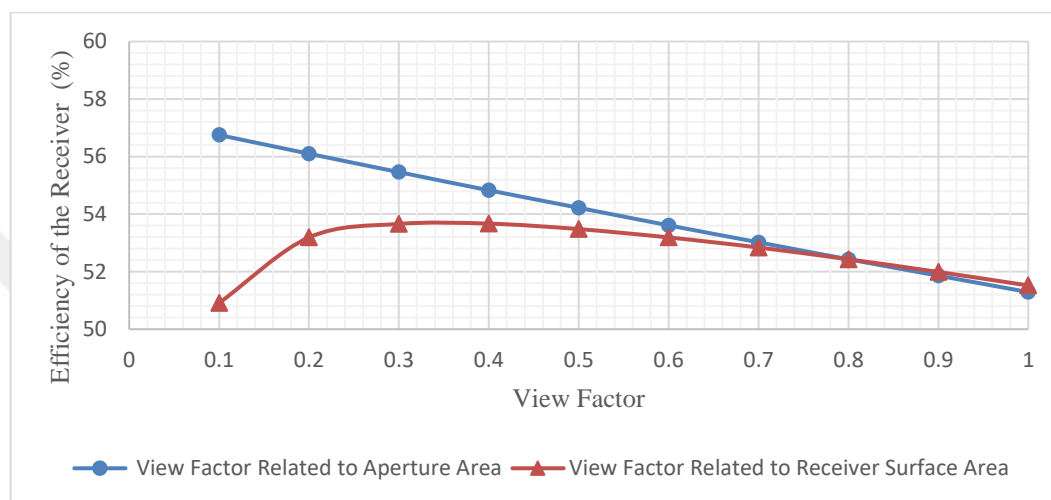


Figure 3.29 Effects of the view factor on the exergy efficiencies of the receiver for the cases of aperture area dependence and receiver surface area dependence

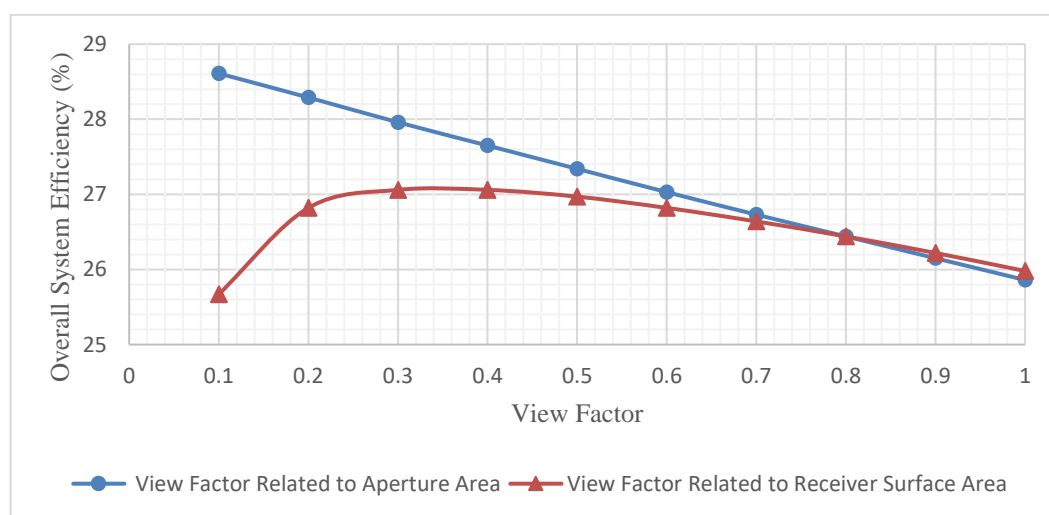


Figure 3.30 Effects of the view factor on the exergy efficiencies of the overall system for the cases of aperture area dependence and receiver surface area dependence

Effects of the view factor on the receiver surface temperature can be seen in Figure 3.31. As seen from the figure, when view factor is increased from 0.1 to 1.0, the surface temperature of the receiver is increased from 724.83 K to 943.82 K.

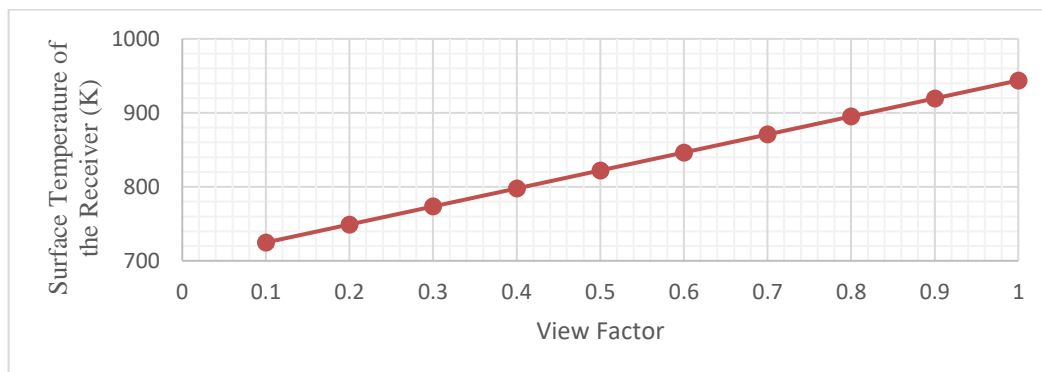


Figure 3.31 Effects of the view factor on the receiver surface temperature

The receiver total heat loss for the both cases can be seen in Figure 3.32. According to the figure total heat loss in the case of aperture area dependence Show increase from 358.31 kW to the 1449.33 kW with the increase of view factor from 0.1 to 1.0. On the other hand, in the case of the surface area dependence receiver total heat loss follows a distinct behavior which first decrease from view factor of 0.1, to the view factor of 0.4, then increase up to the view factor of 1.0, with total heat losses of 1525.11 kW, 973.57 kW and 1403.51 kW, respectively.

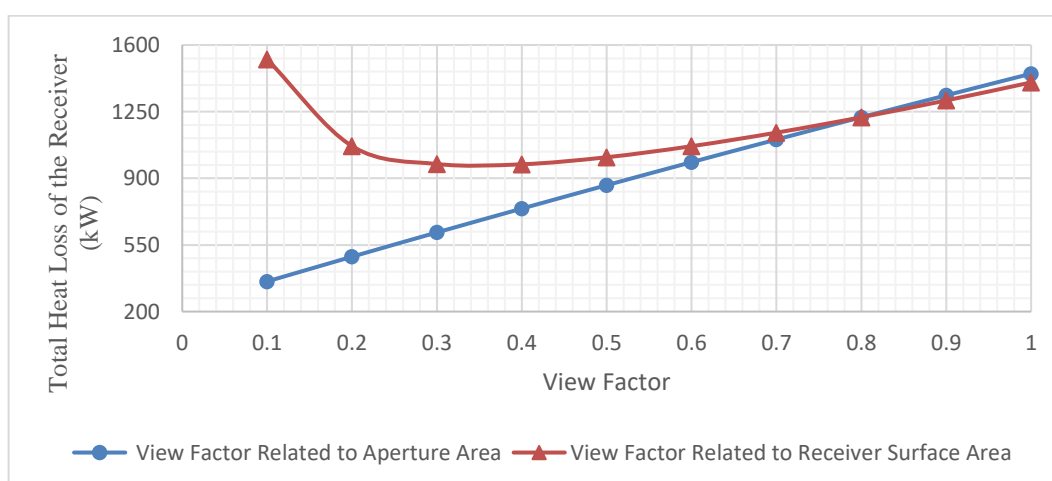


Figure 3.32 Effects of the view factor on the receiver total heat loss for the cases of aperture area dependence and receiver surface area dependence

Individual heat losses by convection, conduction, reflection, and emission for the case of aperture area dependence and surface area dependence is shown in Figure 3.33 and Figure 3.34, respectively. Individual heat losses except for conductive heat loss continuously increased with the increase of the view factor for the case of the aperture area dependence. While the view factor changed from 0.1 to 1.0, even though conductive heat loss stays constant at 69.72 kW, convective heat loss, reflective heat loss, and emissive heat loss increased from 166.86 kW, 46.83 kW, and 74.91 kW to 263.33 kW, 468.31 kW, and 647.98 kW, respectively. On the other hand, for the case of the surface area dependence, while convective and conductive heat losses decrease from 835.14 kW and 389.76 kW to 232.41 kW and 60.63 kW, with the increase of the view factor from 0.1 to 1.0, reflective and emissive heat losses increase from 46.83 kW and 253.38 kW to 468.31 kW and 642.16 kW. These can explain the distinct behavior of the efficiencies for the case of surface area dependence.

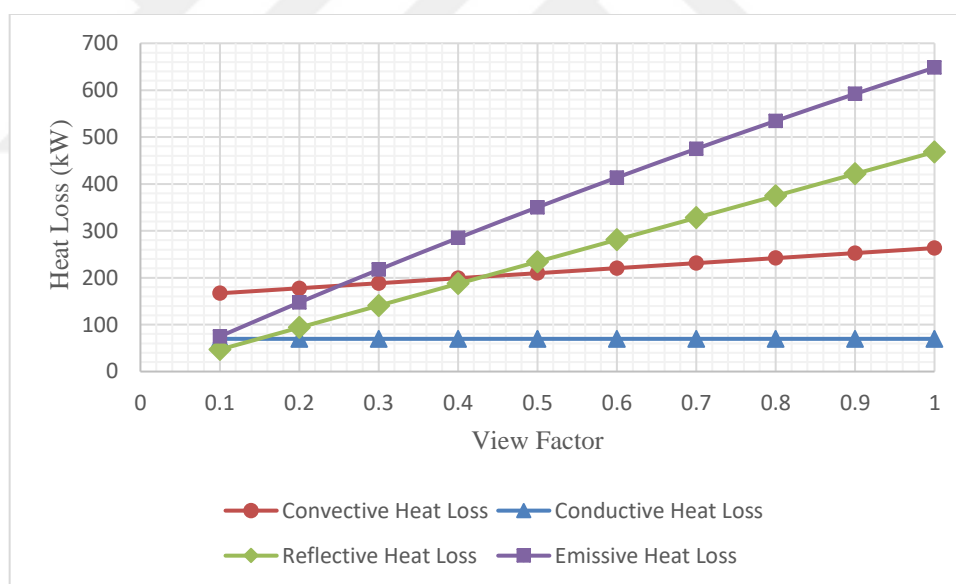


Figure 3.33 Effects of the view factor on the receiver conduction, convection, emission and reflection heat losses related to aperture area

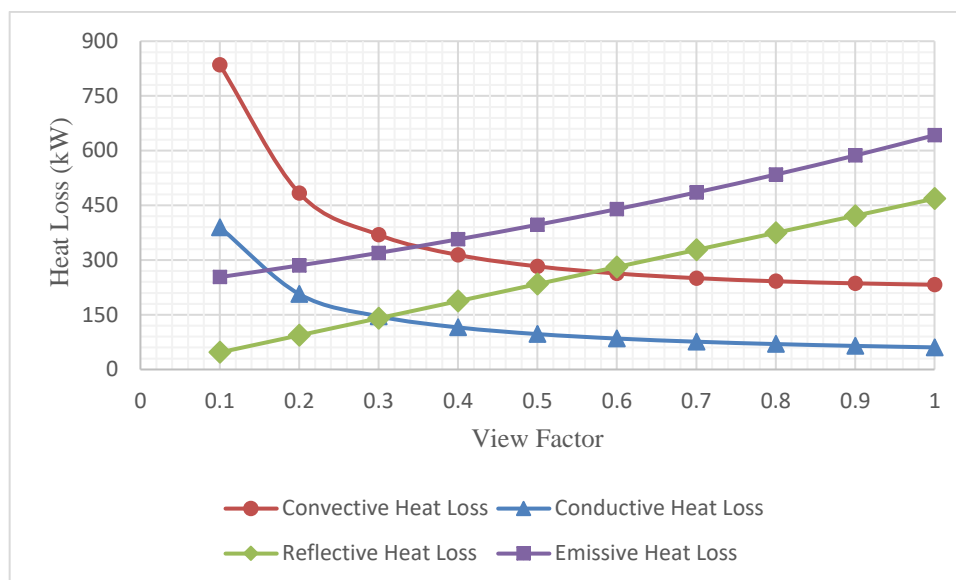


Figure 3.34 Effects of the view factor on the receiver conduction, convection, emission and reflection heat losses related to receiver surface area

Percentages of different type of heat losses, for the both cases can be seen in Figure 3.35 and Figure 3.36. For both cases, with the increase of the view factor, the percentages of conductive and convective heat losses decrease. On the other hand, percentages of reflective and emissive heat losses increases.

For receiver aperture area dependence when view factor is 0.1, percentages of convective, conductive, reflective and emissive heat losses are 19.46%, 46.57%, 13.07% and 20.91%, respectively. Furthermore, when view factor is 1.0, percentages of convective, conductive, reflective and emissive heat losses found as 4.81%, 1.17%, 32.31% and 44.71%, respectively.

For receiver surface area dependence, when view factor is 0.1, percentages of convective, conductive, reflective and emissive heat losses are 25.56%, 54.76%, 3.07% and 16.61%, respectively. Furthermore, when view factor is 1.0, percentages of convective, conductive, reflective and emissive heat losses found as 4.32%, 16.56%, 33.37% and 45.75%, respectively.

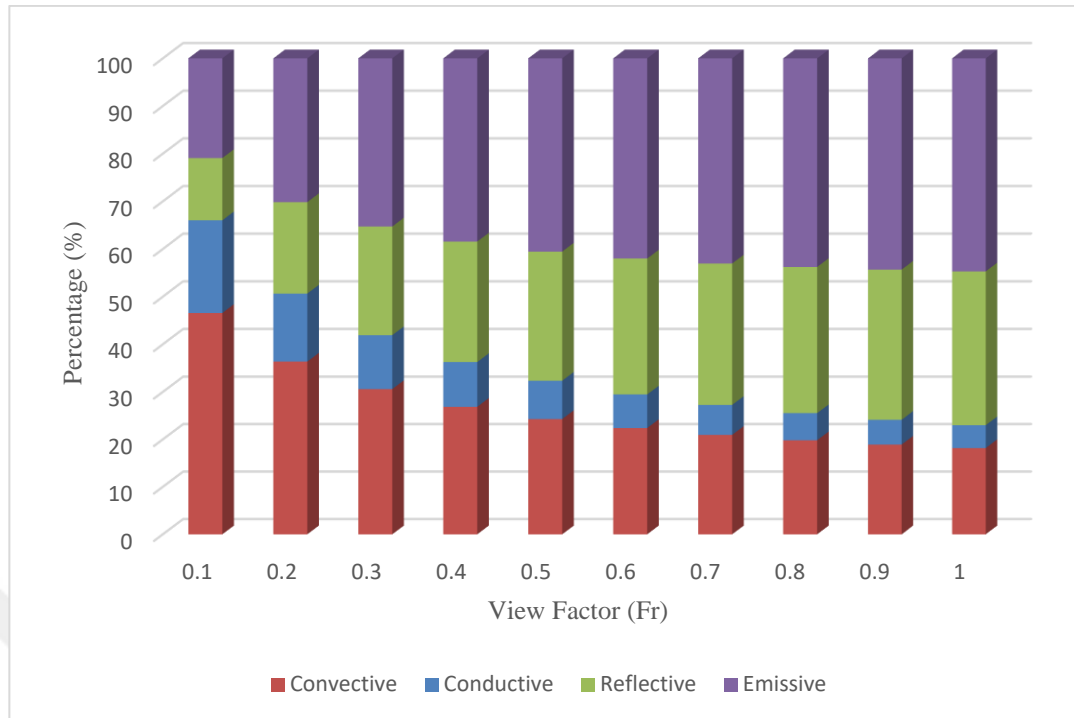


Figure 3.35 Percentages different type of heat losses for the cases of aperture area dependence

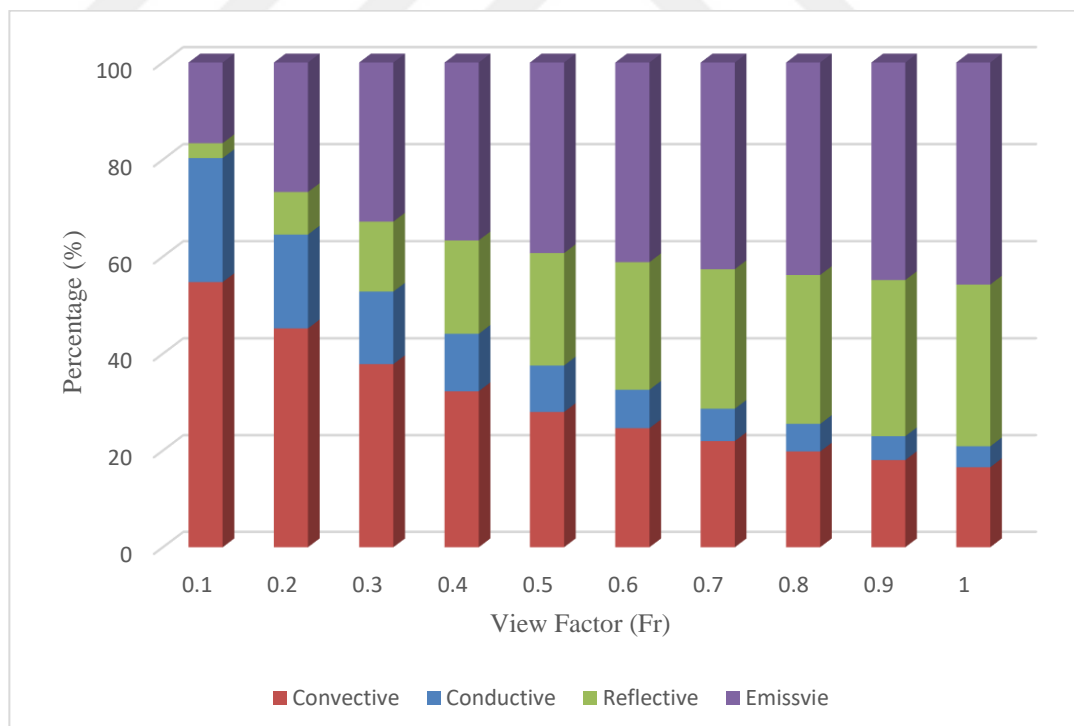


Figure 3.36 Percentages of different type of heat losses for the cases of receiver surface area dependence

3.6 Effects of the Concentration Ratio

Concentration ratio can be defined as the ratio of heliostat field area to receiver aperture area. In the analysis different concentration ratios obtained by changing the aperture area. Therefore, the corresponding surface area is changed to keep the view factor constant value.

Changing the concentration ratio effects on the receiver energy and exergy efficiencies dramatically and can be seen in Figure 3.37. At concentration ratio of 300, receiver energy and exergy efficiencies are 83.43% and 48.83%, respectively. With the increase of concentration ratio, receiver energy and exergy efficiencies are increased, making its peak at around concentration ratio of 1200. At concentration ratio of 1200, efficiencies are found 89.9% and 52.62%, respectively. Further increase of the concentration ratio, result decreases at the energy and exergy efficiencies. At concentration ratio of 2000, receiver and overall efficiencies are found to be 89.19% and 51.62%, respectively.

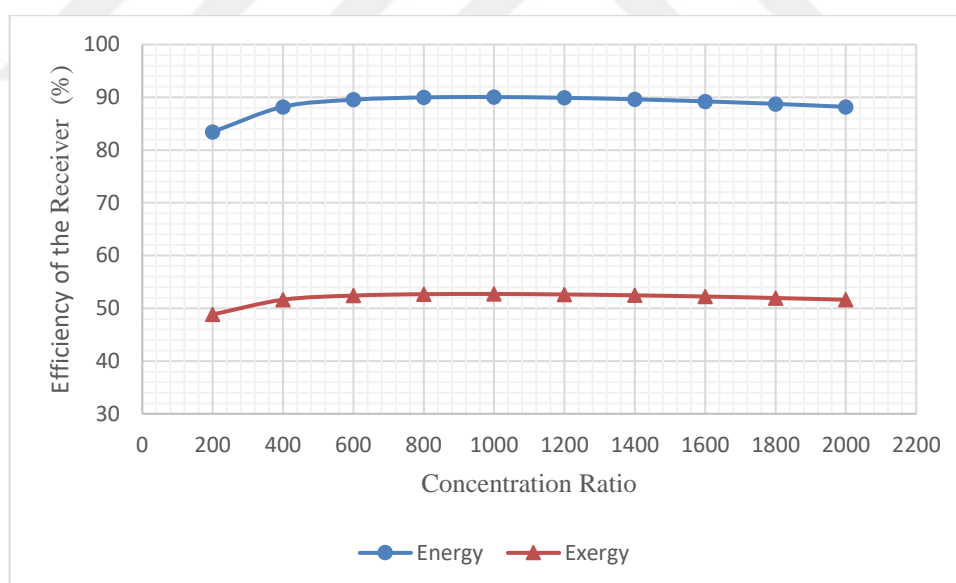


Figure 3.37 Effects of the concentration ratio on the receiver energy and exergy efficiencies

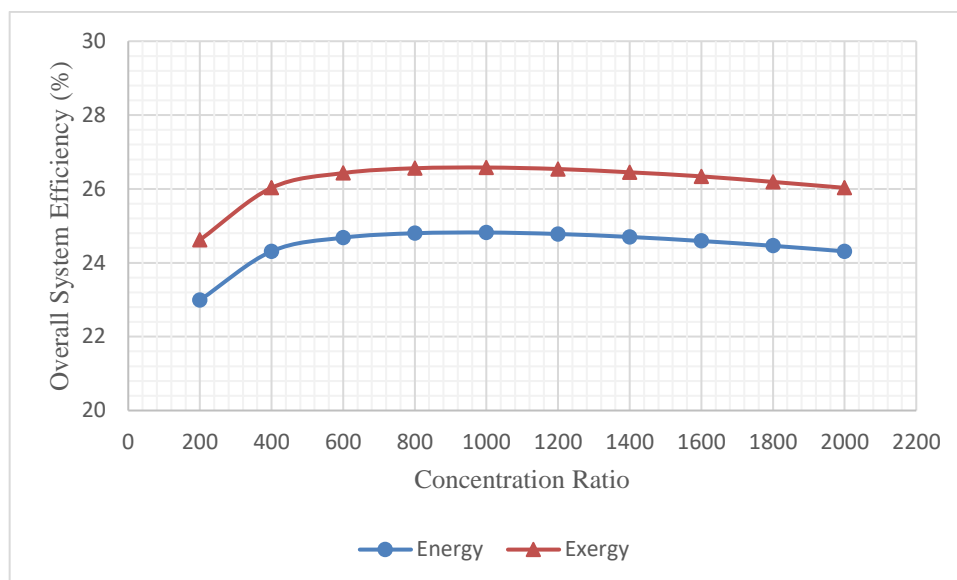


Figure 3.38 Effects of the concentration ratio on the overall energy and exergy efficiencies

Furthermore, overall energy and exergy efficiencies change depending on concentration ratio can be seen in Figure 3.38. At concentration ratio of 300, overall system energy and exergy efficiencies are found 22.99% and 24.62%, respectively. Energy and exergy efficiencies of the overall system are Showed increase with the increase of concentration ratio making its peak at around concentration ratio of 1200. At concentration ratio of 1200, efficiencies are found 24.78% and 26.54%, respectively. Further increase of the concentration ratio results decreases at the energy and exergy efficiencies. At Concentration ratio of 2000, overall system energy and exergy efficiencies are found to be 24.31% and 26.03%, respectively.

Effects of the surface temperature and total heat loss of the receiver with a change of concentration ratio can be seen in Figure 3.39 and Figure 3.40, respectively. Even though the change of the receiver surface temperature shows a linear increase with a change from 763.95 K to 1334.96 K with a change of concentration ratio, receiver total heat loss shows an interesting behavior. With the increase of the concentration ratio receiver total heat loss decrease substantially until the concentration ratio of 1000. At concentration ratio of 200, receiver total heat loss is found 1940.55 kW and at the concentration ratio of 1000, receiver total heat loss is calculated as 1165.95 kW. Further increase of concentration ratio shows a behavior of linearly increasing

the receiver heat loss. At concentration ratio of 2000, receiver total heat loss is found 1383.14 kW.

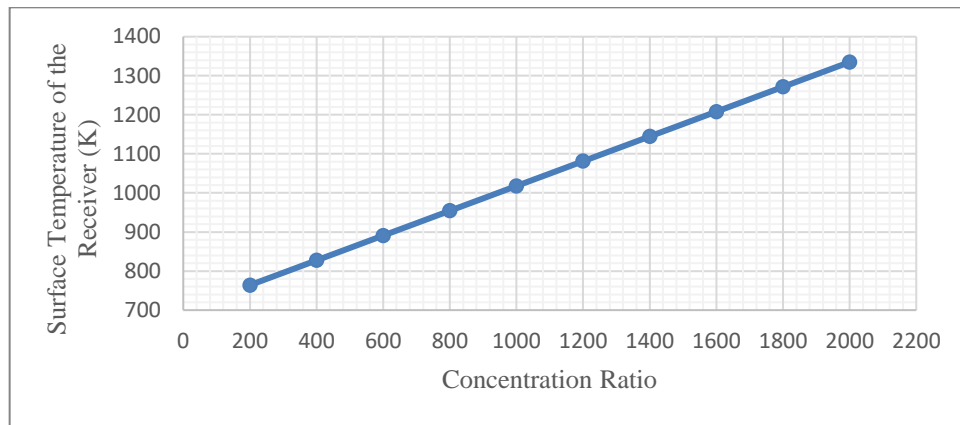


Figure 3.39 Effects of the concentration ratio of the receiver surface temperature

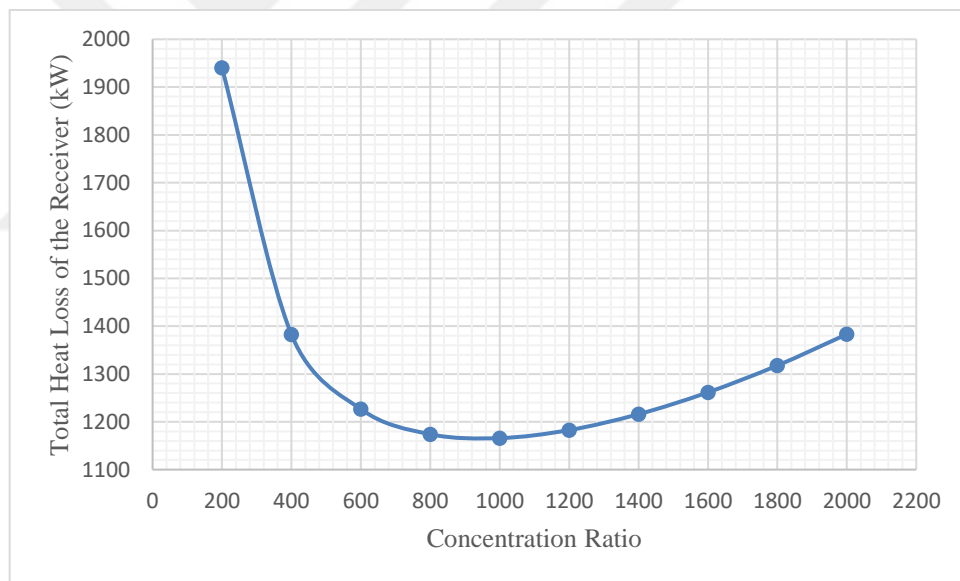


Figure 3.40 Effects of the concentration ratio of the receiver total heat loss

This particular behavior of the receiver total heat loss can be explained by investigating the conduction, convection, reflection, and emission heat losses of the receiver separately which is given in Figure 3.41. According to the figure, reflective heat loss does not show any change staying at the same value of 374.65 kW with the change of the concentration ratio. On the other hand, conductive and convective heat

losses show a decrease which is very minimal after the 1000 concentration ratio. While Convective and conductive heat losses, at the concentration ratio of 200, is found to be 541.58 kW and 164.13 kW, respectively. At the concentration ratio of 1000, the rapid decrease can be seen with values of 188.45 kW and 52.2 kW for convective and conductive heat losses. Further increase of the concentration ratio does not affect the convective and conductive heat losses dearly. At the concentration ratio of 2000, convective and conductive heat losses are found 150.92 kW and 38.52 kW, respectively.

Emissive heat loss shows a decrease from 200 concentration ratio to until the 800 concentration ratio with values of 860.19 kW and 530.91 kW, respectively, and increase after that with a value of 819.05 kW at 2000 concentration ratio. This can explain the behavior of the total heat loss of receiver.

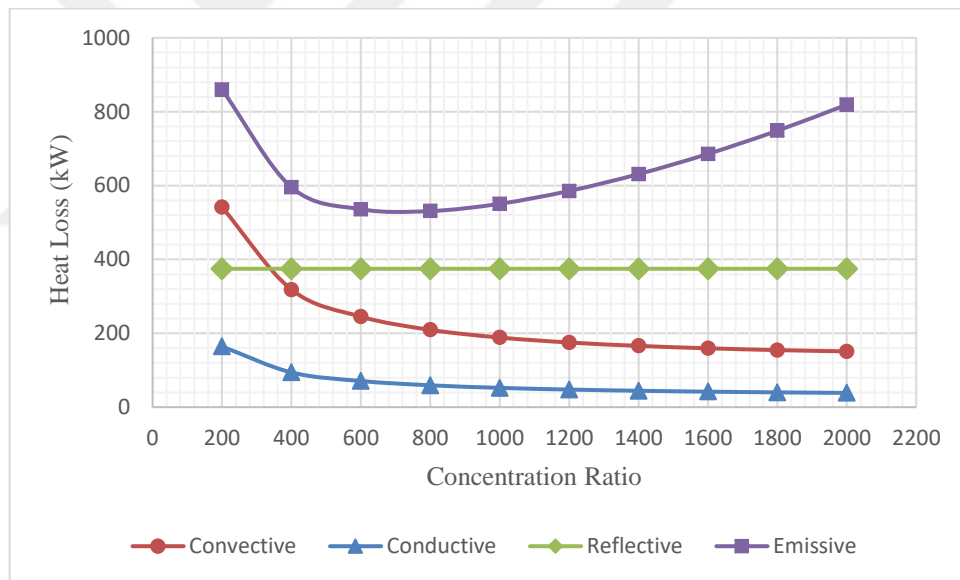


Figure 3.41 Effects of the concentration ratio of the receiver conduction, convection, emission and reflection heat losses

CHAPTER 4

OPTIMUM PERFORMANCE ANALYSIS OF AN SPTS WITH FINITE-RATE HEAT TRANSFER

A simplified schematic diagram of an SPTS considered in this study can be seen in Figure 3.1.

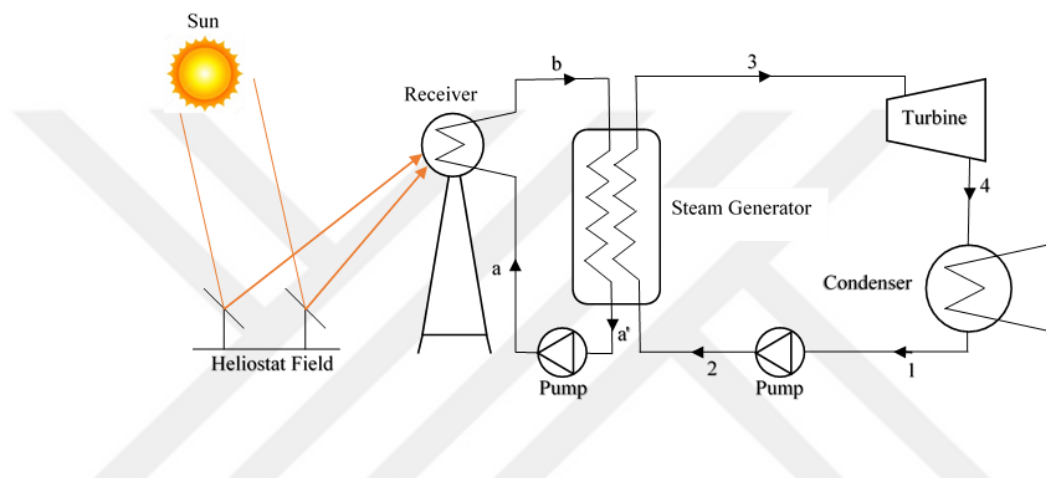


Figure 4.1 Simplified schematic diagram of an SPTS

In order to perform a performance analysis for this system first, its T-s diagram with a simple ideal Rankine cycle is drawn as seen in Figure 3.2. Then, it is modified to an equivalent Carnot-like cycle with finite-rate heat transfer.

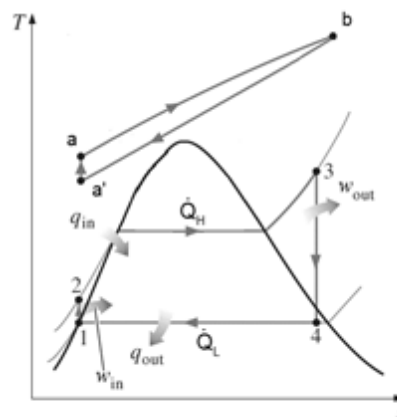


Figure 4.2 T-s diagram of a simple ideal Rankine cycle [modified from 43]

For the Carnot-like cycle, hot temperature of the working fluid is denoted by T_W and expressed by [26]

$$T_W = \frac{q}{\Delta S} \quad (4.1)$$

Carnot cycle efficiency shows the upper limit of a thermal efficiency for an ideal system. However, it is not sufficient in the case of the performance for an actual heat engine. In order to perform an analysis for a finite amount of power production with finite size devices, another ideal Carnot cycle heat engine model is needed [26]. Chambadal [49], Novikov [50] and Curzon-Ahlborn [51] are extended this Carnot cycle model by considering the difference between the temperatures of the working fluid and the thermal reservoirs. They studied the performance of their model for the maximum power (mp) and maximum power density (mpd) conditions. They obtained the efficiency of their Carnot heat engine at mp conditions by using the second law of thermodynamics as a constraint and taking only convective heat transfer on both sides of the system. The efficiency at mp conditions is obtained and given as

$$\eta_{mp} = 1 - \sqrt{\frac{T_L}{T_H}} \quad (4.2)$$

This efficiency is called Chambadal-Novikov-Curzon-Ahlborn efficiency or CNCA efficiency (η_{CNCA}) as an abbreviation by Bejan [52].

Maximum power density (mpd) as a ratio of the power output to the maximum specific volume in the cycle is defined to consider the effect of engine size on the performance analysis [53]. To show the thermal efficiency at mpd conditions is always greater than the efficiency at mp conditions, an analysis by using mpd criterion for Carnot-like heat engine also is needed [26,54].

The model of the Carnot-like heat engine for a solar power tower system with an ideal simple Rankine cycle working at mp and mpd conditions having finite temperature difference can be shown in Figure 3.3.

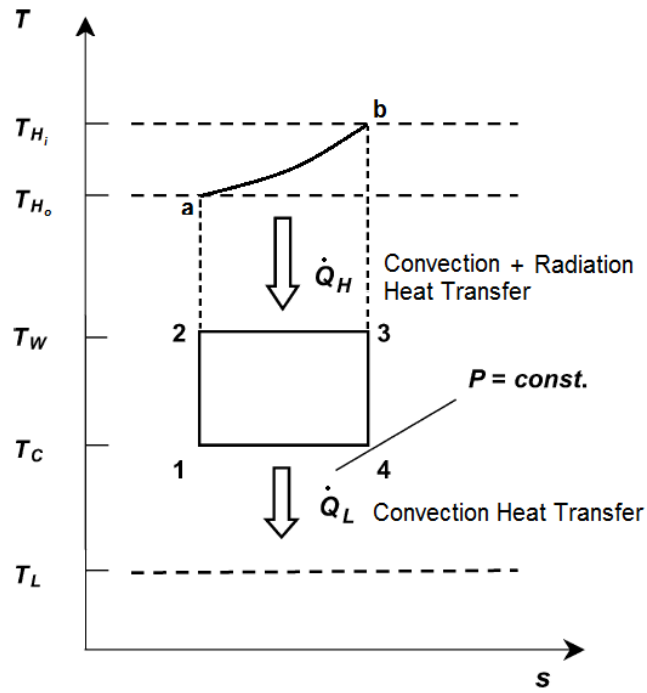


Figure 4.3 Carnot-like heat engine model

where $T_{H,i}$ and $T_{H,o}$ are expressed as inlet and outlet of the hot thermal reservoir and T_L is cold thermal reservoir. Furthermore, the hot and cold side working fluid temperatures are denoted by T_W and T_C . The heat transfer rate from the hot thermal reservoir to the working fluid is assumed by convection and radiation together which are expressed as

$$\dot{Q}_H = \alpha_{H,c}(T_H - T_W) + \alpha_{H,r}(T_H^4 - T_W^4) \quad (4.3)$$

$$\dot{Q}_H = \alpha_{H,c}(T_H - T_W) + \alpha_{H,r}(T_H - T_W)(T_H + T_W)((T_H^2 + T_W^2)) \quad (4.4)$$

where T_H is an expression to show its related to hot thermal reservoir, $\alpha_{H,c}$ and $\alpha_{H,r}$ are convection and radiation heat transfer per unit temperature difference at the hot side of the system, respectively and expressed as

$$\alpha_{H,c} = U_{H,c}A_H \quad (4.5)$$

$$\alpha_{H,r} = U_{H,r}A_H \quad (4.6)$$

$T_H - T_W$ can be defined as

$$T_H - T_W = \frac{(T_{H,i} - T_W) - (T_{H,o} - T_W)}{\ln\left(\frac{T_{H,i} - T_W}{T_{H,o} - T_W}\right)} = LMTD \quad (4.7)$$

where $LMTD$ is the logarithmic mean temperature difference.

In addition T_H can be defined as

$$T_H = LMTD + T_W \quad (4.8)$$

Thus \dot{Q}_H can be expressed as

$$\dot{Q}_H = \alpha_{H,c}(LMTD) + \alpha_{H,r}(LMTD)(LMTD + 2T_W) \left((LMTD + T_W)^2 + T_W^2 \right) \quad (4.9)$$

$$\begin{aligned} \dot{Q}_H = & \alpha_{H,c}(LMTD) \\ & + \alpha_{H,r}[(LMTD)^4 + 4(LMTD)^3T_W + 6(LMTD)^2T_W^2 \\ & + 4(LMTD)T_W^3] \end{aligned} \quad (4.10)$$

Similarly working fluid's heat transfer rate to the cold thermal reservoir is assumed only by convection and expressed as

$$\dot{Q}_L = \alpha_{L,c}(T_C - T_L) \quad (4.11)$$

where $\alpha_{L,c}$ is refer to convective heat transfer per unit temperature difference from cold thermal reservoir and expressed as

$$\alpha_{L,c} = U_{L,c}A_L \quad (4.12)$$

From the first law of thermodynamics

$$\dot{W} = \dot{Q}_H - \dot{Q}_L = \eta\dot{Q}_H \quad (4.13)$$

From the second law of thermodynamics, following equation can be written as

$$\frac{\dot{Q}_H}{T_W} = \frac{\dot{Q}_L}{T_C} \quad (4.14)$$

By substituting of Eqs. (3.8) and (3.9) into Eq. (3.11) yields a relationship between $T_{H,i}$, $T_{H,o}$, T_W and T_C as

$$T_C = T_L / \left[1 - \frac{\alpha_{H,c}}{\alpha_{L,c}} \left(\frac{LMTD}{T_W} \right) - \frac{\alpha_{H,r}}{\alpha_{L,c}} \frac{(LMTD)^4 + 4(LMTD)^3 T_W + 6(LMTD)^2 T_W^2 + 4(LMTD) T_W^3}{T_W} \right] \quad (4.15)$$

By substitution of Eq. (3.11) into Eq. (3.10) power output can be defined as

$$\dot{W} = \left(1 - \frac{T_C}{T_W} \right) \dot{Q}_H \quad (4.16)$$

And the power density can be expressed as

$$\dot{W}_d = \frac{\dot{W}}{V_{max}} \quad (4.17)$$

Where $V_{max} = \frac{mRT_C}{P_{min}}$, which is obtained from $V_{max} = V_4$ and $P_{min} = P_4$ while $P_4 = \text{constant}$.

In order to calculate \dot{W} , \dot{W}_d and η non dimensionalization process is carried out. *Non-dimensional allocation parameters* of the convection-convection and radiation-convection heat transfer can be written as

$$\beta_{c-c} = \frac{\alpha_{H,c}}{\alpha_{L,c}} \quad (4.18)$$

$$\beta_{r-c} = \frac{\alpha_{H,r} T_{H,i}^3}{\alpha_{L,c}} \quad (4.19)$$

Temperature ratios can be expressed as

$$\tau = \frac{T_L}{T_{H,i}} \quad (4.20)$$

$$x = \frac{T_W}{T_{H,i}} \quad (4.21)$$

$$y = \frac{T_{H,o}}{T_{H,i}} \quad (4.22)$$

Non-dimensional heat transfer rate can be defined as

$$\bar{Q}_H = \frac{\dot{Q}_H}{\alpha_{L,c} T_{H,i}} \quad (4.23)$$

Non-dimensional power output can be defined as

$$\bar{W} = \frac{\dot{W}}{\alpha_{L,c} T_{H,i}} \quad (4.24)$$

Non-dimensional power density can be defined as

$$\bar{W}_d = \frac{\dot{W}_d}{\left(\frac{\alpha_{L,c} P_{min}}{mR}\right)} \quad (4.25)$$

Thermal efficiency can be expressed as

$$\eta = 1 - \left(\frac{T_C}{T_W}\right) = \frac{\bar{W}}{\bar{Q}_H} \quad (4.26)$$

Non-dimensional LMTD can be expressed as

$$LMTD = \frac{1 - y}{Ln\left(\frac{1 - x}{y - x}\right)} = A \quad (4.27)$$

By substituting non-dimensional parameters into \bar{Q}_H , η , \bar{W} and \bar{W}_d , following equations can also be expressed as

$$\bar{Q}_H = \beta_{c-c}(A) + \beta_{r-c}[A^4 + 4xA^3 + 6x^2A^2 + 4x^3A] \quad (4.28)$$

$$\eta = 1 - \frac{\tau}{x - \beta_{c-c}(A) - \beta_{r-c}[A^4 + 4xA^3 + 6x^2A^2 + 4x^3A]} \quad (4.29)$$

$$\begin{aligned} \bar{W} &= \bar{q}_H \eta \\ &= [\beta_{c-c}(A) + \beta_{r-c}[A^4 + 4xA^3 + 6x^2A^2 + 4x^3A]] \left[1 - \frac{\tau}{x - \beta_{c-c}(A) - \beta_{r-c}[A^4 + 4xA^3 + 6x^2A^2 + 4x^3A]} \right] \end{aligned} \quad (4.30)$$

$$\begin{aligned} \bar{W}_d &= \frac{[\beta_{c-c}(A) + \beta_{r-c}[A^4 + 4xA^3 + 6x^2A^2 + 4x^3A]]}{x\tau} [x - \beta_{c-c}(A) \\ &\quad - \beta_{r-c}[A^4 + 4xA^3 + 6x^2A^2 + 4x^3A] - \tau] \end{aligned} \quad (4.31)$$

To obtain the maximum power and maximum power density functions for a solar energy driven heat engine, Eq. (4.30) and Eq. (4.31) should be differentiated with respect to x , then resultant equations sets to be equal to zero as $\frac{\partial \bar{W}}{\partial x} = 0$ and $\frac{\partial \bar{W}_d}{\partial x} = 0$, respectively. The calculation details are given in Appendix A and B.

The result of $\frac{\partial \bar{W}}{\partial x} = 0$ is given as

$$\begin{aligned} \frac{\partial \bar{W}}{\partial x} &= \left(\beta_{r-c}(y-1)^4 - 4\beta_{r-c}x(y-1)^3 \text{Ln} \left(\frac{x-1}{x-y} \right) \right. \\ &\quad \left. + 6\beta_{r-c}x^2(y-1)^2 \text{Ln} \left(\frac{x-1}{x-y} \right)^2 \right. \\ &\quad \left. - (\beta_{c-c} + 4\beta_{r-c}x^3)(y-1) \text{Ln} \left(\frac{x-1}{x-y} \right)^3 + (\tau-x) \text{Ln} \left(\frac{x-1}{x-y} \right)^4 \right) \\ &= \left(\beta_{r-c}(y-1)^4 - 4\beta_{r-c}x(y-1)^3 \text{Ln} \left(\frac{x-1}{x-y} \right) + 6\beta_{r-c}x^2(y-1)^2 \text{Ln} \left(\frac{x-1}{x-y} \right)^2 \right. \\ &\quad \left. - (\beta_{c-c} + 4\beta_{r-c}x^3)(y-1) \text{Ln} \left(\frac{x-1}{x-y} \right)^3 + x \text{Ln} \left(\frac{x-1}{x-y} \right)^4 \right) \end{aligned}$$

$$\begin{aligned}
& \left(4\beta_{r-c}(y-1)^4 - 12\beta_{r-c}x(y-1)^3 \text{Ln}\left(\frac{x-1}{x-y}\right) \right. \\
& \quad + 4\beta_{r-c}(y-1)^2(x+2x^2-y+xy) \text{Ln}\left(\frac{x-1}{x-y}\right)^2 \\
& \quad - (y-1)(\beta_{c-c} + 4\beta_{r-c}x(-2x^2-3y+3x(y+1))) \text{Ln}\left(\frac{x-1}{x-y}\right)^3 \\
& \quad \left. - 12\beta_{r-c}(x-1)x^2(x-y) \text{Ln}\left(\frac{x-1}{x-y}\right)^4 \right) + \\
& \tau \text{Ln}\left(\frac{x-1}{x-y}\right)^4 \left(-\beta_{r-c}(y-1)^3 + 4\beta_{r-c}x(y-1)^2 \text{Ln}\left(\frac{x-1}{x-y}\right) \right. \\
& \quad \left. - 6\beta_{r-c}x^2(y-1) \text{Ln}\left(\frac{x-1}{x-y}\right)^2 + (\beta_{c-c} + 4\beta_{r-c}x^3) \text{Ln}\left(\frac{x-1}{x-y}\right)^3 \right) \\
& \left(4\beta_{r-c}(y-1)^5 - 12\beta_{r-c}x(y-1)^4 \text{Ln}\left(\frac{x-1}{x-y}\right) \right. \\
& \quad + 4\beta_{r-c}(y-1)^3(x+2x^2-y+xy) \text{Ln}\left(\frac{x-1}{x-y}\right)^2 \\
& \quad - (y-1)^2(\beta_{c-c} + 4\beta_{r-c}x(-2x^2-3y+3x(y+1))) \text{Ln}\left(\frac{x-1}{x-y}\right)^3 \\
& \quad \left. - 12\beta_{r-c}(x-1)x^2(x-y)(y-1) \text{Ln}\left(\frac{x-1}{x-y}\right)^4 - (x-1)(x-y) \text{Ln}\left(\frac{x-1}{x-y}\right)^5 \right) \\
& = 0 \tag{4.32}
\end{aligned}$$

Similarly, the result of $\frac{\partial \bar{W}_d}{\partial x} = 0$ is given as

$$\begin{aligned}
\frac{\partial \bar{W}_d}{\partial x} &= 8\beta_{r-c}^2 x(y-1)^8 + \beta_{r-c}^2 (y-1)^7 (x-57x^2-y+xy) \text{Ln}\left(\frac{x-1}{x-y}\right) \\
& \quad + 168\beta_{r-c}^2 x^3(y-1)^6 \text{Ln}\left(\frac{x-1}{x-y}\right)^2 \\
& \quad - 2\beta_{r-c}x(y-1)^5(5\beta_{c-c} \\
& \quad + 14\beta_{r-c}x(x+9x^2-y+xy)) \text{Ln}\left(\frac{x-1}{x-y}\right)^3 \\
& \quad + 2\beta_{r-c}(y-1)^4(\beta_{c-c}(17x^2+y-x(y+1)) +
\end{aligned}$$

$$\begin{aligned}
& 2x \left(\tau + x \left(-1 + 4\beta_{r-c}x(10x^2 - 7y + 7x(y+1)) \right) \right) \operatorname{Ln} \left(\frac{x-1}{x-y} \right)^4 \\
& \quad + \beta_{r-c}(y-1)^3 \left(\tau(x - 13x^2 - y + xy) \right. \\
& \quad \left. + 12x^3 \left(1 - 3\beta_{c-c} + \beta_{r-c}x(5x^2 + 17y - 17x(y+1)) \right) \right) \\
& \operatorname{Ln} \left(\frac{x-1}{x-y} \right)^5 + 2x(y-1)^2 \left(\beta_{c-c}^2 + 2\beta_{c-c}\beta_{r-c}x(x^2 - 3y + 3x(y+1)) \right. \\
& \quad - 2\beta_{r-c}x(2x^2 + 40\beta_{r-c}x^5 - y + 48\beta_{r-c}x^3y \\
& \quad \left. - 48\beta_{r-c}x^4(y+1) + x(1 - 3\tau + y)) \right) \operatorname{Ln} \left(\frac{x-1}{x-y} \right)^6 \\
& \quad + (y-1) \left(\beta_{c-c}x \left(-\tau + x(1 + 16\beta_{r-c}(x-1)x(x-y)) \right) \right. \\
& \quad - \beta_{c-c}^2(x-1)(x-y) \\
& \quad + 2\beta_{r-c}x^2 \left(\tau(x^2 + 3y - 3x(y+1)) \right. \\
& \quad \left. + 2x(-2x^2 + 20\beta_{r-c}x^5 - 3y + 20\beta_{r-c}x^3y + 3x(y+1) \right. \\
& \quad \left. \left. - 20\beta_{r-c}x^4(y+1)) \right) \right) \operatorname{Ln} \left(\frac{x-1}{x-y} \right)^7 + (x-1)(\beta_{c-c}\tau \\
& \quad + 4\beta_{r-c}x^3(-2\tau + 3x))(x-y) \operatorname{Ln} \left(\frac{x-1}{x-y} \right)^8 = 0 \quad (4.33)
\end{aligned}$$

Finally, \dot{W}_{max} , $\dot{W}_{d,max}$, η_{mp} and η_{mpd} can be obtained by solving Equations (4.32) and (4.33) numerically by using the real roots of x which is between 0 and 1.

The real roots of these equations provide the optimum design parameters for the *Carnot-like heat engine* of the solar power tower system at mp and mpd conditions for any given τ , y , β_{c-c} and β_{r-c} values.

Equations (4.28) – (4.31) define the generalized performance functions of the solar driven Carnot heat engine. Equations (4.32) and (4.33) indicate the optimum conditions where the power output is maximized [26].

CHAPTER 5

OPTIMUM PERFORMANCE ANALYSIS RESULTS

In order to determine the effects of convection-convection ($\beta_{c-c} = \alpha_{H,c}/\alpha_{L,c}$) and convection-radiation allocation parameters ($\beta_{r-c} = \alpha_{H,r}T_{Hi}^3/\alpha_{L,c}$), reservoir temperature ratio ($\tau = T_L/T_{Hi}$), molten salt temperature ratio ($y = T_{Ho}/T_{Hi}$) and design parameter ($x = T_W/T_{Hi}$) on the thermal efficiency at maximum power (mp) and maximum power density (mpd) conditions, a numerical study is carried out. In this section, comparisons for the design parameters of the Carnot like heat engines for SPTS working at mp and mpd conditions are provided.

Due to the constraints caused by the nature of SPTS and performance optimization technique, some rules need to be established. These are,

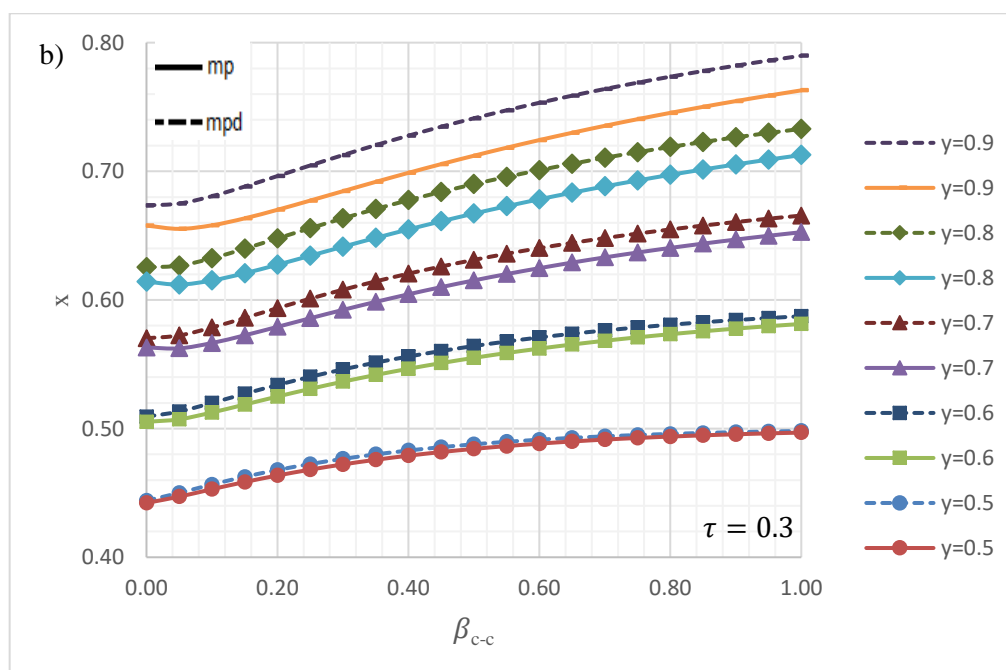
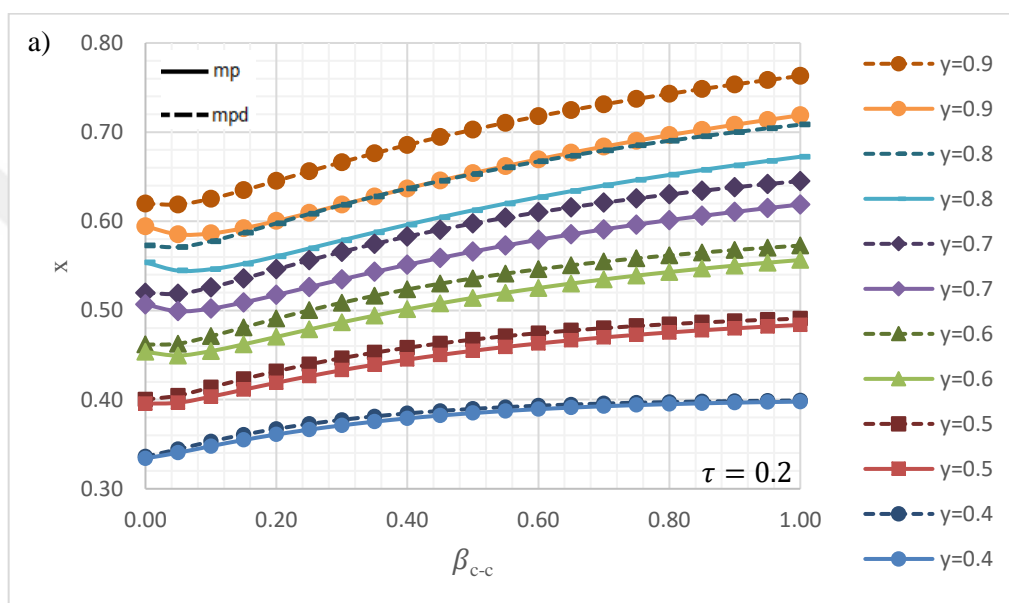
- T_L is assumed 300 K.
- Due to the solidification problem caused by the molten salt, T_{Ho} cannot be less than 494 K (221 C).
- Because of the nature of heat exchangers, T_w cannot be more than T_{Ho} .
- T_{Hi} 's maximum temperature is assumed 1500 K.

Due to the assumptions mentioned above, y is investigated between the values of 0.4–0.9. depending on τ values which are investigated between the 0.2–0.5. Finally β_{c-c} and β_{r-c} values are investigated between 0.0–1.0.

The change of x with relation to β_{c-c} for different τ and y values when $\beta_{r-c} = 0.1$ mp and mpd conditions are given in Figure 5.1.

The change of reservoir temperatures ratio and molten salt temperature ratio can be done in two ways which can be seen from their formulas ($\tau = T_L/T_{Hi}$, $y = T_{Ho}/T_{Hi}$). The increase in y values are caused by the change of T_{Hi} also affects the design parameter ($x = T_W/T_{Hi}$) which causes further increases of design parameters as seen in Figure 5.1. Furthermore, according to the figure at mpd conditions x values shows

higher increase than the mp conditions. Also at lower τ and β_{c-c} values, x values show slight decrease before start to increase. In addition increasing the y values which means the hot source temperature change is to become smaller, further increase the x values. While x values at $\tau = 0.2$ and $y = 0.4$ shows change around 0.33–0.40 range for both mp and mpd conditions, increasing τ and y values to 0.5 and 0.9, respectively, increases x values to a range around 0.75–0.83 for mp conditions and 0.76–0.84 for mpd conditions.



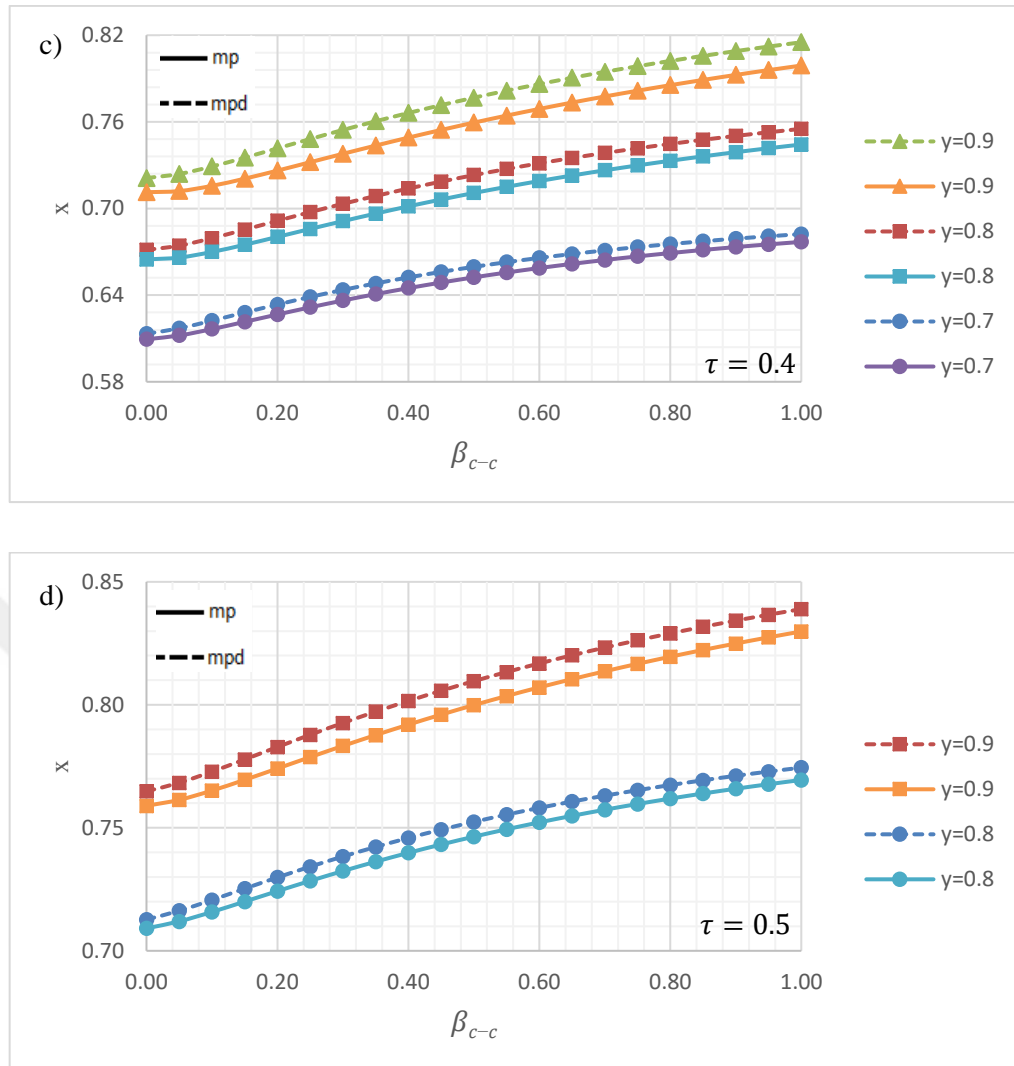
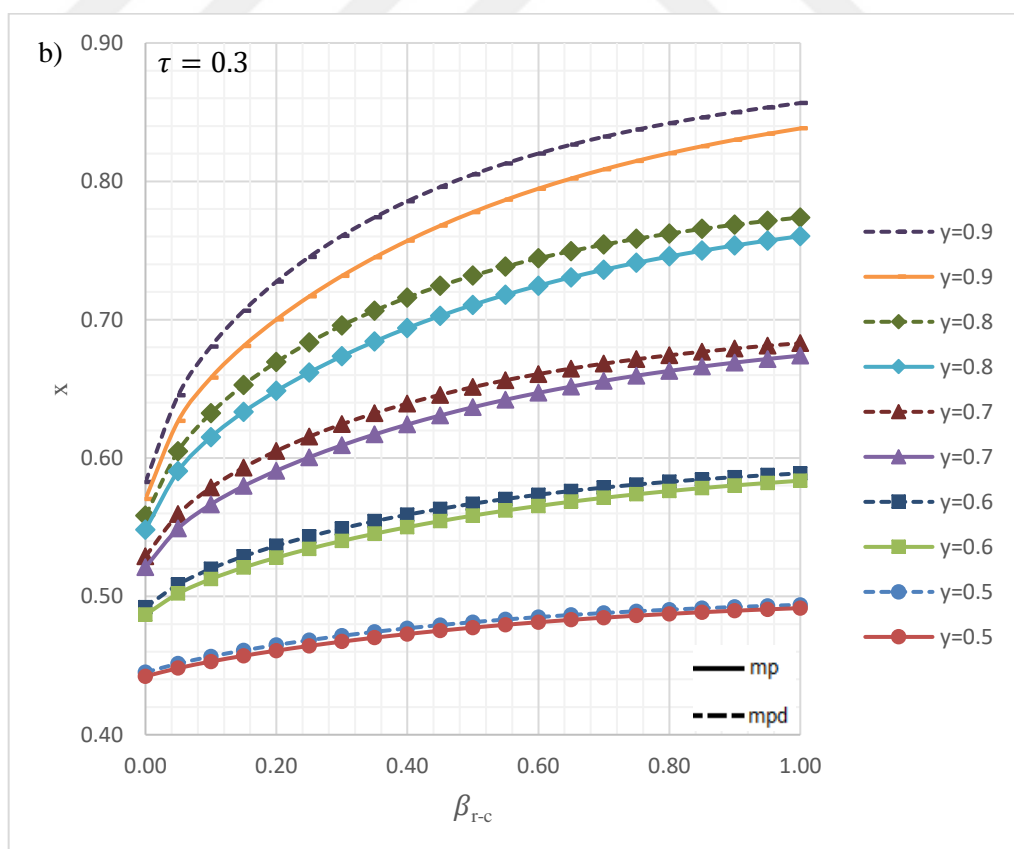
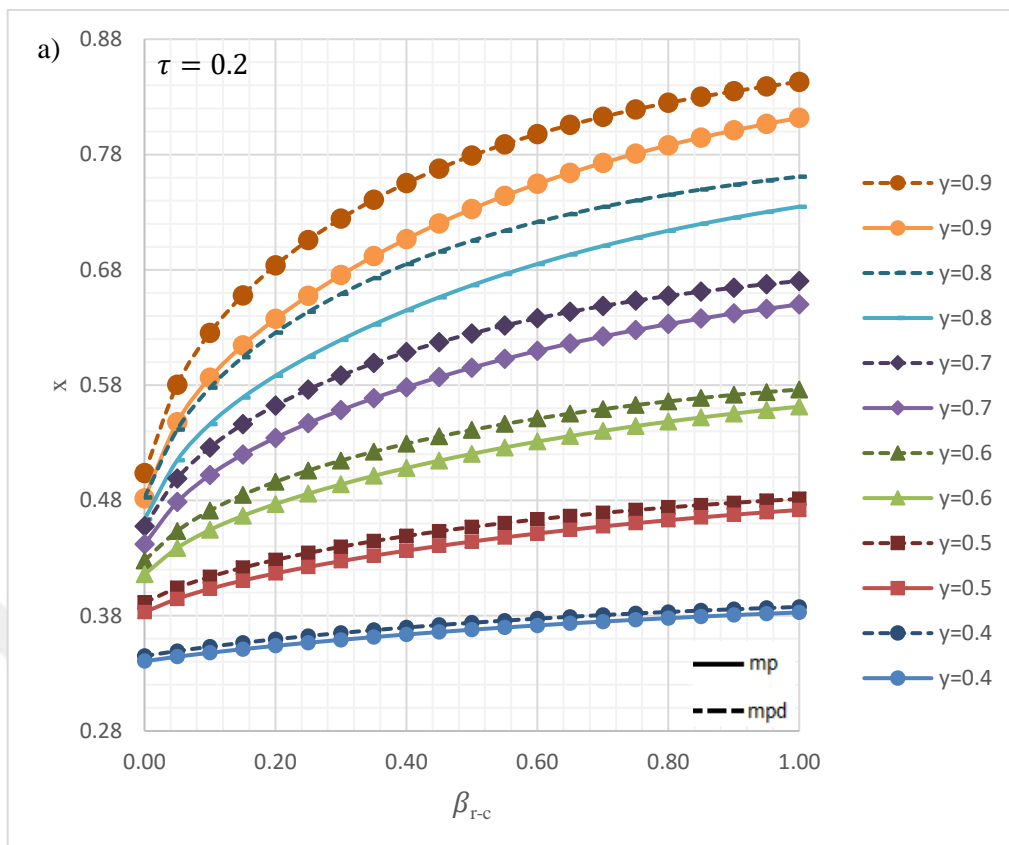


Figure 5.1 Change of x with respect to β_{c-c} for different τ and y values when $\beta_{r-c} = 0.1$

Furthermore, the change of x with relation to β_{r-c} for different τ and y values when $\beta_{c-c} = 0.1$ at mp and mpd conditions are given in Figure 5.2. According to the figure increasing the β_{r-c} values increase x values with a decreasing increment. Similar to the effects of the β_{r-c} change, increase of τ and y values further increases x values. While x values at $\tau = 0.2$ and $y = 0.4$ shows change around 0.34–0.39 range for both mp and mpd conditions, increasing τ and y values to 0.5 and 0.9, respectively, increases x values to a range around 0.71–0.88 for mp mpd conditions. Also noted that at mpd conditions always yield an higher x values compare to the mp conditions.



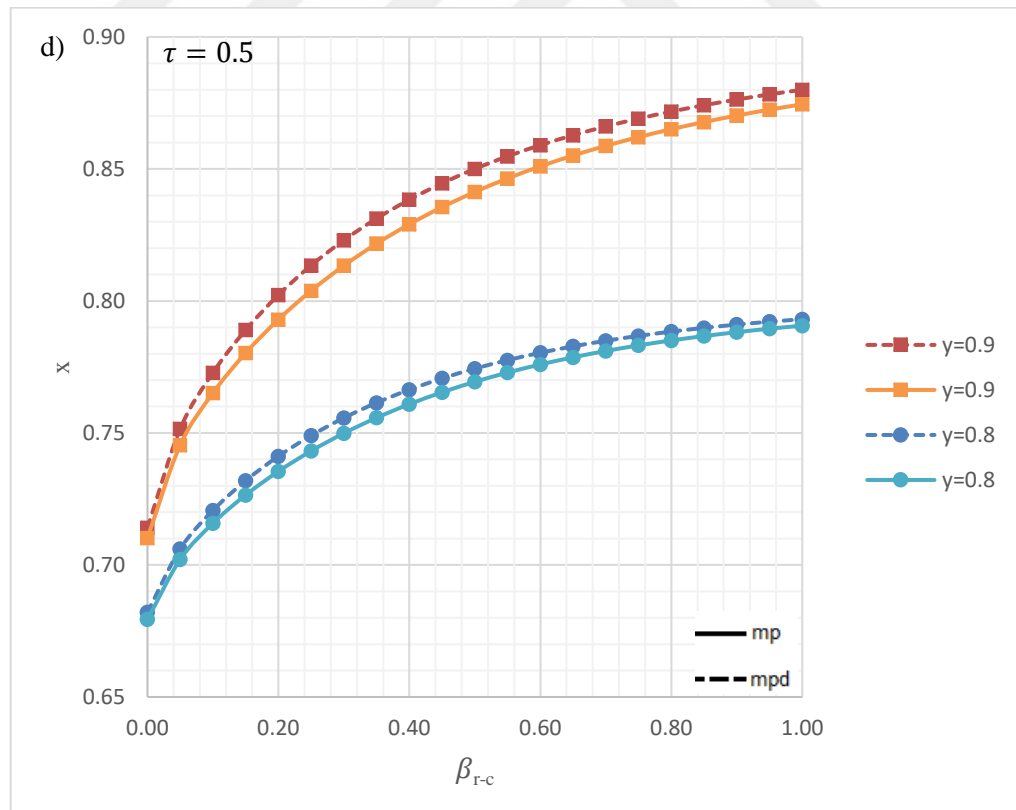
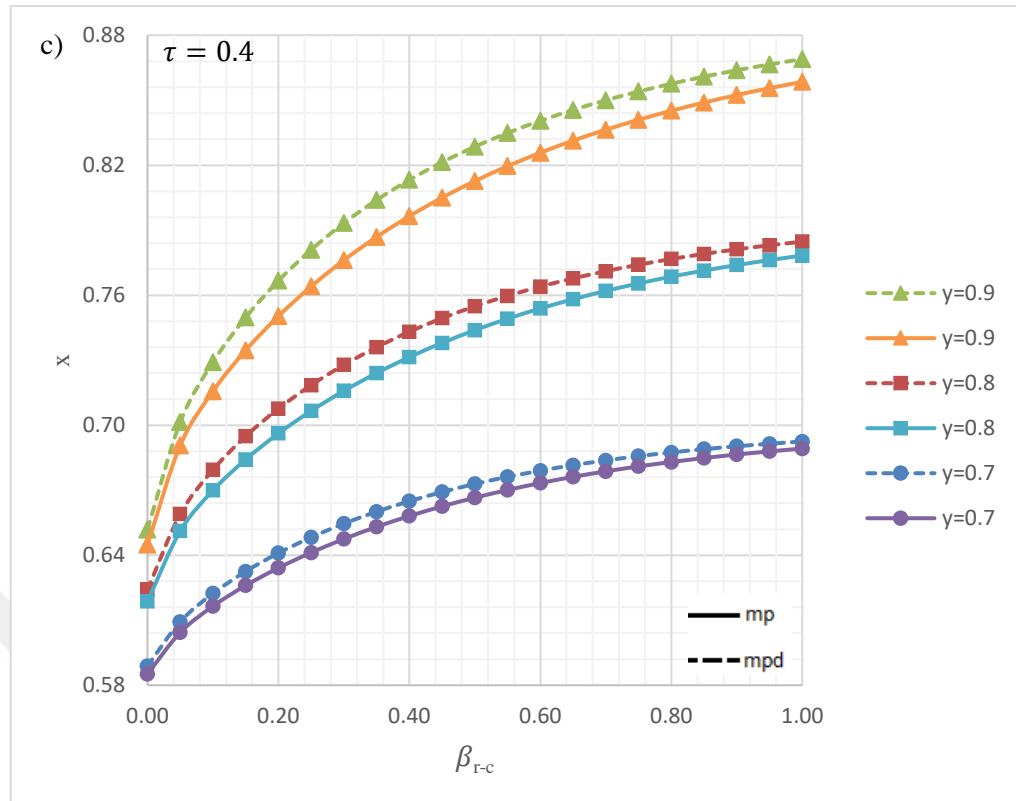
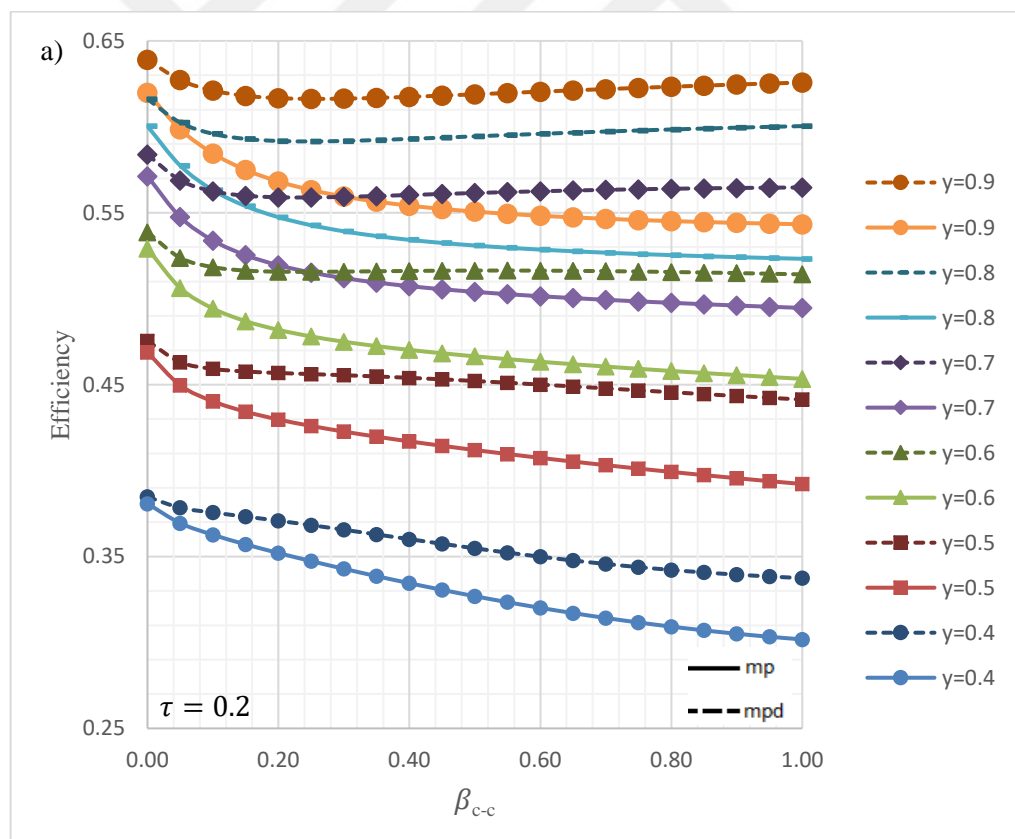
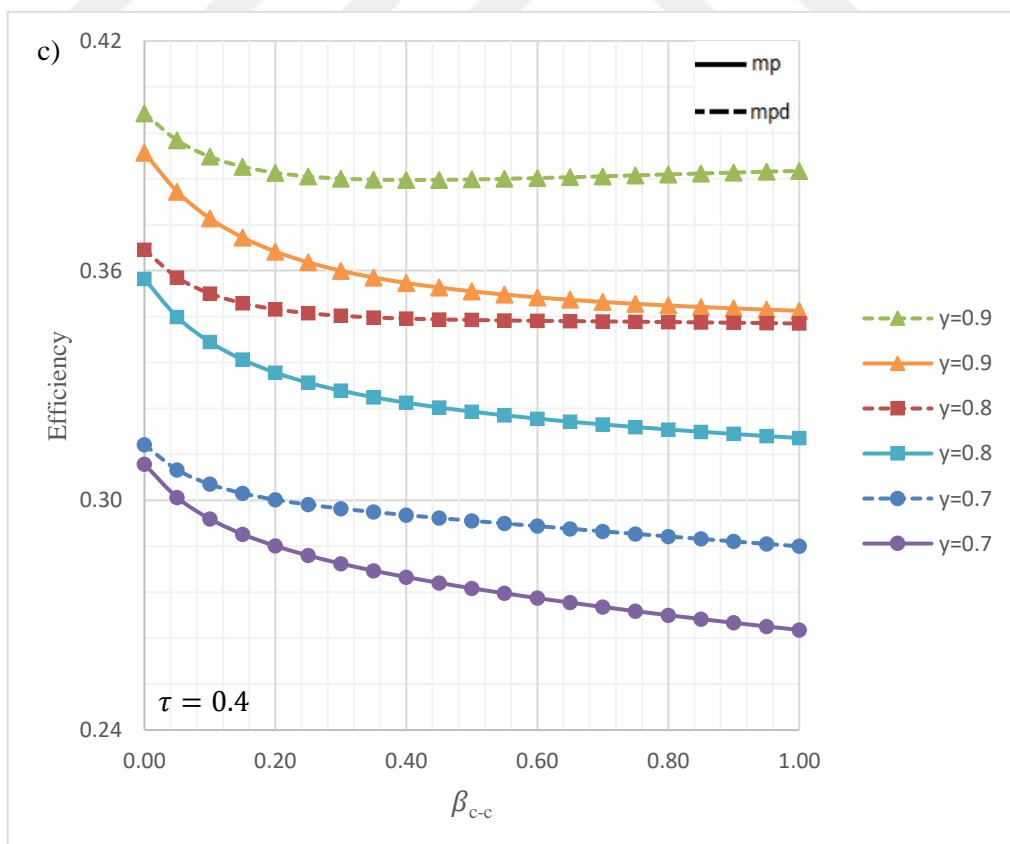
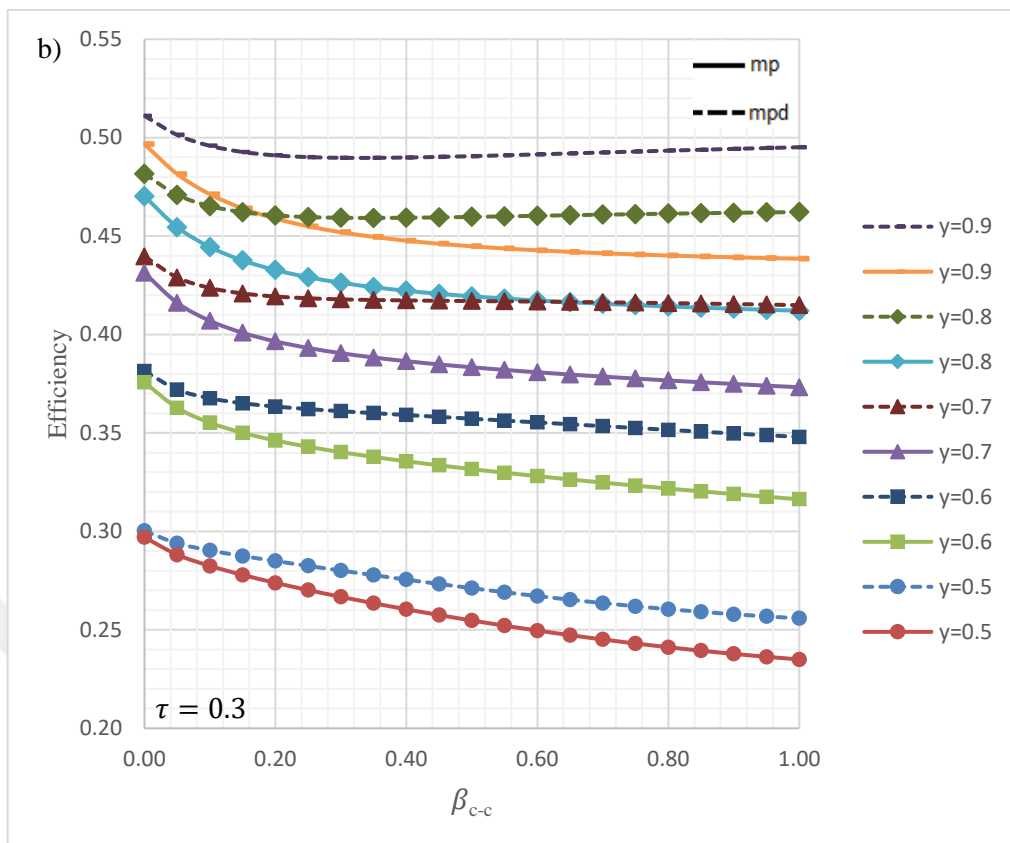


Figure 5.2 Change of x with respect to β_{r-c} for different τ and γ values when $\beta_{c-c} = 0.1$

Similarly, the change of η with relation to β_{c-c} for different τ and y values when $\beta_{r-c} = 0.1$ at mp and mpd conditions are given in Figure 5.3. According to the figure increasing the β_{c-c} decrease the efficiencies for both mp and mpd conditions with a decreasing increment. Also it is noted, that the decrease of the efficiencies at the mp conditions is greater than the mpd conditions which proves the argument presented by the Shain et al. [55]. In addition it is seen that at lower τ and y values Change of the efficiencies became more linear. Furthermore, according to the figure while increasing the y values causes efficiencies to increase, increasing the τ values causes the efficiencies to decrease greater percentages. While efficiencies at $\tau = 0.2$ and $y = 0.9$ shows change around 62–54% range for mp conditions and 64–62% range for mpd conditions, increasing τ values to 0.5 and at $y = 0.9$, yields efficiencies in a range around 30–27% for mp conditions and 31–29% at mpd conditions.





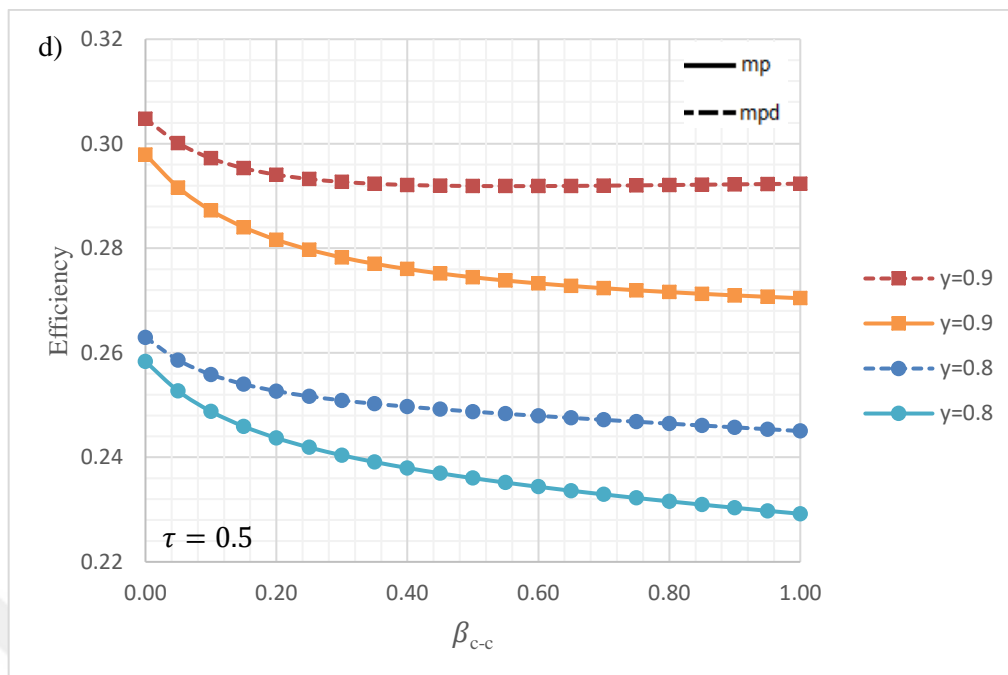
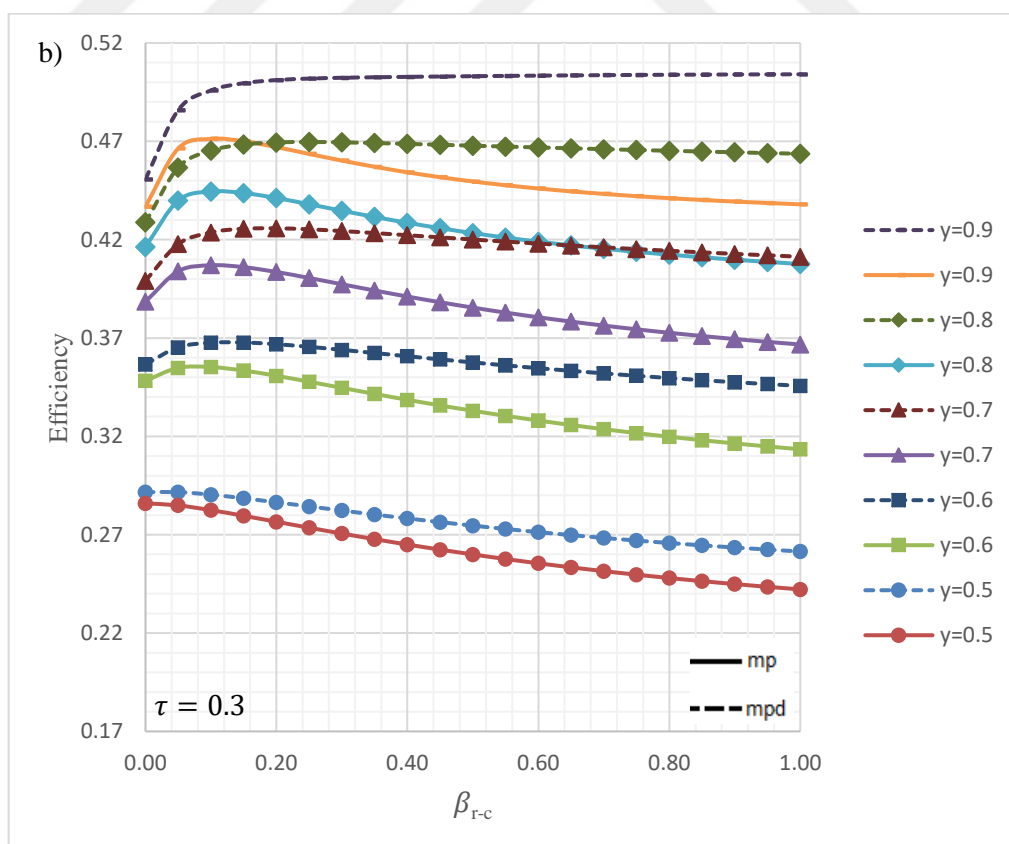
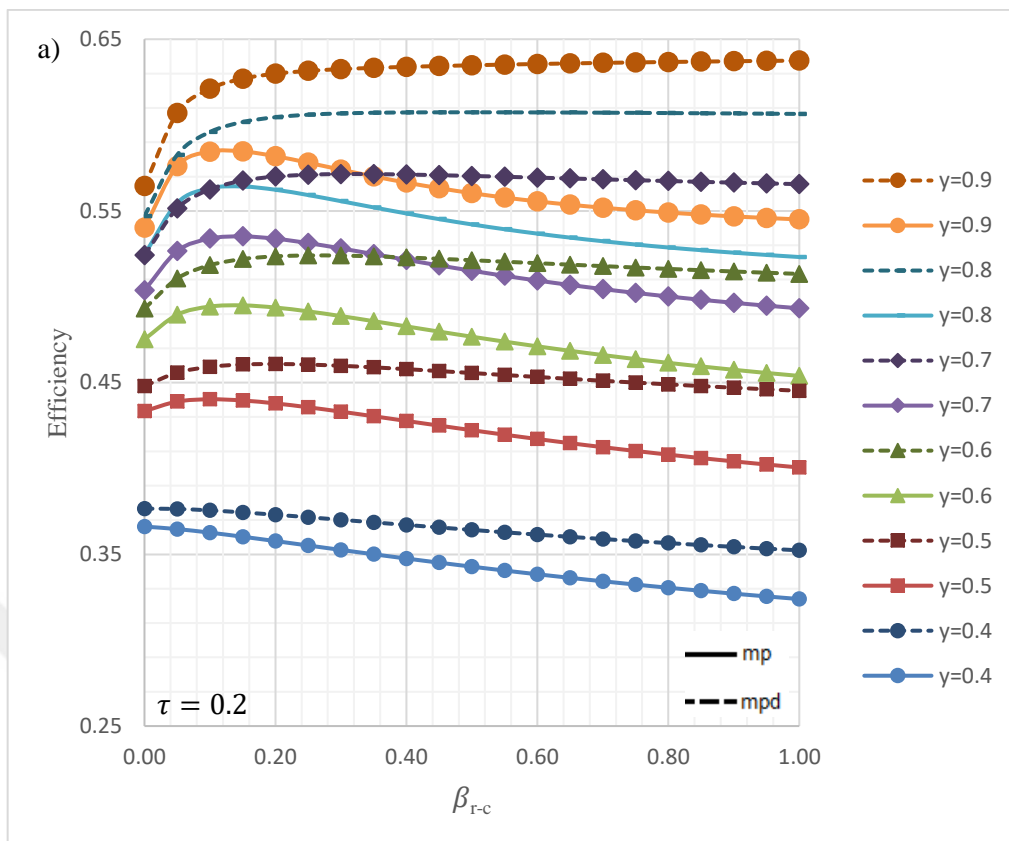


Figure 5.3 Change of η with respect to β_{c-c} for different τ and y values when $\beta_{r-c} = 0.1$

In addition, the change of η with relation to β_{r-c} for different τ and y values when $\beta_{c-c} = 0.1$ at mp and mpd conditions are given in Figure 5.4. According to the figure change of β_{r-c} values from 0 to 0.15 causes efficiencies to increase substantially for both mp and mpd conditions. However further increase of β_{r-c} values effects the efficiencies negatively causes them to decrease. In addition at higher y values efficiencies at the mpd conditions show an increase with a change of β_{r-c} . Furthermore, Similar to Figure 4.3 while increasing the y values causes efficiencies to increase, increasing τ values causes the efficiencies to decrease greater percentages. While efficiencies at $\tau = 0.2$ and $y = 0.9$ shows change around 58–54% range for mp conditions and 56–64% range for mpd conditions, increasing τ values to 0.5 and at $y = 0.9$, yields efficiencies in a range around 29–26% for mp conditions and 27–30% at mpd conditions.



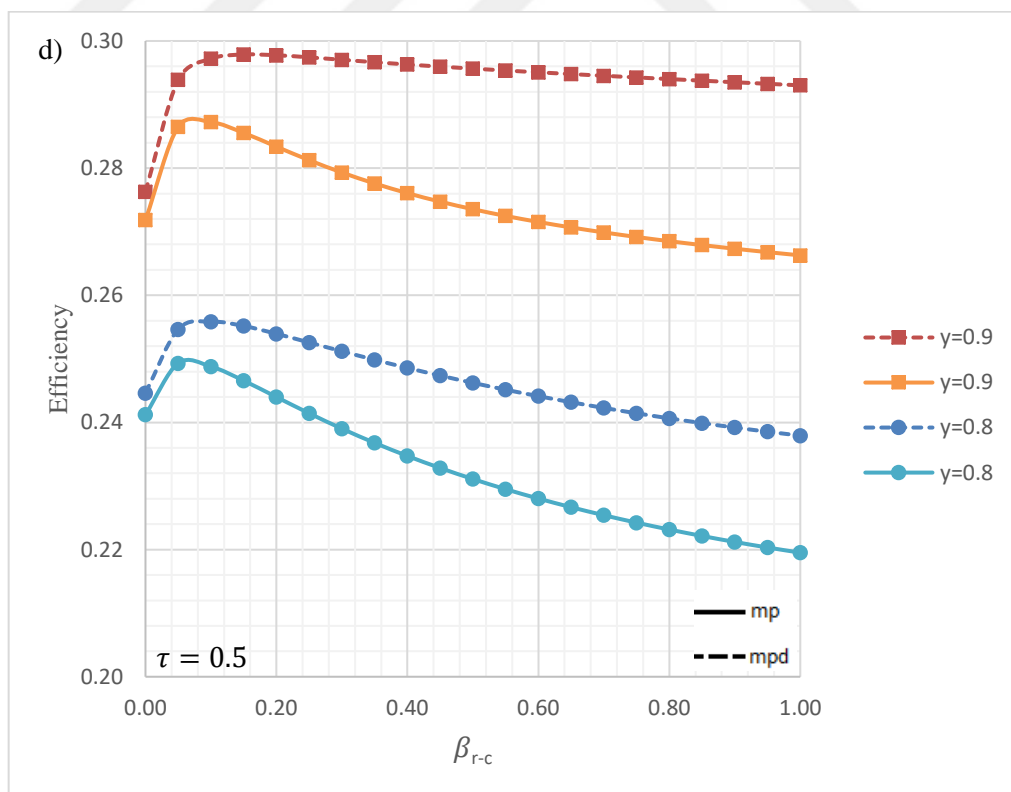
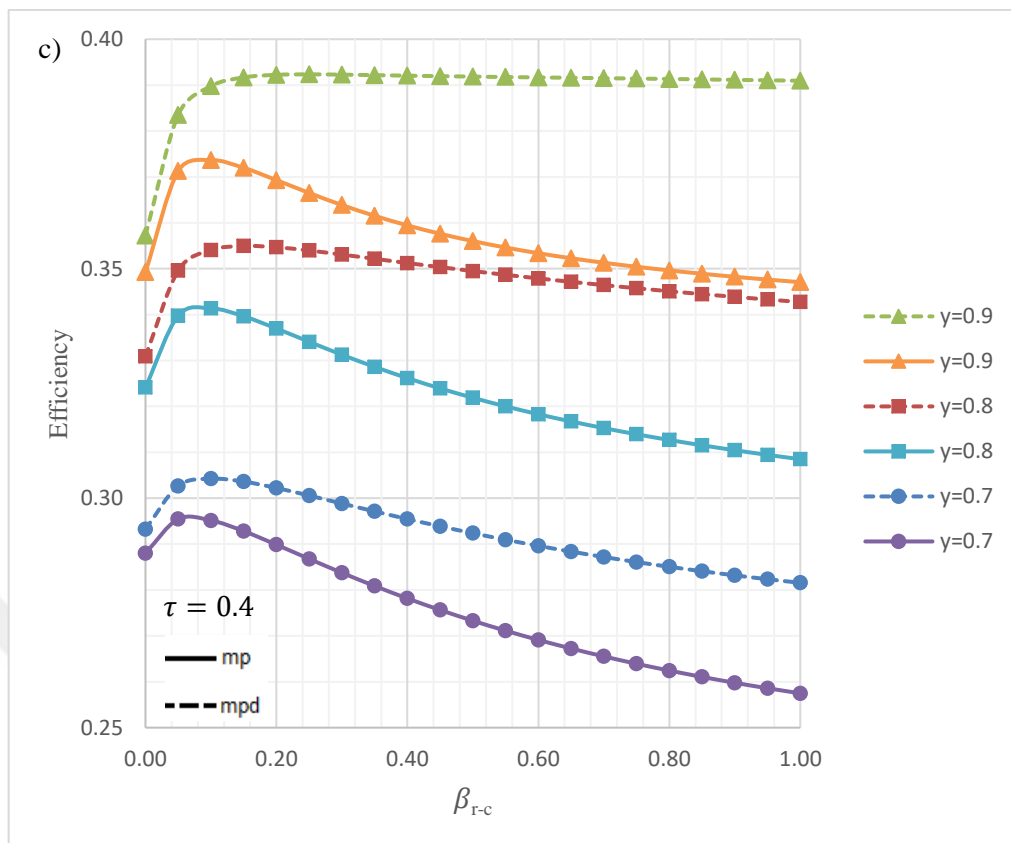


Figure 5.4 Change of η with respect to β_{r-c} for different τ and γ values when $\beta_{c-c} = 0.1$

Also, variation of η is given as a 3d plot with respect to β_{r-c} and β_{c-c} with different τ and y values at mp and mpd conditions can be seen in Figure 5.5 and Figure 5.6, respectively. As seen from the figures efficiencies at mpd conditions is always greater than the efficiencies at mp conditions for the all β_{r-c} and β_{c-c} values. Furthermore, at higher β_{r-c} and β_{c-c} values regardless of τ and y values efficiencies change became minimal. In addition at lower β_{r-c} and β_{c-c} values efficiencies at mp and mpd conditions are close to each other. However increasing β_{r-c} and β_{c-c} values causes the gap between them to widen.

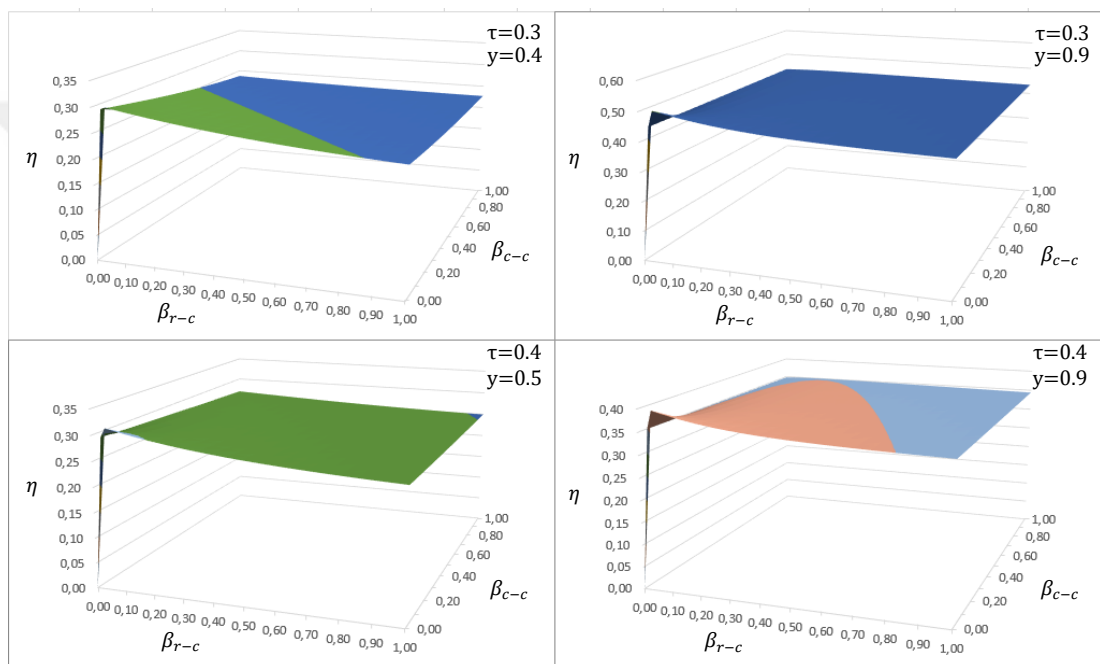


Figure 5.5 Variation of η with respect to β_{r-c} and β_{c-c} with different τ and y values at mp conditions

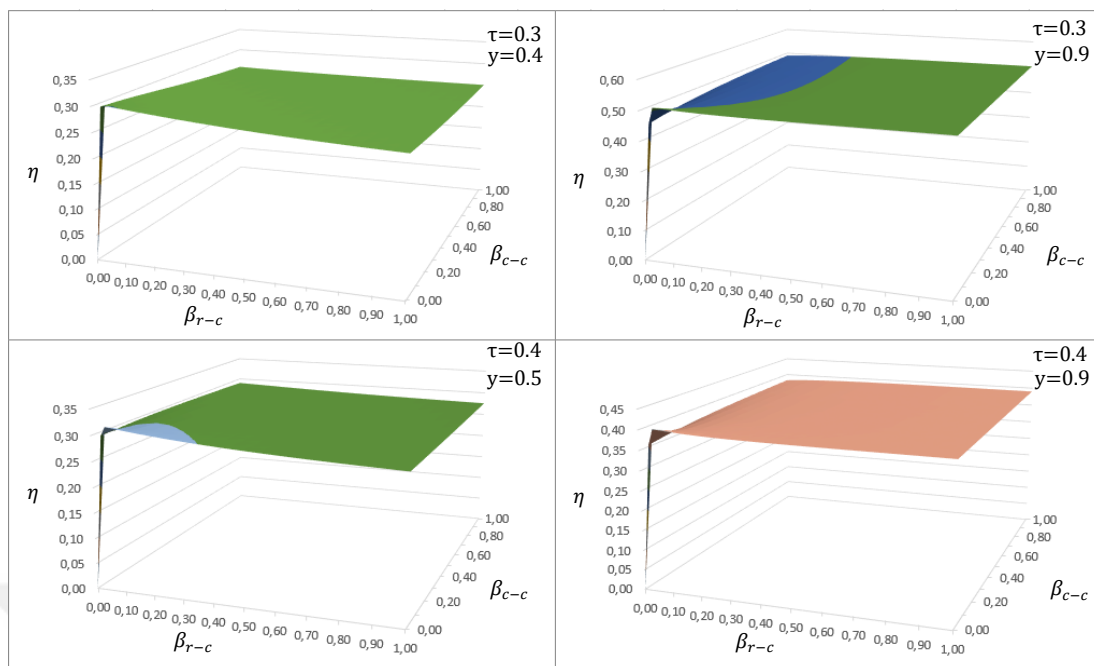


Figure 5.6 Variation of η with respect to β_{r-c} and β_{c-c} with different τ and y values at mpd conditions

The effect of τ on the efficiencies at constant y and 0.1 β_{r-c} and β_{c-c} values can be seen in Figure 5.7. As seen from the figure $\eta_{mp,r-c}$ and $\eta_{mpd,r-c}$ is greater than the η_{CNCA} and $\eta_{mpd,c-c}$. Further more efficiencies working at the mpd conditions are always bigger than the ones working at the mp conditions.

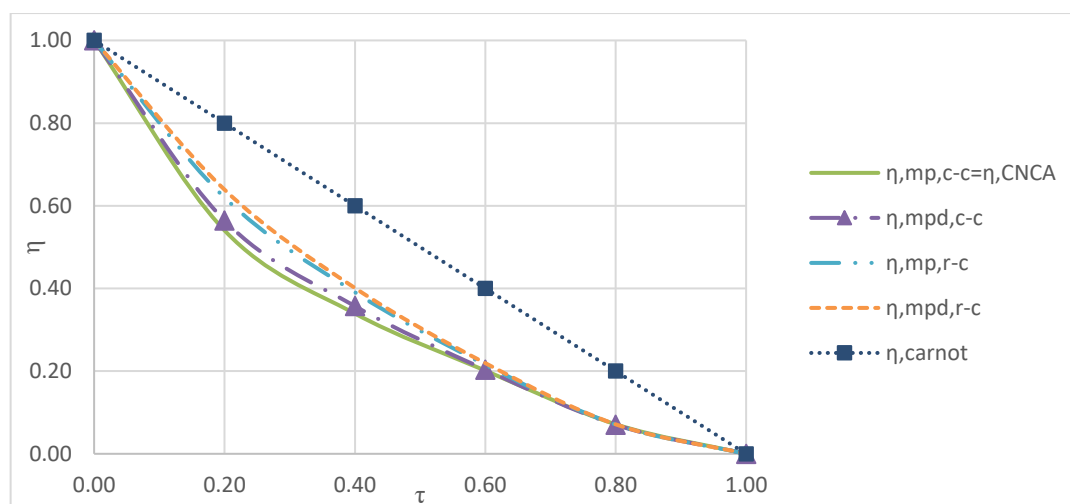


Figure 5.7 Effect of τ on the efficiencies at $y = 0.9$ and different cases of $\beta_{r-c} = 0.1$ and $\beta_{c-c} = 0.1$ values

CHAPTER 6

DISCUSSION AND CONCLUSION

In this study, first, an energy and exergy analysis for a solar power tower system with a cavity receiver and a molten salt as its working fluid is achieved. The parameters needed for the analysis are taken from the literature. After the analysis, design parameters such as energy and exergy efficiencies for the receiver and system, the surface temperature of the receiver and total heat loss of the receiver are obtained. Then, the effects on the design parameters of the system are investigated by changing direct normal irradiation, heliostat field area, reflectivity and emissivity of the receiver, tube diameter of the receiver, view factor and concentration ratio in specific ranges.

The energy and exergy analysis is carried out by dividing the system into four subsystems which are the heliostat field subsystem, receiver subsystem, steam generation subsystem and power generation subsystem. After the analysis, energy and exergy efficiencies of each subsystem and overall system are obtained. From the results of this analysis, it is understood that energy efficiencies of the system differ dramatically as compared to the exergy efficiencies of the system. For example, highest energy loss occurs at the power generating system even though it has the highest exergy efficiency. This behavior is caused by the quality of the energy used in the different subsystems, which would not be seen from the energy analysis alone.

The energy and exergy efficiencies of the receiver and the system, surface temperature of the receiver and total heat loss of the receiver are depicted by changing of the direct normal irradiation in a range of 200–2000 W/m². It is seen from the results that surface temperature and total heat loss of the receiver are changed linearly. However, even if both of them are increased while the surface temperature of the receiver is increased 50% of its initial temperature, total heat loss of the receiver is increased over three fold of its initial value. Receiver and overall energy and exergy efficiencies are showed an unexpected behavior. They increased

with a decreasing rate when direct normal irradiation increased. For example, when DNI is increased two times from 200 to 400 Energy and exergy efficiencies of the receiver are increased more than 13 and 7%, respectively. However when DNI is increased ten times from 200 to 2000, energy and exergy efficiencies of the receiver are increased about 21 and 12%, respectively.

Heliostat field area of the system is changed between 3000 m² and 18000 m². By depending on the change of heliostat field area of the system, the surface temperature of the receiver increased linearly. In addition, because of emissive heat loss depending on the surface temperature of the receiver, the total heat loss of receiver increases with a slightly increasing rate. Energy and exergy efficiencies of the receiver and overall system are increased with a decreasing rate. The increase in the efficiencies with heliostat field area is increased from 300 to 6000 m² are bigger than the increase in the efficiencies when heliostat field area increased from 6000 to 18000 m².

Reflectivity and emissivity of the receiver changed in a range of 0.1–0.9. The total heat loss of the receiver is increased substantially with the increase of the reflectivity and emissivity. Furthermore, it is observed that receiver and the overall system energy and exergy efficiencies are decreased for the increase of both parameters. However, the effect of emissivity on the receiver and the overall system energy and exergy efficiencies are not affected as much as the case of the reflectivity. Increasing the emissivity from 0.1 to 0.9 are causing the energy and exergy efficiencies of the receiver to drop about 4% and 2.5%, respectively. In addition, the change at the overall system energy and exergy efficiencies are noted about 1%. On the other hand, increasing the reflectivity from 0.1 to 0.9, caused the energy and exergy efficiencies of the receiver to drop 65% and 37.5%, respectively. Furthermore, the change at the overall system energy and exergy efficiencies are noted around 17.5% and 19%. Respectively. It is understood that even though both parameters are important for the system efficiencies, reflectivity is one of the most important parameters that affect the efficiencies of the system.

Tube diameter of receiver changed in the range of 8–24. The surface temperature of the receiver is shown a continuous decrease with a decreasing rate, From the behavior of the total heat loss of the receiver with a change of the tube diameter, it is understood that at the smaller tube diameters with < 18 mm, the total heat loss of the receiver is effected mainly by emissive heat loss. However, at the bigger tube diameters with > 18 mm, the variation of total heat loss of the receiver is affected by convective and conductive heat losses. Furthermore, calculations are showed that about 16 mm tube diameter is yielded the highest efficiencies for the receiver and the system.

View factor can be changed depending on the either aperture area or receiver surface area. The change of the view factor is changed in a range of 0.1–1.0 for two different areas. Calculations are showed that surface temperature of the receiver increases from about 720 K to 950 K depending on receiver surface area. The total heat loss of the receiver is increased linearly from about 350 kW to 1450 kW depending on aperture area. However, when view factor is depending on the surface area, the total heat loss of the receiver is first decreased from about 1550 kW to 1000 kW until the view factor of 0.4, then is increased up to about 1400 kW at the view factor of 1.0.

The energy and exergy efficiencies of the receiver with a change of view factor related to aperture area are decreased and are found between the ranges of about 87–97% and 51–57%, respectively. Furthermore, the energy and exergy efficiencies of the overall system via view factor related to aperture area are decreased and are found between the ranges of about 24–27 and 26–29%, respectively.

When the view factor is changed related to receiver surface area, energy and exergy efficiencies increase until the view factor of 0.4. However, after the view factor of 0.4, both efficiencies decrease linearly up to 1.0. Energy and exergy efficiencies of the receiver via the view factor related to receiver surface area change in the range of about 87–92% and 51–54%, respectively. In addition, energy and exergy efficiencies of the overall system via the view factor related to receiver surface change in the range of about 24–26% and 25–27%, respectively.

In this study, change of concentration ratio is investigated in a range of 200–2000. The surface temperature is increased from about 750 K to 1350 K via concentration ratio in this range. So, the total heat loss of the receiver first decreases from about 1950 kW to about 1150 kW between 200–1000 of the concentration ratio, and then increases until concentration ratio of 2000 at about 1400 kW of a total heat loss of the receiver. Energy and exergy efficiencies of the receiver via concentration ratio change in a range about 83–90% and 48–53%, respectively. As a result, energy and exergy efficiencies of the overall system via concentration ratio change in a range of about 23–25% and 24–27%, respectively.

In this study, a performance optimization for the solar power tower system is also carried out. For this purpose, a *Carnot-like heat engine* is modeled by using the non-dimensionalized design parameters. At the hot side of the Carnot-like heat engine is considered to receive the heat as convection and radiation in order to simulate receiver of the system. Furthermore, cold end of the Carnot-like heat engine considered to be working only by convection heat transfer in order to simulate the condenser of the Rankine cycle. For non-dimensionalization process, temperature ratios (τ , y , and x), Non-dimensional allocation parameters (β_{c-c} and β_{r-c}), nondimensional heat transfer rate (\bar{q}_H), non-dimensional power output (\bar{w}) and non-dimensional power density (\bar{w}_d) are defined. Then, two main equations which are power and power density depending on β_{c-c} , β_{r-c} , x , y and τ are obtained. Then, these main equations are derived by using MATHEMATICA program in order to obtain max power and max power density. After the derivations, the variations of x versus β_{c-c} by changing of β_{r-c} , y and τ , and the variations of x versus β_{r-c} by changing of β_{c-c} , y and τ are depicted, respectively by using MATLAB program. At the end of the performance analysis, variations of the efficiencies for mp and mpd conditions are obtained by using the non-dimensionalized design parameters.

From the results of the optimum performance analysis, it is found that the higher y values and smaller τ values cause the efficiency to increase. For example while changing the β_{c-c} at $\beta_{r-c} = 0.1$, $\tau = 0.2$ and $y = 0.9$ efficiencies are change around 62–54% range for mp conditions and 64–62% range for mpd conditions,

increasing τ value to 0.5 and at $\gamma = 0.9$, yields efficiencies in a range around 30–27% for mp conditions and 31-29% at mpd conditions. Furthermore, Carnot-like heat engine of an SPTS working at mpd conditions always has a greater efficiency than Carnot-like heat engine of an SPTS working at the mp conditions. Performance analysis of a SPTS helps to obtain optimum system parameters in order to achieve max efficiency by depending on working conditions.



REFERENCES

- [1] Freris, L. and Infield, D., “Renewable Energy in Power Systems”, WILEY, United Kingdom, 2008.
- [2] Sorensen, B., “Renewable Energy Conversion, Transmission and Storage”, Academic Press, United Kingdom, 2007.
- [3] Kalogirou, S.A., “Solar Energy Engineering: Processes and Systems”, Academic Press, United States of America, 2014.
- [4] McMordie, R.K., “Solar Energy Fundamentals”, The Fairmont Press, United States of America, 2012.
- [5] Sabonnadière, J.C., “Renewable Energies”, WILEY, France, 2007.
- [6] Quaschnig, V., “Understanding Renewable Energy Systems”, Earthscan, London, 2005.
- [7] Solar Power Towers, http://lisas.de/projects/alt_energy/sol_thermal.html, Retrieved April 05, 2017.
- [8] Gevorkian, P., “Sustainable Energy Systems Engineering: The Complete Green Building Design Resource”, Mc Graw Hill, United States of America, 2006.
- [9] Xu, C., Wang, Z., Li, X. and Sun, F., “Energy and exergy analysis of solar power tower plants”, Applied Thermal Engineering, 31, 3904-3913, 2011.
- [10] Taggart, S., “CSP and the power tower”, Renewable Energy Focus, May-June, 51-54, 2008.
- [11] Fernandez, P. and Miller, F.J., “Performance analysis and preliminary design optimization of a Small Particle Heat Exchange Receiver for solar tower power plants”, Solar Energy, 112, 458-468, 2015.
- [12] Ataei, S. and Ameri, M., “Energy and exergy analysis of all-glass evacuated solar collector tubes with coaxial fluid conduit”, Solar Energy, 118, 575-591, 2015.
- [13] McGovern, R.K. and Smith, W.J., “Optimal concentration and temperatures of solar thermal power plants”, Energy Conversion and Management, 60, 226-232, 2012.

- [14] Ranjan, K.R. and Kaushik, S.C., “Energy, exergy and thermo-economic analysis of solar distillation systems: A review”, *Renewable and Sustainable Energy Reviews*, 27, 709-723, 2013.
- [15] Arora, R., Kaushik, S.C., Kumar, R. and Arora, R., “Multi-objective thermo-economic optimization of solar parabolic dish Stirling heat engine with regenerative losses using NSGA-II and decision making”, *Electrical Power and Energy Systems*, 74, 25-35, 2016.
- [16] Zhao, Y., Hong, H. and Jin, H., “Thermo-economic optimization of Solar–Coal Hybrid Systems”, *Energy Procedia*, 75, 457 – 461, 2015.
- [17] Calise, F., d’Accadia, M.D. and Vanoli, L., “Thermoeconomic optimization of solar heating and cooling systems”, *Energy Conversion and Management*, 52, 1562-1573, 2011.
- [18] Silva, R., Berenguel, M., Perez, M. and Fernandez-Garcia, A., “Thermo-economic design optimization of parabolic trough solar plants for industrial process heat applications with memetic algorithms”, *Applied Energy*, 113, 603-614, 2014.
- [19] Zhu, J., Wang, K., Wu, H., Wang, D., Du, J. and Olabi, A.G., “Experimental investigation on the energy and exergy performance of a coiled tube solar receiver”, *Applied Energy*, 156, 519-527, 2015.
- [20] Gholampour, M. and Ameri, M., “Energy and exergy analyses of Photovoltaic/Thermal flat transpired collectors: Experimental and theoretical study”, *Applied Energy*, 164, 837-856, 2016.
- [21] Spelling, J., Favrat, D., Martin, A. and Augsburger, G., “Thermoeconomic optimization of a combined-cycle solar tower power plant”, *Energy*, 41, 113-120, 2012.
- [22] Tempesti, D. and Fiaschi, D., “Thermo-economic assessment of a micro CHP system fueled by geothermal and solar energy”, *Energy*, 58, 45-51, 2013.
- [23] Petela, R., “Exergy of Heat Radiation”, *ASME Journal of Heat Transfer*, Vol. 86, 1964, p. 187.
- [24] Al-Sulaiman, F.A. and Atif, M., “Performance comparison of different supercritical carbon dioxide Brayton cycles integrated with a solar power tower”, *Energy*, 82, 61-71, 2015.

- [25] Carrizosa, E., Dominguez-Bravo, C., Fernandez-Cara, E. and Quero, M., "Optimization of multiple receivers solar power tower systems", *Energy*, 90, 2085-2093, 2015.
- [26] Sogut, O.S. and Durmayaz, A., "Performance optimization of a solar driven heat engine with finite-rate heat transfer", *Renewable Energy*, 30, 1329-1344, 2005.
- [27] Li, X., Kong, W., Wang, Z., Chang, C. and Bai, F., "Thermal model and thermodynamic performance of molten salt cavity receiver", *Renewable Energy*, 35, 981-988, 2010.
- [28] Kalogirou, S.A., Karellas, S., Badescu, V. and Braimakis, K., "Exergy analysis on solar thermal systems: A better understanding of their sustainability", *Renewable Energy*, 85, 1328-1333, 2016.
- [29] Wang, K., He, Y., Qiu, Y. and Zhang, Y., "A novel integrated simulation approach couples MCRT and Gebhart methods to simulate solar radiation transfer in a solar power tower system with a cavity receiver", *Renewable Energy*, 89, 93-107, 2016.
- [30] Ntsoukpoe, K.E., Azoumah, K.Y., Ramde, E., Fiagbe, A.K.Y., Neveu, P., Py, X., Gaye, M. and Jourdan, A., "Integrated design and construction of a micro-central tower power plant", *Energy for Sustainable Development*, 31, 1-13, 2016.
- [31] Zheng, H., Yu, X., Su, Y., Riffat, S. and Xiong, J., "Thermodynamic analysis of an idealized solar tower thermal power plant", *Applied Thermal Engineering*, 81, 271-278, 2015.
- [32] Luo, Y., Du, X. and Wen, D., "Novel design of central dual-receiver for solar power tower", *Applied Thermal Engineering*, 91, 1071-1081, 2015.
- [33] Desai, N.B. and Bandyopadhyay, S., "Thermo-economic analysis and selection of working fluid for solar organic Rankine cycle", *Applied Thermal Engineering*, 95, 471-481, 2016.
- [34] Okoroigwe, E. and Madhlopa, A., "An integrated combined cycle system driven by a solar tower: A review", *Renewable and Sustainable Energy Reviews*, 57, 337-350, 2016.

- [35] Faille, D., Liu, S., Wang, Z. and Yang, Z., “Control design model for a solar tower plant”, *Energy Procedia*, 49, 2080 – 2089, 2014.
- [36] Desai, N.B., Kedare, S.B. and Bandyopadhyay, S., “Optimization of design radiation for concentrating solar thermal power plants without storage”, *Solar Energy*, 107, 98-112, 2014.
- [37] Han, W., Jin, H., Lin, R. and Liu, Q., “Performance enhancement of a solar trough power plant by integrating tower collectors”, *Energy Procedia*, 49, 1391-1399, 2014.
- [38] Kalogirou, S.A., “Solar thermal collectors and applications”, *Progress in Energy and Combustion Science*, 30, 231–295, 2004.
- [39] Yao, Z., Wang, Z., Lu, Z. and Wei, X., “Modeling and simulation of the pioneer 1MW solar thermal central receiver system in China”, *Renewable Energy*, 34, 2437–2446, 2009.
- [40] Liu, Q., Bai, Z., Sun, J., Yan, Y., Gao, Z. and Jin, H., “Thermodynamics investigation of a solar power system integrated oil and molten salt as heat transfer fluids”, *Applied Thermal Engineering*, 93, 967–977, 2016.
- [41] Behar, O., Khellaf, A. and Mohammedi, K., “A review of studies on central receiver solar thermal power plants”, *Renewable and Sustainable Energy Reviews*, 23, 12–39, 2013.
- [42] Bejan, A., Kearney, D.W. and Kreith, F., “Second law analysis and synthesis of solar collector systems”, *Journal of Solar Energy Engineering* 103 23-28, 1981.
- [43] Çengel, Y. A. and Boles, M. A., “Thermodynamics: An Engineering Approach”, McGraw-Hill, Boston, 2006.
- [44] Melchior T, Perkins, C. A., Weimer, W. and Steinfeld. A., “A cavity-receiver containing a tubular absorber for high-temperature thermochemical processing using concentrated solar energy”, *International Journal of Thermal Sciences*, 47, 11, 1496-1503, 2008.
- [45] Collado, F.J., “Quick evaluation of the annual heliostat field efficiency”, *Solar Energy*, 82, 379-384, 2008.

- [46] Collado, F.J. and Guallar, j., “A review of optimized design layouts for solar power tower plants with campo code”, *Renewable and Sustainable Energy Reviews*, 20, 142–154, 2013.
- [47] Behar, O., Khellaf, A. and Mohammedi, K., “A review of studies on central receiver solar thermal power plants”, *Renewable and Sustainable Energy Reviews*, 23, 12–39, 2013.
- [48] Clifford K.H. and Brian D.I., “Review of high-temperature central receiver designs for concentrating solar power”, *Renewable and Sustainable Energy Reviews*, 29, 835–846, 2014.
- [49] Chambadal P., “Le choix du cycle thermique dans une usine géne´ratrice nucle´aire”, *Rev Ge´n E´lect*, 67, 332–45 1958.
- [50] Novikov II., “The efficiency of atomic power stations (a review)”, *J Nucl Energy*, 7 125–8, 1958.
- [51] Curzon F.L. and Ahlborn B., “Efficiency of a Carnot engine at maximum power output”, *Am J Phys.*, 43, 22–4, 1975.
- [52] Bejan A., “Entropy generation minimization: the new thermodynamics of finite-size devices and finite-time processes”, *J Appl Phys*, 79(3), 1191–218, 1996.
- [53] Sahin B., Kodal A. and Yavuz H., “Efficiency of a Joule-Brayton engine at maximum power-density”, *J Phys.*, 28, 1309–1313, 1995.
- [54] Sahin B., Kodal A. and Yavuz H., “Maximum power density for an endoreversible Carnot heat engine”, *Energy*, 21, 1219–25, 1996.

APPENDICES

Appendix A: $\partial \bar{W} / \partial x = 0$ performance optimization derivation by
MATHEMATICA

Appendix B: $\partial \bar{W}_d / \partial x = 0$ performance optimization derivation by
MATHEMATICA

Appendix C: The performance optimization codes written in MATLAB



$$\begin{aligned}
& \frac{12 x^2 (1-y)^2 (-x+y) \left(\frac{1-x}{(-x+y)^2} - \frac{1}{-x+y} \right)}{(1-x) \operatorname{Log} \left[\frac{1-x}{-x+y} \right]^3} + \frac{12 x (1-y)^2}{\operatorname{Log} \left[\frac{1-x}{-x+y} \right]^2} - \\
& \left. \frac{4 x^3 (1-y) (-x+y) \left(\frac{1-x}{(-x+y)^2} - \frac{1}{-x+y} \right)}{(1-x) \operatorname{Log} \left[\frac{1-x}{-x+y} \right]^2} + \frac{12 x^2 (1-y)}{\operatorname{Log} \left[\frac{1-x}{-x+y} \right]} \right) + \\
& \frac{\operatorname{Bcc} (1-y) (-x+y) \left(\frac{1-x}{(-x+y)^2} - \frac{1}{-x+y} \right)}{(1-x) \operatorname{Log} \left[\frac{1-x}{-x+y} \right]^2} \Bigg) \\
& \left(\operatorname{Brc} \left(\frac{(1-y)^4}{\operatorname{Log} \left[\frac{1-x}{-x+y} \right]^4} + \frac{4 x (1-y)^3}{\operatorname{Log} \left[\frac{1-x}{-x+y} \right]^3} + \frac{6 x^2 (1-y)^2}{\operatorname{Log} \left[\frac{1-x}{-x+y} \right]^2} + \frac{4 x^3 (1-y)}{\operatorname{Log} \left[\frac{1-x}{-x+y} \right]} \right) + \right. \\
& \left. \frac{\operatorname{Bcc} (1-y)}{\operatorname{Log} \left[\frac{1-x}{-x+y} \right]} \right) \Bigg) / \\
& \left(x - \operatorname{Brc} \left(\frac{(1-y)^4}{\operatorname{Log} \left[\frac{1-x}{-x+y} \right]^4} + \frac{4 x (1-y)^3}{\operatorname{Log} \left[\frac{1-x}{-x+y} \right]^3} + \frac{6 x^2 (1-y)^2}{\operatorname{Log} \left[\frac{1-x}{-x+y} \right]^2} + \frac{4 x^3 (1-y)}{\operatorname{Log} \left[\frac{1-x}{-x+y} \right]} \right) - \right. \\
& \left. \frac{\operatorname{Bcc} (1-y)}{\operatorname{Log} \left[\frac{1-x}{-x+y} \right]} \right)^2 = 0
\end{aligned}$$

Cancel [%]

$$\begin{aligned}
& - \left((-1+y) \left(-\operatorname{Brc} + 4 \operatorname{Brc} y - 6 \operatorname{Brc} y^2 + 4 \operatorname{Brc} y^3 - \operatorname{Brc} y^4 - 4 \operatorname{Brc} x \operatorname{Log} \left[\frac{1-x}{-x+y} \right] + \right. \right. \\
& \quad 12 \operatorname{Brc} x y \operatorname{Log} \left[\frac{1-x}{-x+y} \right] - 12 \operatorname{Brc} x y^2 \operatorname{Log} \left[\frac{1-x}{-x+y} \right] + \\
& \quad 4 \operatorname{Brc} x y^3 \operatorname{Log} \left[\frac{1-x}{-x+y} \right] - 6 \operatorname{Brc} x^2 \operatorname{Log} \left[\frac{1-x}{-x+y} \right]^2 + \\
& \quad 12 \operatorname{Brc} x^2 y \operatorname{Log} \left[\frac{1-x}{-x+y} \right]^2 - 6 \operatorname{Brc} x^2 y^2 \operatorname{Log} \left[\frac{1-x}{-x+y} \right]^2 - \\
& \quad \operatorname{Bcc} \operatorname{Log} \left[\frac{1-x}{-x+y} \right]^3 - 4 \operatorname{Brc} x^3 \operatorname{Log} \left[\frac{1-x}{-x+y} \right]^3 + \operatorname{Bcc} y \operatorname{Log} \left[\frac{1-x}{-x+y} \right]^3 + \\
& \quad \left. \left. 4 \operatorname{Brc} x^3 y \operatorname{Log} \left[\frac{1-x}{-x+y} \right]^3 - \operatorname{to} \operatorname{Log} \left[\frac{1-x}{-x+y} \right]^4 + x \operatorname{Log} \left[\frac{1-x}{-x+y} \right]^4 \right) \right) \\
& \left(-4 \operatorname{Brc} + 16 \operatorname{Brc} y - 24 \operatorname{Brc} y^2 + 16 \operatorname{Brc} y^3 - 4 \operatorname{Brc} y^4 - \right. \\
& \quad 12 \operatorname{Brc} x \operatorname{Log} \left[\frac{1-x}{-x+y} \right] + 36 \operatorname{Brc} x y \operatorname{Log} \left[\frac{1-x}{-x+y} \right] - \\
& \quad 36 \operatorname{Brc} x y^2 \operatorname{Log} \left[\frac{1-x}{-x+y} \right] + 12 \operatorname{Brc} x y^3 \operatorname{Log} \left[\frac{1-x}{-x+y} \right] - \\
& \quad \left. 4 \operatorname{Brc} x \operatorname{Log} \left[\frac{1-x}{-x+y} \right]^2 - 8 \operatorname{Brc} x^2 \operatorname{Log} \left[\frac{1-x}{-x+y} \right]^2 + 4 \operatorname{Brc} y \operatorname{Log} \left[\frac{1-x}{-x+y} \right]^2 + \right.
\end{aligned}$$

$$\begin{aligned}
& 4 \text{Brc } x y \text{ Log} \left[\frac{1-x}{-x+y} \right]^2 + 16 \text{Brc } x^2 y \text{ Log} \left[\frac{1-x}{-x+y} \right]^2 - \\
& 8 \text{Brc } y^2 \text{ Log} \left[\frac{1-x}{-x+y} \right]^2 + 4 \text{Brc } x y^2 \text{ Log} \left[\frac{1-x}{-x+y} \right]^2 - \\
& 8 \text{Brc } x^2 y^2 \text{ Log} \left[\frac{1-x}{-x+y} \right]^2 + 4 \text{Brc } y^3 \text{ Log} \left[\frac{1-x}{-x+y} \right]^2 - \\
& 4 \text{Brc } x y^3 \text{ Log} \left[\frac{1-x}{-x+y} \right]^2 - \text{Bcc} \text{ Log} \left[\frac{1-x}{-x+y} \right]^3 - \\
& 12 \text{Brc } x^2 \text{ Log} \left[\frac{1-x}{-x+y} \right]^3 + 8 \text{Brc } x^3 \text{ Log} \left[\frac{1-x}{-x+y} \right]^3 + \text{Bcc } y \text{ Log} \left[\frac{1-x}{-x+y} \right]^3 + \\
& 12 \text{Brc } x y \text{ Log} \left[\frac{1-x}{-x+y} \right]^3 - 8 \text{Brc } x^3 y \text{ Log} \left[\frac{1-x}{-x+y} \right]^3 - \\
& 12 \text{Brc } x y^2 \text{ Log} \left[\frac{1-x}{-x+y} \right]^3 + 12 \text{Brc } x^2 y^2 \text{ Log} \left[\frac{1-x}{-x+y} \right]^3 - \\
& 12 \text{Brc } x^3 \text{ Log} \left[\frac{1-x}{-x+y} \right]^4 + 12 \text{Brc } x^4 \text{ Log} \left[\frac{1-x}{-x+y} \right]^4 + \\
& 12 \text{Brc } x^2 y \text{ Log} \left[\frac{1-x}{-x+y} \right]^4 - 12 \text{Brc } x^3 y \text{ Log} \left[\frac{1-x}{-x+y} \right]^4 \Big) / \\
& \left((-1+x) (x-y) \text{ Log} \left[\frac{1-x}{-x+y} \right]^5 \left(-\text{Brc} + 4 \text{Brc } y - 6 \text{Brc } y^2 + \right. \right. \\
& \quad 4 \text{Brc } y^3 - \text{Brc } y^4 - 4 \text{Brc } x \text{ Log} \left[\frac{1-x}{-x+y} \right] + 12 \text{Brc } x y \text{ Log} \left[\frac{1-x}{-x+y} \right] - \\
& \quad 12 \text{Brc } x y^2 \text{ Log} \left[\frac{1-x}{-x+y} \right] + 4 \text{Brc } x y^3 \text{ Log} \left[\frac{1-x}{-x+y} \right] - \\
& \quad 6 \text{Brc } x^2 \text{ Log} \left[\frac{1-x}{-x+y} \right]^2 + 12 \text{Brc } x^2 y \text{ Log} \left[\frac{1-x}{-x+y} \right]^2 - \\
& \quad 6 \text{Brc } x^2 y^2 \text{ Log} \left[\frac{1-x}{-x+y} \right]^2 - \text{Bcc} \text{ Log} \left[\frac{1-x}{-x+y} \right]^3 - 4 \text{Brc } x^3 \text{ Log} \left[\frac{1-x}{-x+y} \right]^3 + \\
& \quad \left. \left. \text{Bcc } y \text{ Log} \left[\frac{1-x}{-x+y} \right]^3 + 4 \text{Brc } x^3 y \text{ Log} \left[\frac{1-x}{-x+y} \right]^3 + x \text{ Log} \left[\frac{1-x}{-x+y} \right]^4 \right) \right) - \\
& \left(\text{to } (-1+y) \left(\text{Brc} - 3 \text{Brc } y + 3 \text{Brc } y^2 - \text{Brc } y^3 + 4 \text{Brc } x \text{ Log} \left[\frac{1-x}{-x+y} \right] - \right. \right. \\
& \quad 8 \text{Brc } x y \text{ Log} \left[\frac{1-x}{-x+y} \right] + 4 \text{Brc } x y^2 \text{ Log} \left[\frac{1-x}{-x+y} \right] + \\
& \quad 6 \text{Brc } x^2 \text{ Log} \left[\frac{1-x}{-x+y} \right]^2 - 6 \text{Brc } x^2 y \text{ Log} \left[\frac{1-x}{-x+y} \right]^2 + \\
& \quad \left. \left. \text{Bcc} \text{ Log} \left[\frac{1-x}{-x+y} \right]^3 + 4 \text{Brc } x^3 \text{ Log} \left[\frac{1-x}{-x+y} \right]^3 \right) \right) \\
& \left(4 \text{Brc} - 20 \text{Brc } y + 40 \text{Brc } y^2 - 40 \text{Brc } y^3 + 20 \text{Brc } y^4 - 4 \text{Brc } y^5 + \right. \\
& \quad 12 \text{Brc } x \text{ Log} \left[\frac{1-x}{-x+y} \right] - 48 \text{Brc } x y \text{ Log} \left[\frac{1-x}{-x+y} \right] + \\
& \quad 72 \text{Brc } x y^2 \text{ Log} \left[\frac{1-x}{-x+y} \right] - 48 \text{Brc } x y^3 \text{ Log} \left[\frac{1-x}{-x+y} \right] + \\
& \quad 12 \text{Brc } x y^4 \text{ Log} \left[\frac{1-x}{-x+y} \right] + 4 \text{Brc } x \text{ Log} \left[\frac{1-x}{-x+y} \right]^2 + \\
& \quad 8 \text{Brc } x^2 \text{ Log} \left[\frac{1-x}{-x+y} \right]^2 - 4 \text{Brc } y \text{ Log} \left[\frac{1-x}{-x+y} \right]^2 - \\
& \quad \left. \left. 8 \text{Brc } x y \text{ Log} \left[\frac{1-x}{-x+y} \right]^2 - 24 \text{Brc } x^2 y \text{ Log} \left[\frac{1-x}{-x+y} \right]^2 + \right. \right.
\end{aligned}$$

$$\begin{aligned}
& 12 \text{Brc } y^2 \text{Log} \left[\frac{1-x}{-x+y} \right]^2 + 24 \text{Brc } x^2 y^2 \text{Log} \left[\frac{1-x}{-x+y} \right]^2 - \\
& 12 \text{Brc } y^3 \text{Log} \left[\frac{1-x}{-x+y} \right]^2 + 8 \text{Brc } x y^3 \text{Log} \left[\frac{1-x}{-x+y} \right]^2 - \\
& 8 \text{Brc } x^2 y^3 \text{Log} \left[\frac{1-x}{-x+y} \right]^2 + 4 \text{Brc } y^4 \text{Log} \left[\frac{1-x}{-x+y} \right]^2 - \\
& 4 \text{Brc } x y^4 \text{Log} \left[\frac{1-x}{-x+y} \right]^2 + \text{Bcc} \text{Log} \left[\frac{1-x}{-x+y} \right]^3 + 12 \text{Brc } x^2 \text{Log} \left[\frac{1-x}{-x+y} \right]^3 - \\
& 8 \text{Brc } x^3 \text{Log} \left[\frac{1-x}{-x+y} \right]^3 - 2 \text{Bcc } y \text{Log} \left[\frac{1-x}{-x+y} \right]^3 - \\
& 12 \text{Brc } x y \text{Log} \left[\frac{1-x}{-x+y} \right]^3 - 12 \text{Brc } x^2 y \text{Log} \left[\frac{1-x}{-x+y} \right]^3 + \\
& 16 \text{Brc } x^3 y \text{Log} \left[\frac{1-x}{-x+y} \right]^3 + \text{Bcc } y^2 \text{Log} \left[\frac{1-x}{-x+y} \right]^3 + \\
& 24 \text{Brc } x y^2 \text{Log} \left[\frac{1-x}{-x+y} \right]^3 - 12 \text{Brc } x^2 y^2 \text{Log} \left[\frac{1-x}{-x+y} \right]^3 - \\
& 8 \text{Brc } x^3 y^2 \text{Log} \left[\frac{1-x}{-x+y} \right]^3 - 12 \text{Brc } x y^3 \text{Log} \left[\frac{1-x}{-x+y} \right]^3 + \\
& 12 \text{Brc } x^2 y^3 \text{Log} \left[\frac{1-x}{-x+y} \right]^3 + 12 \text{Brc } x^3 \text{Log} \left[\frac{1-x}{-x+y} \right]^4 - \\
& 12 \text{Brc } x^4 \text{Log} \left[\frac{1-x}{-x+y} \right]^4 - 12 \text{Brc } x^2 y \text{Log} \left[\frac{1-x}{-x+y} \right]^4 + \\
& 12 \text{Brc } x^4 y \text{Log} \left[\frac{1-x}{-x+y} \right]^4 + 12 \text{Brc } x^2 y^2 \text{Log} \left[\frac{1-x}{-x+y} \right]^4 - \\
& 12 \text{Brc } x^3 y^2 \text{Log} \left[\frac{1-x}{-x+y} \right]^4 - x \text{Log} \left[\frac{1-x}{-x+y} \right]^5 + \\
& x^2 \text{Log} \left[\frac{1-x}{-x+y} \right]^5 + y \text{Log} \left[\frac{1-x}{-x+y} \right]^5 - x y \text{Log} \left[\frac{1-x}{-x+y} \right]^5 \Big) \Big/ \\
& \left((-1+x) (x-y) \text{Log} \left[\frac{1-x}{-x+y} \right] \left(-\text{Brc} + 4 \text{Brc } y - 6 \text{Brc } y^2 + 4 \text{Brc } y^3 - \right. \right. \\
& \quad \text{Brc } y^4 - 4 \text{Brc } x \text{Log} \left[\frac{1-x}{-x+y} \right] + 12 \text{Brc } x y \text{Log} \left[\frac{1-x}{-x+y} \right] - \\
& \quad 12 \text{Brc } x y^2 \text{Log} \left[\frac{1-x}{-x+y} \right] + 4 \text{Brc } x y^3 \text{Log} \left[\frac{1-x}{-x+y} \right] - \\
& \quad 6 \text{Brc } x^2 \text{Log} \left[\frac{1-x}{-x+y} \right]^2 + 12 \text{Brc } x^2 y \text{Log} \left[\frac{1-x}{-x+y} \right]^2 - \\
& \quad 6 \text{Brc } x^2 y^2 \text{Log} \left[\frac{1-x}{-x+y} \right]^2 - \text{Bcc} \text{Log} \left[\frac{1-x}{-x+y} \right]^3 - 4 \text{Brc } x^3 \text{Log} \left[\frac{1-x}{-x+y} \right]^3 + \\
& \quad \left. \left. \text{Bcc } y \text{Log} \left[\frac{1-x}{-x+y} \right]^3 + 4 \text{Brc } x^3 y \text{Log} \left[\frac{1-x}{-x+y} \right]^3 + x \text{Log} \left[\frac{1-x}{-x+y} \right]^4 \right)^2 \right) = 0
\end{aligned}$$

Simplify [%]

$$\begin{aligned}
& \left((-1+y) \left(\left(\text{Brc} (-1+y)^4 - \right. \right. \right. \\
& \quad 4 \text{Brc } x (-1+y)^3 \text{Log} \left[\frac{-1+x}{x-y} \right] + 6 \text{Brc } x^2 (-1+y)^2 \text{Log} \left[\frac{-1+x}{x-y} \right]^2 - \\
& \quad \left. \left. \left(\text{Bcc} + 4 \text{Brc } x^3 \right) (-1+y) \text{Log} \left[\frac{-1+x}{x-y} \right]^3 + (to - x) \text{Log} \left[\frac{-1+x}{x-y} \right]^4 \right) \right)
\end{aligned}$$

$$\begin{aligned}
& \left(\text{Brc } (-1+y)^4 - 4 \text{Brc } x (-1+y)^3 \text{Log} \left[\frac{-1+x}{x-y} \right] + \right. \\
& \quad \left. 6 \text{Brc } x^2 (-1+y)^2 \text{Log} \left[\frac{-1+x}{x-y} \right]^2 - \right. \\
& \quad \left. (\text{Bcc} + 4 \text{Brc } x^3) (-1+y) \text{Log} \left[\frac{-1+x}{x-y} \right]^3 - x \text{Log} \left[\frac{-1+x}{x-y} \right]^4 \right) \\
& \left(4 \text{Brc } (-1+y)^4 - 12 \text{Brc } x (-1+y)^3 \text{Log} \left[\frac{-1+x}{x-y} \right] + \right. \\
& \quad \left. 4 \text{Brc } (-1+y)^2 (x + 2x^2 - y + xy) \text{Log} \left[\frac{-1+x}{x-y} \right]^2 - \right. \\
& \quad \left. (-1+y) (\text{Bcc} + 4 \text{Brc } x (-2x^2 - 3y + 3x(1+y))) \text{Log} \left[\frac{-1+x}{x-y} \right]^3 - \right. \\
& \quad \left. 12 \text{Brc } (-1+x) x^2 (x-y) \text{Log} \left[\frac{-1+x}{x-y} \right]^4 \right) + \\
& \text{to } \text{Log} \left[\frac{-1+x}{x-y} \right]^4 \left(-\text{Brc } (-1+y)^3 + 4 \text{Brc } x (-1+y)^2 \text{Log} \left[\frac{-1+x}{x-y} \right] - \right. \\
& \quad \left. 6 \text{Brc } x^2 (-1+y) \text{Log} \left[\frac{-1+x}{x-y} \right]^2 + (\text{Bcc} + 4 \text{Brc } x^3) \text{Log} \left[\frac{-1+x}{x-y} \right]^3 \right) \\
& \left(4 \text{Brc } (-1+y)^5 - 12 \text{Brc } x (-1+y)^4 \text{Log} \left[\frac{-1+x}{x-y} \right] + \right. \\
& \quad \left. 4 \text{Brc } (-1+y)^3 (x + 2x^2 - y + xy) \text{Log} \left[\frac{-1+x}{x-y} \right]^2 - \right. \\
& \quad \left. (-1+y)^2 (\text{Bcc} + 4 \text{Brc } x (-2x^2 - 3y + 3x(1+y))) \text{Log} \left[\frac{-1+x}{x-y} \right]^3 - \right. \\
& \quad \left. 12 \text{Brc } (-1+x) x^2 (x-y) (-1+y) \text{Log} \left[\frac{-1+x}{x-y} \right]^4 - \right. \\
& \quad \left. (-1+x) (x-y) \text{Log} \left[\frac{-1+x}{x-y} \right]^5 \right) \Bigg) / \\
& \left((-1+x) (x-y) \text{Log} \left[\frac{-1+x}{x-y} \right]^5 \left(-\text{Brc } (-1+y)^4 + \right. \right. \\
& \quad \left. \left. 4 \text{Brc } x (-1+y)^3 \text{Log} \left[\frac{-1+x}{x-y} \right] - 6 \text{Brc } x^2 (-1+y)^2 \text{Log} \left[\frac{-1+x}{x-y} \right]^2 + \right. \right. \\
& \quad \left. \left. (\text{Bcc} + 4 \text{Brc } x^3) (-1+y) \text{Log} \left[\frac{-1+x}{x-y} \right]^3 + x \text{Log} \left[\frac{-1+x}{x-y} \right]^4 \right)^2 \right) = \theta
\end{aligned}$$

$$dw / dx = \theta,$$

$$\begin{aligned}
& \left(\left(\text{Brc } (-1+y)^4 - 4 \text{Brc } x (-1+y)^3 \text{Log} \left[\frac{-1+x}{x-y} \right] + \right. \right. \\
& \quad \left. \left. 6 \text{Brc } x^2 (-1+y)^2 \text{Log} \left[\frac{-1+x}{x-y} \right]^2 - \right. \right. \\
& \quad \left. \left. (\text{Bcc} + 4 \text{Brc } x^3) (-1+y) \text{Log} \left[\frac{-1+x}{x-y} \right]^3 + (to - x) \text{Log} \left[\frac{-1+x}{x-y} \right]^4 \right) \right) \\
& \left(\text{Brc } (-1+y)^4 - 4 \text{Brc } x (-1+y)^3 \text{Log} \left[\frac{-1+x}{x-y} \right] + \right. \\
& \quad \left. 6 \text{Brc } x^2 (-1+y)^2 \text{Log} \left[\frac{-1+x}{x-y} \right]^2 - \right. \\
& \quad \left. (\text{Bcc} + 4 \text{Brc } x^3) (-1+y) \text{Log} \left[\frac{-1+x}{x-y} \right]^3 - x \text{Log} \left[\frac{-1+x}{x-y} \right]^4 \right)
\end{aligned}$$

$$\begin{aligned}
& \left(4 \operatorname{Brc} (-1+y)^4 - 12 \operatorname{Brc} x (-1+y)^3 \operatorname{Log} \left[\frac{-1+x}{x-y} \right] + \right. \\
& \quad 4 \operatorname{Brc} (-1+y)^2 (x+2x^2-y+xy) \operatorname{Log} \left[\frac{-1+x}{x-y} \right]^2 - \\
& \quad (-1+y) (\operatorname{Bcc} + 4 \operatorname{Brc} x (-2x^2-3y+3x(1+y))) \operatorname{Log} \left[\frac{-1+x}{x-y} \right]^3 - \\
& \quad \left. 12 \operatorname{Brc} (-1+x) x^2 (x-y) \operatorname{Log} \left[\frac{-1+x}{x-y} \right]^4 \right) + \\
& \text{to } \operatorname{Log} \left[\frac{-1+x}{x-y} \right]^4 \\
& \left(-\operatorname{Brc} (-1+y)^3 + 4 \operatorname{Brc} x (-1+y)^2 \operatorname{Log} \left[\frac{-1+x}{x-y} \right] - \right. \\
& \quad \left. 6 \operatorname{Brc} x^2 (-1+y) \operatorname{Log} \left[\frac{-1+x}{x-y} \right]^2 + (\operatorname{Bcc} + 4 \operatorname{Brc} x^3) \operatorname{Log} \left[\frac{-1+x}{x-y} \right]^3 \right) \\
& \left(4 \operatorname{Brc} (-1+y)^5 - 12 \operatorname{Brc} x (-1+y)^4 \operatorname{Log} \left[\frac{-1+x}{x-y} \right] + \right. \\
& \quad 4 \operatorname{Brc} (-1+y)^3 (x+2x^2-y+xy) \operatorname{Log} \left[\frac{-1+x}{x-y} \right]^2 - \\
& \quad (-1+y)^2 (\operatorname{Bcc} + 4 \operatorname{Brc} x (-2x^2-3y+3x(1+y))) \operatorname{Log} \left[\frac{-1+x}{x-y} \right]^3 - \\
& \quad \left. 12 \operatorname{Brc} (-1+x) x^2 (x-y) (-1+y) \operatorname{Log} \left[\frac{-1+x}{x-y} \right]^4 - \right. \\
& \quad \left. (-1+x) (x-y) \operatorname{Log} \left[\frac{-1+x}{x-y} \right]^5 \right) = \theta
\end{aligned}$$

**Appendix B – $\partial \bar{W}_d / \partial x = 0$ Performance Optimization Derivation
by *MATHEMATICA***

$$\begin{aligned}
 & D [\\
 & \quad (((Bcc * ((1 - y) / \text{Log}[((1 - x) / (y - x))])) + \\
 & \quad \quad Brc * ((((1 - y) / \text{Log}[(1 - x) / (y - x)]) ^4) + \\
 & \quad \quad \quad 4 * x * (((1 - y) / \text{Log}[(1 - x) / (y - x)]) ^3) + \\
 & \quad \quad \quad 6 * (x^2) * (((1 - y) / \text{Log}[(1 - x) / (y - x)]) ^2) + \\
 & \quad \quad \quad 4 * (x^3) * ((1 - y) / \text{Log}[(1 - x) / (y - x)]))) * \\
 & \quad (x - (Bcc * ((1 - y) / \text{Log}[(1 - x) / (y - x)]) + \\
 & \quad \quad Brc * ((((1 - y) / \text{Log}[(1 - x) / (y - x)]) ^4) + \\
 & \quad \quad \quad 4 * x * (((1 - y) / \text{Log}[(1 - x) / (y - x)]) ^3) + \\
 & \quad \quad \quad 6 * (x^2) * (((1 - y) / \text{Log}[(1 - x) / (y - x)]) ^2) + \\
 & \quad \quad \quad 4 * (x^3) * ((1 - y) / \text{Log}[(1 - x) / (y - x)]))) - to)) / \\
 & \quad (x * to)) = 0, x] \\
 & \frac{1}{to \ x} \left(Brc \left(- \frac{4 (1 - y)^4 (-x + y) \left(\frac{1-x}{(-x+y)^2} - \frac{1}{-x+y} \right)}{(1 - x) \text{Log} \left[\frac{1-x}{-x+y} \right]^5} - \right. \right. \\
 & \quad \frac{12 x (1 - y)^3 (-x + y) \left(\frac{1-x}{(-x+y)^2} - \frac{1}{-x+y} \right)}{(1 - x) \text{Log} \left[\frac{1-x}{-x+y} \right]^4} + \frac{4 (1 - y)^3}{\text{Log} \left[\frac{1-x}{-x+y} \right]^3} - \\
 & \quad \frac{12 x^2 (1 - y)^2 (-x + y) \left(\frac{1-x}{(-x+y)^2} - \frac{1}{-x+y} \right)}{(1 - x) \text{Log} \left[\frac{1-x}{-x+y} \right]^3} + \frac{12 x (1 - y)^2}{\text{Log} \left[\frac{1-x}{-x+y} \right]^2} - \\
 & \quad \left. \frac{4 x^3 (1 - y) (-x + y) \left(\frac{1-x}{(-x+y)^2} - \frac{1}{-x+y} \right)}{(1 - x) \text{Log} \left[\frac{1-x}{-x+y} \right]^2} + \frac{12 x^2 (1 - y)}{\text{Log} \left[\frac{1-x}{-x+y} \right]} \right) - \\
 & \quad \left. \frac{Bcc (1 - y) (-x + y) \left(\frac{1-x}{(-x+y)^2} - \frac{1}{-x+y} \right)}{(1 - x) \text{Log} \left[\frac{1-x}{-x+y} \right]^2} \right) \\
 & \quad \left(-to + x - Brc \left(\frac{(1 - y)^4}{\text{Log} \left[\frac{1-x}{-x+y} \right]^4} + \frac{4 x (1 - y)^3}{\text{Log} \left[\frac{1-x}{-x+y} \right]^3} + \frac{6 x^2 (1 - y)^2}{\text{Log} \left[\frac{1-x}{-x+y} \right]^2} + \frac{4 x^3 (1 - y)}{\text{Log} \left[\frac{1-x}{-x+y} \right]} \right) - \right. \\
 & \quad \left. \frac{Bcc (1 - y)}{\text{Log} \left[\frac{1-x}{-x+y} \right]} \right) + \\
 & \frac{1}{to \ x} \left(1 - Brc \left(- \frac{4 (1 - y)^4 (-x + y) \left(\frac{1-x}{(-x+y)^2} - \frac{1}{-x+y} \right)}{(1 - x) \text{Log} \left[\frac{1-x}{-x+y} \right]^5} - \right. \right. \\
 & \quad \left. \frac{12 x (1 - y)^3 (-x + y) \left(\frac{1-x}{(-x+y)^2} - \frac{1}{-x+y} \right)}{(1 - x) \text{Log} \left[\frac{1-x}{-x+y} \right]^4} + \frac{4 (1 - y)^3}{\text{Log} \left[\frac{1-x}{-x+y} \right]^3} - \right.
 \end{aligned}$$

$$\begin{aligned}
& \frac{12 x^2 (1-y)^2 (-x+y) \left(\frac{1-x}{(-x+y)^2} - \frac{1}{-x+y} \right)}{(1-x) \operatorname{Log} \left[\frac{1-x}{-x+y} \right]^3} + \frac{12 x (1-y)^2}{\operatorname{Log} \left[\frac{1-x}{-x+y} \right]^2} - \\
& \frac{4 x^3 (1-y) (-x+y) \left(\frac{1-x}{(-x+y)^2} - \frac{1}{-x+y} \right)}{(1-x) \operatorname{Log} \left[\frac{1-x}{-x+y} \right]^2} + \frac{12 x^2 (1-y)}{\operatorname{Log} \left[\frac{1-x}{-x+y} \right]} \Bigg) + \\
& \frac{\operatorname{Bcc} (1-y) (-x+y) \left(\frac{1-x}{(-x+y)^2} - \frac{1}{-x+y} \right)}{(1-x) \operatorname{Log} \left[\frac{1-x}{-x+y} \right]^2} \Bigg) \\
& \left(\operatorname{Brc} \left(\frac{(1-y)^4}{\operatorname{Log} \left[\frac{1-x}{-x+y} \right]^4} + \frac{4 x (1-y)^3}{\operatorname{Log} \left[\frac{1-x}{-x+y} \right]^3} + \frac{6 x^2 (1-y)^2}{\operatorname{Log} \left[\frac{1-x}{-x+y} \right]^2} + \frac{4 x^3 (1-y)}{\operatorname{Log} \left[\frac{1-x}{-x+y} \right]} \right) + \right. \\
& \left. \frac{\operatorname{Bcc} (1-y)}{\operatorname{Log} \left[\frac{1-x}{-x+y} \right]} \right) - \frac{1}{\operatorname{to} x^2} \\
& \left(-\operatorname{to} + x - \operatorname{Brc} \left(\frac{(1-y)^4}{\operatorname{Log} \left[\frac{1-x}{-x+y} \right]^4} + \frac{4 x (1-y)^3}{\operatorname{Log} \left[\frac{1-x}{-x+y} \right]^3} + \frac{6 x^2 (1-y)^2}{\operatorname{Log} \left[\frac{1-x}{-x+y} \right]^2} + \frac{4 x^3 (1-y)}{\operatorname{Log} \left[\frac{1-x}{-x+y} \right]} \right) - \right. \\
& \left. \frac{\operatorname{Bcc} (1-y)}{\operatorname{Log} \left[\frac{1-x}{-x+y} \right]} \right) \\
& \left(\operatorname{Brc} \left(\frac{(1-y)^4}{\operatorname{Log} \left[\frac{1-x}{-x+y} \right]^4} + \frac{4 x (1-y)^3}{\operatorname{Log} \left[\frac{1-x}{-x+y} \right]^3} + \frac{6 x^2 (1-y)^2}{\operatorname{Log} \left[\frac{1-x}{-x+y} \right]^2} + \frac{4 x^3 (1-y)}{\operatorname{Log} \left[\frac{1-x}{-x+y} \right]} \right) + \right. \\
& \left. \frac{\operatorname{Bcc} (1-y)}{\operatorname{Log} \left[\frac{1-x}{-x+y} \right]} \right) = \theta
\end{aligned}$$

Cancel [%]

$$\begin{aligned}
& - \frac{1}{\operatorname{to} x^2 \operatorname{Log} \left[\frac{1-x}{-x+y} \right]^8} \\
& (-1+y) \left(\operatorname{Brc} - 3 \operatorname{Brc} y + 3 \operatorname{Brc} y^2 - \operatorname{Brc} y^3 + 4 \operatorname{Brc} x \operatorname{Log} \left[\frac{1-x}{-x+y} \right] - \right. \\
& \quad 8 \operatorname{Brc} x y \operatorname{Log} \left[\frac{1-x}{-x+y} \right] + 4 \operatorname{Brc} x y^2 \operatorname{Log} \left[\frac{1-x}{-x+y} \right] + 6 \operatorname{Brc} x^2 \operatorname{Log} \left[\frac{1-x}{-x+y} \right]^2 - \\
& \quad \left. 6 \operatorname{Brc} x^2 y \operatorname{Log} \left[\frac{1-x}{-x+y} \right]^2 + \operatorname{Bcc} \operatorname{Log} \left[\frac{1-x}{-x+y} \right]^3 + 4 \operatorname{Brc} x^3 \operatorname{Log} \left[\frac{1-x}{-x+y} \right]^3 \right) \\
& \left(\operatorname{Brc} - 4 \operatorname{Brc} y + 6 \operatorname{Brc} y^2 - 4 \operatorname{Brc} y^3 + \operatorname{Brc} y^4 + 4 \operatorname{Brc} x \operatorname{Log} \left[\frac{1-x}{-x+y} \right] - \right. \\
& \quad 12 \operatorname{Brc} x y \operatorname{Log} \left[\frac{1-x}{-x+y} \right] + 12 \operatorname{Brc} x y^2 \operatorname{Log} \left[\frac{1-x}{-x+y} \right] - \\
& \quad \left. 4 \operatorname{Brc} x y^3 \operatorname{Log} \left[\frac{1-x}{-x+y} \right] + 6 \operatorname{Brc} x^2 \operatorname{Log} \left[\frac{1-x}{-x+y} \right]^2 - \right.
\end{aligned}$$

$$\begin{aligned}
& 12 \text{Brc } x^2 y \text{ Log} \left[\frac{1-x}{-x+y} \right]^2 + 6 \text{Brc } x^2 y^2 \text{ Log} \left[\frac{1-x}{-x+y} \right]^2 + \\
& \text{Bcc Log} \left[\frac{1-x}{-x+y} \right]^3 + 4 \text{Brc } x^3 \text{ Log} \left[\frac{1-x}{-x+y} \right]^3 - \text{Bcc } y \text{ Log} \left[\frac{1-x}{-x+y} \right]^3 - \\
& 4 \text{Brc } x^3 y \text{ Log} \left[\frac{1-x}{-x+y} \right]^3 + \text{to Log} \left[\frac{1-x}{-x+y} \right]^4 - x \text{ Log} \left[\frac{1-x}{-x+y} \right]^4 + \\
& \left((-1+y) \left(\text{Brc} - 4 \text{Brc } y + 6 \text{Brc } y^2 - 4 \text{Brc } y^3 + \text{Brc } y^4 + 4 \text{Brc } x \text{ Log} \left[\frac{1-x}{-x+y} \right] - \right. \right. \\
& \quad 12 \text{Brc } x y \text{ Log} \left[\frac{1-x}{-x+y} \right] + 12 \text{Brc } x y^2 \text{ Log} \left[\frac{1-x}{-x+y} \right] - \\
& \quad 4 \text{Brc } x y^3 \text{ Log} \left[\frac{1-x}{-x+y} \right] + 6 \text{Brc } x^2 \text{ Log} \left[\frac{1-x}{-x+y} \right]^2 - \\
& \quad 12 \text{Brc } x^2 y \text{ Log} \left[\frac{1-x}{-x+y} \right]^2 + 6 \text{Brc } x^2 y^2 \text{ Log} \left[\frac{1-x}{-x+y} \right]^2 + \\
& \quad \text{Bcc Log} \left[\frac{1-x}{-x+y} \right]^3 + 4 \text{Brc } x^3 \text{ Log} \left[\frac{1-x}{-x+y} \right]^3 - \text{Bcc } y \text{ Log} \left[\frac{1-x}{-x+y} \right]^3 - \\
& \quad \left. \left. 4 \text{Brc } x^3 y \text{ Log} \left[\frac{1-x}{-x+y} \right]^3 + \text{to Log} \left[\frac{1-x}{-x+y} \right]^4 - x \text{ Log} \left[\frac{1-x}{-x+y} \right]^4 \right) \right) \\
& \left(-4 \text{Brc} + 16 \text{Brc } y - 24 \text{Brc } y^2 + 16 \text{Brc } y^3 - 4 \text{Brc } y^4 - 12 \text{Brc } x \right. \\
& \quad \text{Log} \left[\frac{1-x}{-x+y} \right] + 36 \text{Brc } x y \text{ Log} \left[\frac{1-x}{-x+y} \right] - 36 \text{Brc } x y^2 \text{ Log} \left[\frac{1-x}{-x+y} \right] + \\
& \quad 12 \text{Brc } x y^3 \text{ Log} \left[\frac{1-x}{-x+y} \right] - 4 \text{Brc } x \text{ Log} \left[\frac{1-x}{-x+y} \right]^2 - 8 \text{Brc } x^2 \text{ Log} \left[\frac{1-x}{-x+y} \right]^2 + \\
& \quad 4 \text{Brc } y \text{ Log} \left[\frac{1-x}{-x+y} \right]^2 + 4 \text{Brc } x y \text{ Log} \left[\frac{1-x}{-x+y} \right]^2 + \\
& \quad 16 \text{Brc } x^2 y \text{ Log} \left[\frac{1-x}{-x+y} \right]^2 - 8 \text{Brc } y^2 \text{ Log} \left[\frac{1-x}{-x+y} \right]^2 + \\
& \quad 4 \text{Brc } x y^2 \text{ Log} \left[\frac{1-x}{-x+y} \right]^2 - 8 \text{Brc } x^2 y^2 \text{ Log} \left[\frac{1-x}{-x+y} \right]^2 + \\
& \quad 4 \text{Brc } y^3 \text{ Log} \left[\frac{1-x}{-x+y} \right]^2 - 4 \text{Brc } x y^3 \text{ Log} \left[\frac{1-x}{-x+y} \right]^2 - \text{Bcc Log} \left[\frac{1-x}{-x+y} \right]^3 - \\
& \quad 12 \text{Brc } x^2 \text{ Log} \left[\frac{1-x}{-x+y} \right]^3 + 8 \text{Brc } x^3 \text{ Log} \left[\frac{1-x}{-x+y} \right]^3 + \text{Bcc } y \text{ Log} \left[\frac{1-x}{-x+y} \right]^3 + \\
& \quad 12 \text{Brc } x y \text{ Log} \left[\frac{1-x}{-x+y} \right]^3 - 8 \text{Brc } x^3 y \text{ Log} \left[\frac{1-x}{-x+y} \right]^3 - \\
& \quad 12 \text{Brc } x y^2 \text{ Log} \left[\frac{1-x}{-x+y} \right]^3 + 12 \text{Brc } x^2 y^2 \text{ Log} \left[\frac{1-x}{-x+y} \right]^3 - \\
& \quad 12 \text{Brc } x^3 \text{ Log} \left[\frac{1-x}{-x+y} \right]^4 + 12 \text{Brc } x^4 \text{ Log} \left[\frac{1-x}{-x+y} \right]^4 + \\
& \quad \left. \left. 12 \text{Brc } x^2 y \text{ Log} \left[\frac{1-x}{-x+y} \right]^4 - 12 \text{Brc } x^3 y \text{ Log} \left[\frac{1-x}{-x+y} \right]^4 \right) \right) / \\
& \left(\text{to } (-1+x) \times (x-y) \text{ Log} \left[\frac{1-x}{-x+y} \right]^9 \right) - \\
& \left((-1+y) \left(\text{Brc} - 3 \text{Brc } y + 3 \text{Brc } y^2 - \text{Brc } y^3 + 4 \text{Brc } x \text{ Log} \left[\frac{1-x}{-x+y} \right] - \right. \right. \\
& \quad \left. \left. 8 \text{Brc } x y \text{ Log} \left[\frac{1-x}{-x+y} \right] + 4 \text{Brc } x y^2 \text{ Log} \left[\frac{1-x}{-x+y} \right] + 6 \text{Brc } x^2 \text{ Log} \left[\frac{1-x}{-x+y} \right]^2 - \right. \right.
\end{aligned}$$

$$\begin{aligned}
& 6 \text{Brc } x^2 y \text{ Log} \left[\frac{1-x}{-x+y} \right]^2 + \text{Bcc} \text{ Log} \left[\frac{1-x}{-x+y} \right]^3 + 4 \text{Brc } x^3 \text{ Log} \left[\frac{1-x}{-x+y} \right]^3 \Big) \\
& \left(4 \text{Brc} - 20 \text{Brc } y + 40 \text{Brc } y^2 - 40 \text{Brc } y^3 + 20 \text{Brc } y^4 - 4 \text{Brc } y^5 + \right. \\
& 12 \text{Brc } x \text{ Log} \left[\frac{1-x}{-x+y} \right] - 48 \text{Brc } x y \text{ Log} \left[\frac{1-x}{-x+y} \right] + \\
& 72 \text{Brc } x y^2 \text{ Log} \left[\frac{1-x}{-x+y} \right] - 48 \text{Brc } x y^3 \text{ Log} \left[\frac{1-x}{-x+y} \right] + \\
& 12 \text{Brc } x y^4 \text{ Log} \left[\frac{1-x}{-x+y} \right] + 4 \text{Brc } x \text{ Log} \left[\frac{1-x}{-x+y} \right]^2 + \\
& 8 \text{Brc } x^2 \text{ Log} \left[\frac{1-x}{-x+y} \right]^2 - 4 \text{Brc } y \text{ Log} \left[\frac{1-x}{-x+y} \right]^2 - 8 \text{Brc } x y \text{ Log} \left[\frac{1-x}{-x+y} \right]^2 - \\
& 24 \text{Brc } x^2 y \text{ Log} \left[\frac{1-x}{-x+y} \right]^2 + 12 \text{Brc } y^2 \text{ Log} \left[\frac{1-x}{-x+y} \right]^2 + \\
& 24 \text{Brc } x^2 y^2 \text{ Log} \left[\frac{1-x}{-x+y} \right]^2 - 12 \text{Brc } y^3 \text{ Log} \left[\frac{1-x}{-x+y} \right]^2 + \\
& 8 \text{Brc } x y^3 \text{ Log} \left[\frac{1-x}{-x+y} \right]^2 - 8 \text{Brc } x^2 y^3 \text{ Log} \left[\frac{1-x}{-x+y} \right]^2 + \\
& 4 \text{Brc } y^4 \text{ Log} \left[\frac{1-x}{-x+y} \right]^2 - 4 \text{Brc } x y^4 \text{ Log} \left[\frac{1-x}{-x+y} \right]^2 + \text{Bcc} \text{ Log} \left[\frac{1-x}{-x+y} \right]^3 + \\
& 12 \text{Brc } x^2 \text{ Log} \left[\frac{1-x}{-x+y} \right]^3 - 8 \text{Brc } x^3 \text{ Log} \left[\frac{1-x}{-x+y} \right]^3 - 2 \text{Bcc } y \text{ Log} \left[\frac{1-x}{-x+y} \right]^3 - \\
& 12 \text{Brc } x y \text{ Log} \left[\frac{1-x}{-x+y} \right]^3 - 12 \text{Brc } x^2 y \text{ Log} \left[\frac{1-x}{-x+y} \right]^3 + 16 \text{Brc } x^3 y \\
& \text{Log} \left[\frac{1-x}{-x+y} \right]^3 + \text{Bcc } y^2 \text{ Log} \left[\frac{1-x}{-x+y} \right]^3 + 24 \text{Brc } x y^2 \text{ Log} \left[\frac{1-x}{-x+y} \right]^3 - \\
& 12 \text{Brc } x^2 y^2 \text{ Log} \left[\frac{1-x}{-x+y} \right]^3 - 8 \text{Brc } x^3 y^2 \text{ Log} \left[\frac{1-x}{-x+y} \right]^3 - \\
& 12 \text{Brc } x y^3 \text{ Log} \left[\frac{1-x}{-x+y} \right]^3 + 12 \text{Brc } x^2 y^3 \text{ Log} \left[\frac{1-x}{-x+y} \right]^3 + \\
& 12 \text{Brc } x^3 \text{ Log} \left[\frac{1-x}{-x+y} \right]^4 - 12 \text{Brc } x^4 \text{ Log} \left[\frac{1-x}{-x+y} \right]^4 - \\
& 12 \text{Brc } x^2 y \text{ Log} \left[\frac{1-x}{-x+y} \right]^4 + 12 \text{Brc } x^4 y \text{ Log} \left[\frac{1-x}{-x+y} \right]^4 + \\
& 12 \text{Brc } x^2 y^2 \text{ Log} \left[\frac{1-x}{-x+y} \right]^4 - 12 \text{Brc } x^3 y^2 \text{ Log} \left[\frac{1-x}{-x+y} \right]^4 - x \text{ Log} \left[\frac{1-x}{-x+y} \right]^5 + \\
& x^2 \text{ Log} \left[\frac{1-x}{-x+y} \right]^5 + y \text{ Log} \left[\frac{1-x}{-x+y} \right]^5 - x y \text{ Log} \left[\frac{1-x}{-x+y} \right]^5 \Big) / \\
& \left(\text{to } (-1+x) \times (x-y) \text{ Log} \left[\frac{1-x}{-x+y} \right]^9 \right) = \theta
\end{aligned}$$

Simplify[%]

$$\begin{aligned}
& \left((-1+y) \left(8 \text{Brc}^2 x (-1+y)^8 + \text{Brc}^2 (-1+y)^7 (x - 57x^2 - y + xy) \text{ Log} \left[\frac{-1+x}{x-y} \right] + \right. \right. \\
& 168 \text{Brc}^2 x^3 (-1+y)^6 \text{ Log} \left[\frac{-1+x}{x-y} \right]^2 - \\
& \left. \left. 2 \text{Brc } x (-1+y)^5 (5 \text{Bcc} + 14 \text{Brc } x (x + 9x^2 - y + xy)) \text{ Log} \left[\frac{-1+x}{x-y} \right]^3 + \right. \right.
\end{aligned}$$

$$\begin{aligned}
& 2 \text{Brc } (-1+y)^4 (\text{Bcc } (17x^2 + y - x(1+y)) + \\
& \quad 2x (\text{to} + x (-1 + 4 \text{Brc } x (10x^2 - 7y + 7x(1+y)))))) \\
& \text{Log} \left[\frac{-1+x}{x-y} \right]^4 + \text{Brc } (-1+y)^3 (\text{to } (x - 13x^2 - y + xy) + \\
& \quad 12x^3 (1 - 3 \text{Bcc} + \text{Brc } x (5x^2 + 17y - 17x(1+y)))) \text{Log} \left[\frac{-1+x}{x-y} \right]^5 + \\
& 2x (-1+y)^2 (\text{Bcc}^2 + 2 \text{Bcc } \text{Brc } x (x^2 - 3y + 3x(1+y)) - \\
& \quad 2 \text{Brc } x (2x^2 + 40 \text{Brc } x^5 - y + 48 \text{Brc } x^3 y - \\
& \quad 48 \text{Brc } x^4 (1+y) + x(1 - 3 \text{to} + y))) \text{Log} \left[\frac{-1+x}{x-y} \right]^6 + \\
& (-1+y) (\text{Bcc } x (-\text{to} + x(1 + 16 \text{Brc } (-1+x)x(x-y))) - \text{Bcc}^2 \\
& \quad (-1+x)(x-y) + 2 \text{Brc } x^2 (\text{to } (x^2 + 3y - 3x(1+y)) + 2x(-2x^2 + \\
& \quad 20 \text{Brc } x^5 - 3y + 20 \text{Brc } x^3 y + 3x(1+y) - 20 \text{Brc } x^4 (1+y)))) \\
& \text{Log} \left[\frac{-1+x}{x-y} \right]^7 + (-1+x) (\text{Bcc } \text{to} + 4 \text{Brc } x^3 (-2 \text{to} + 3x) \\
& \quad (x-y) \text{Log} \left[\frac{-1+x}{x-y} \right]^8) \Big/ \\
& (\text{to } (-1+x)x(x-y) \text{Log} \left[\frac{-1+x}{x-y} \right]) = 0
\end{aligned}$$

$$dw/dx = 0,$$

$$\begin{aligned}
& \left(8 \text{Brc}^2 x (-1+y)^8 + \text{Brc}^2 (-1+y)^7 (x - 57x^2 - y + xy) \text{Log} \left[\frac{-1+x}{x-y} \right] + \right. \\
& \quad 168 \text{Brc}^2 x^3 (-1+y)^6 \text{Log} \left[\frac{-1+x}{x-y} \right]^2 - \\
& \quad 2 \text{Brc } x (-1+y)^5 (5 \text{Bcc} + 14 \text{Brc } x (x + 9x^2 - y + xy)) \text{Log} \left[\frac{-1+x}{x-y} \right]^3 + \\
& \quad 2 \text{Brc } (-1+y)^4 \\
& \quad (\text{Bcc } (17x^2 + y - x(1+y)) + \\
& \quad \quad 2x (\text{to} + x (-1 + 4 \text{Brc } x (10x^2 - 7y + 7x(1+y)))) \text{Log} \left[\frac{-1+x}{x-y} \right]^4 + \\
& \quad \text{Brc } (-1+y)^3 \\
& \quad (\text{to } (x - 13x^2 - y + xy) + \\
& \quad \quad 12x^3 (1 - 3 \text{Bcc} + \text{Brc } x (5x^2 + 17y - 17x(1+y)))) \text{Log} \left[\frac{-1+x}{x-y} \right]^5 + \\
& \quad 2x (-1+y)^2 \\
& \quad (\text{Bcc}^2 + 2 \text{Bcc } \text{Brc } x (x^2 - 3y + 3x(1+y)) - \\
& \quad \quad 2 \text{Brc } x (2x^2 + 40 \text{Brc } x^5 - y + 48 \text{Brc } x^3 y - 48 \text{Brc } x^4 (1+y) + \\
& \quad \quad \quad x(1 - 3 \text{to} + y)) \text{Log} \left[\frac{-1+x}{x-y} \right]^6 +
\end{aligned}$$

$$\begin{aligned}
& (-1+y) \left(Bcc x (-to + x (1 + 16 Brc (-1+x) x (x-y))) - \right. \\
& \quad Bcc^2 (-1+x) (x-y) + \\
& \quad 2 Brc x^2 (to (x^2 + 3y - 3x (1+y)) + \\
& \quad \quad 2x (-2x^2 + 20 Brc x^5 - 3y + 20 Brc x^3 y + 3x (1+y) - \\
& \quad \quad \quad 20 Brc x^4 (1+y))) \left. \right) \text{Log} \left[\frac{-1+x}{x-y} \right]^7 + \\
& (-1+x) \left(Bcc to + 4 Brc x^3 (-2 to + 3x) \right) (x-y) \text{Log} \left[\frac{-1+x}{x-y} \right]^8 \Big) = 0
\end{aligned}$$



Appendix C – The Performance Optimization Codes Written in *MATLAB*

```

clear all;
clc;
format long
syms x;
counter = 1;
i = 1;
twthi = zeros(10000,1);
twthid = zeros(10000,1);
efficiency = zeros(10000,1);
efficiencyd = zeros(10000,1);
    for brc = 0:0.05:1
        for y = 0.4:0.1:0.9
            for to = 0.2:0.1:0.5
                for bcc = 0:0.05:1
                    % Maximum power can be written as
                    w = @(x) (((brc*(-1+y)^4)-(log((-1+x)/(x-y)))*4*brc*x*...
((-1+y)^3)+6*brc*(x^2)*((-1+y)^2)*(log((-1+x)/(x-y))^2)-...
(bcc+4*brc*(x^3))*(-1+y)*(log((-1+x)/(x-y))^3)+...
(to-x)*(log((-1+x)/(x-y))^4)*(brc*((-1+y)^4)-...
4*brc*x*((-1+y)^3)*(log((-1+x)/(x-y)))+...
(6*brc*(x^2))*((-1+y)^2)*(log((-1+x)/(x-y))^2)-...
(bcc+4*brc*(x^3))*(-1+y)*(log((-1+x)/(x-y))^3)-...
x*(log((-1+x)/(x-y))^4))*((4*brc*((-1+y)^4))-...
12*brc*x*((-1+y)^3)*(log((-1+x)/(x-y)))+...
4*brc*((-1+y)^2)*(x+2*(x^2)-y+x*y)*...
(log((-1+x)/(x-y))^2)-(-1+y)*(bcc+4*brc*x*...
(-2*(x^2)-3*y+3*x*(1+y)))*(log((-1+x)/(x-y))^3)-...
12*brc*(-1+x)*(x^2)*(x-y)*(log((-1+x)/(x-y))^4))+...
to*(log((-1+x)/(x-y))^4)*(-brc*((-1+y)^3)+...

```

```

4*brc*x*(-1+y)^2*(log((-1+x)/(x-y)))-...
6*brc*(x^2)*(-1+y)*(log((-1+x)/(x-y))^2)+...
(bcc+4*brc*(x^3))*(log((-1+x)/(x-y))^3)*...
(4*brc*(-1+y)^5)-12*brc*x*(-1+y)^4)*...
(log((-1+x)/(x-y)))+4*brc*(-1+y)^3*(x+2*(x^2)-y+x*y)*...
(log((-1+x)/(x-y))^2)-((-1+y)^2)*(bcc+4*brc*x*...
(-2*(x^2)-3*y+3*x*(1+y)))*(log((-1+x)/(x-y))^3)-...
12*brc*(-1+x)*(x^2)*(x-y)*(-1+y)*(log((-1+x)/(x-y))^4)-...
(-1+x)*(x-y)*(log((-1+x)/(x-y))^5));
x1 = fzero(w,[to (y-0.1e-8)]);
    display (x1)
% Efficiency at maximum power conditions can be
written as
eff1 = (1-(to/(x1-bcc*((1-y)/log((-1+x1)/(x1-y)))-...
brc*(((1-y)/log((-1+x1)/(x1-y)))^4)+...
4*x1*(((1-y)/log((-1+x1)/(x1-y)))^3)+...
6*(x1^2)*(((1-y)/log((-1+x1)/(x1-y)))^2)+...
4*(x1^3)*((1-y)/log((-1+x1)/(x1-y)))));
    display (eff1)
% Maximum power density can be written as
wd = @(x) (8*(brc^2)*x*(-1+y)^8)+(brc^2)*((-1+y)^7)*...
(x-57*(x^2)-y+x*y)*(log((-1+x)/(x-y)))+...
168*(brc^2)*(x^3)*((-1+y)^6)*((log((-1+x)/(x-y)))^2)-...
2*brc*x*(-1+y)^5*(5*bcc+14*brc*x*(x+9*(x^2)-y+x*y))*...
((log((-1+x)/(x-y)))^3)+2*brc*(-1+y)^4)*...
(bcc*(17*(x^2)+y-x*(1+y))+2*x*(to+x*(-1+4*brc*x*...
(10*(x^2)-7*y+7*x*(1+y))))*(log((-1+x)/(x-y))^4)+...
brc*(-1+y)^3*(to*(x-13*(x^2)-y+x*y)+...
12*(x^3)*(1-3*bcc+brc*x*(5*(x^2)+17*y-17*x*(1+y))))*...
((log((-1+x)/(x-y)))^5)+2*x*(-1+y)^2)*...
((bcc^2)+2*bcc*brc*x*((x^2)-3*y+3*x*(1+y))-...
2*brc*x*(2*(x^2)+40*brc*(x^5)-y+48*brc*(x^3)*...
y-48*brc*(x^4)*(1+y)+x*(1-3*to+y))*...

```

```

((log((-1+x)/(x-y)))^6)+(-1+y)*(bcc*x*...
(-to+x*(1+16*brc*(-1+x)*x*(x-y)))-(bcc^2)*(-1+x)*...
(x-y)+2*brc*(x^2)*(to*((x^2)+3*y-3*x*(1+y))+...
2*x*(-2*(x^2)+20*brc*(x^5)-3*y+20*brc*(x^3)*y+3*x*...
(1+y)-20*brc*(x^4)*(1+y)))*((log((-1+x)/(x-y)))^7)+...
(-1+x)*(bcc*to+4*brc*(x^3)*(-2*to+3*x))*(x-y)*...
((log((-1+x)/(x-y)))^8));
2 = fzero(w,[to (y-0.1e-8)]);
    display (x2)

% Efficiency at maximum power density conditions
can be written as
eff2 = (1-(to/(x2-bcc*((1-y)/log((-1+x2)/(x2-y)))-...
brc*(((1-y)/log((-1+x2)/(x2-y)))^4)+...
4*x2*(((1-y)/log((-1+x2)/(x2-y)))^3)+...
6*(x2^2)*(((1-y)/log((-1+x2)/(x2-y)))^2)+...
4*(x2^3)*(((1-y)/log((-1+x2)/(x2-y))))));
    display (eff2)
    twthi (counter,i) = x1;
    efficiency (counter,i) = eff1;
    twthid (counter,i) = x2;
    efficiencyd (counter,i) = eff2;
        if (counter>=21)
            counter = 1;
            i = i+1;
        else
            counter = counter + 1;
        end
    end
end
end
end
end

```

CURRICULUM VITAE

PERSONAL INFORMATION

Name Surname : Gürcan TİRYAKİ
Date of Birth : 28.07.1989
Phone : +90 554 841 95 67
E-mail : gtiryaki@ybu.edu.tr



EDUCATION

High School : Anıttepe Super High School / ANKARA (2003-2007)
Bachelor : Gazi University / ANKARA (2007-2012)
Master Degree : Ankara Yıldırım Beyazıt University / (2014-continued)

WORK EXPERIENCE

Design and Manufacturing Engineer: Turkmak Makine Mühendislik Ltd. Şti. (09.2012-12.2012)
Chief Engineer of Design and Manufacturing Dept.: Evotek Mühendislik A.Ş. (12.2012-06.2013)
Field Engineer: Poyraz İnşaat Ltd. Şti. (06.2013-09.2013)
Field Chief Engineer: RC Rönesans İnşaat Taahhüt A.Ş. / Poyraz İnşaat Ltd. Şti. (09.2013-01.2014)
Research Assist.: Ankara Yıldırım Beyazıt University / (02.2014-continued)

TOPICS OF INTEREST

- Thermodynamics
- Heat Transfer
- Nuclear Energy Systems
- Fluid Mechanics
- Solar Power Technologies

2017 ANKARA	Department of Mechanical Engineering	Gürcan TIRYAKI	
--------------------	---	-----------------------	---